UNIVERSITY OF CALIFORNIA
RIVERSIDE

Kinetics of Stem Cell Stasis and Transformation Through Transcription Factor WUSCHEL and its Interactors.

A Dissertation submitted in partial satisfaction
of the requirements for the degree of

Doctor of Philosophy

in

Genetics, Genomics, and Bioinformatics

by

Albert Do

December 2022

Dissertation Committee:
Dr. Venugopala Reddy Gonehal, Chairperson
Dr. Weitao Chen
Dr. Gregor Blaha

The Dissertation of Albert Do is approved:

_____

_____

_____

Committee Chairperson

University of California, Riverside

Acknowledgements

This research is the result of the active support and resources of individuals too numerous to comprehensively mention. I am especially indebted to my PI Dr. Venu Gonehal for his scientific and personal guidance over the years. His patience and support going above and beyond to take interest in and aid my progress made this project possible. Dr. Kevin Rodriguez has worked closely together with me for as long, as a colleague and second mentor. Without his constant support as well, this research would not have been possible. Dr. Weitao Chen has been our longtime collaborator and a co-PI of sorts for me on the computational end of our project. She along with Dr. Betul Senay-Aras have been instrumental in guiding me through the more unfamiliar aspects of mathematical modeling as we collaborated. I am grateful to my past labmates; Alexander Plong, Dariush Nejad, Dr. Stephen Snipes, and my current colleague Yujiuxiao Zhang, who have been valuable sources of information and discussion as we helped each other along in our respective endeavors. I want to shoutout the many undergraduates and high school students who have worked with and for me including those currently with us like Arely Fernandez, Dorothy Nguyen, Christian and Cameron Delgadillo, Lloyd Kao, and Samin Ullah as well as those who have moved on to other pursuits such as Cora Bright, Raffee Wright, Vanessa Ceja, and others who are too numerous to list for their assistance and providing a lively environment. From my committee I'd like to acknowledge Dr. Stefano Lonardi for the training and help he provided on the computational aspects of my project as well as Dr. Gregor Blaha for his critiques and analysis. I'd also like to thank other UCR faculty who have helped me throughout my time at here. This includes Dr. Thomas Girke, especially when I was new, Dr. Patricia Springer for her support as Department Chair and as a perennial part of the

qualifying exam committee of our lab's members, Dr. Zhenyu Jia who aided me in the process of passing my qualifiers, and Dr. Mark Alber for his assistance on getting our manuscript published. Alber's team, along with former Gonehal lab members; Dr. Mariano Perales, Dr. Ricardo Moreno, and Dr. Ram Yadav provided me with useful technical support as I progressed through my experiments. I'd also like to thank Dr. Houng-Wei-Tsai and Dr. Peggy Farnham and others for helping to set me on my career course.

Chapter 1 of this dissertation is a reprint with minor modifications to figure references of K. Rodriguez, **A. Do**, B. Senay-Aras, M. Perales, M. Alber, W. Chen, G. V. Reddy, Concentration-dependent transcriptional switching through a collective action of cis-elements. *Science Advances*. **8**, eabo6157 (2022). Coauthors W. Chen and G. V. Reddy listed in this publication directed and supervised the research which formed the basis for this dissertation. Parts of the preceding work were in turn derived from K. Rodriguez (2017). WUSCHEL Mediated Bifunctional Transcriptional Regulation of CLAVATA3 Levels and Spatial Pattern in Arabidopsis thaliana. *UC Riverside*. Both of these works are licensed under CC BY 4.0.

The base framework the multicellular model presented in Chapter 1 and 2 was built on was forked from Organism Simulator by Henrik Jonsson et al (https://dev.thep.lu.se/organism) released under the MIT license. Dariush Nejad took the 2 images of the control untransformed LambdaN SAMs in Fig. 4.2A. Alexander Plong scanned the image stacks in Fig 4.6A and D which were subsequently analyzed by me. The WT GFP meristem image in Fig 4.7A was from Dr. Kevin Rodriguez.

Dedication

I dedicate this manuscript to my family. Especially to my parents, who have given me undying love and support all my life.

And of course, I'd like to thank the Big Guy upstairs.

ABSTRACT OF THE DISSERTATION

Kinetics of Stem Cell Stasis and Transformation Through Transcription Factor WUSCHEL and its Interactors

by

Albert Do

Doctor of Philosophy, Graduate Program in Genetics, Genomics and Bioinformatics
University of California, Riverside, December 2022
Dr. Venugopala Reddy Gonehal, Chairperson

The process of growth in plants is driven by the shoot apical meristem (SAM) which is in turn driven by a signaling network centered around the transcription factor WUSCHEL (WUS). The interaction between WUS and its target genes has a key role in determining the structure of the SAM and fate of its stem cells, as well as how it responds and adapts to its environment. The interplay between WUS and a limited number of other targets such as the gene encoding the peptide CLAVATA3 (CLV3) has been outlined on a basic level through previous studies. However, much work remains to gather more detailed information, develop quantitative molecular explanations for the observed gene expression behaviors, generalize the biology to encompass the broad range of WUS targets, and potentially identify similar regulatory systems elsewhere in plants and other organisms. This study uses a multidisciplinary approach combining experimental and computational techniques to proceed toward these objectives through a number of different avenues. The nature of the cis-regulatory module (CRM) through which *CLV3*

interacts with WUS was examined showing that individual cis-elements of the CRM behave distinctly when they are working alone compared to when they are working together. This also provided molecular details about the concentration dependent mechanism where the CRM coordinated a nonlinear response to WUS. A computational simulation of the meristem network was tested and data is being gathered on how the resetting of the CLV3 expression gradient to the outer meristem occurs on a molecular level in *CLV3* complementation assays. Surveying the *CLV3* epigenome revealed a landscape of binding clusters and chromatin looping within the gene and at its ends. This and motif analysis, showed that other targets may share similar features. Imaging studies revealed tissue level dynamics, backing up previously hypothesized mechanisms relating expression to monomeric and multimeric WUS and how it not only regulates but is regulated in turn by a network of interactors.

Table of Contents

List of Figures

Introduction

Chapter 1

Chapter 2

Chapter 3

Chapter 4

List of Abbreviations

3C	chromatin conformation capture
Bp	base pair
ChIP	chromatin immunoprecipitation
CLV	CLAVATA
CK	Cytokinin
CRM	cis regulatory module
Cq	quantification cycle
Dex	dexamethasone
Dm	double mutant
DMSO	dimethyl sulfoxide
EMSA	electromobility shift assay
FCS	fluorescence correlation spectroscopy
FD	forced dimer
FL	full length
GFP	eGFP green fluorescence
GO	gene ontology
GR	Rattus Glucocorticoid Receptor
HAM	HAIRY MERISTEM
HDAC	histone deacetylase
HMM	hidden markov model
HOD	homodimerization domain
IGg	immunoglobulin G
Kb	kilobase
Lep	leptomycin
NLS	nuclear localization signal
nM	nanomolar
NPA	napthylphthalmic acid
H2B	Histone 2B
ODE	ordinary differential equation
PCR	sqPCR qPCR polymerase
PIN	PIN-FORMED
PSF	point spread function
Pol II	polymerase II
RK4	Runge Kutta 4th
RICS	Raster image correlation
SAM	shoot apical meristem
TAR2	TRYPTOPHAN AMINOTRANSFERASE RELATED
TF	transcription factor
uM	micromolar
UTR	untranslated region

WUS	WUSCHEL
WT	wild type
YFP	yellow fluorescence protein

Introduction

Within the biosphere, plants serve as the fulcrum of terrestrial ecosystems interacting with and depended on by numerous organisms. Humans rely on plants for virtually every imaginable purpose from food, to shelter, to medicine among other things (1). Learning about the underlying mechanisms by which plants function is important not just for straightforward applications such as improving agriculture and manufacturing products but to also derive a basic scientific understanding of important processes that can be applied to other systems (2).

The Shoot Apical Meristem and how it controls growth in plants.

The central biological process plants depend on is growth. Plants use growth to perform functions that would be fulfilled by faster movement in other organisms such as defense, finding resources, and general adaptation to the environment. (3) Growth in higher order plants is coordinated by a structure known as the meristem which is a bundle of tissue containing undifferentiated stem cells. (4) There are different types of meristems controlling different parts of the plants. Meristems that control above ground growth are known as shoot apical meristems (SAM). SAM structure can be divided in the apical-basal axis into different layers L1, L2, etc representing different layers of mature tissue or the radial axis, with the undifferentiated central zone and the surrounding peripheral zone. (Fig. 0.1) (5) SAM development is controlled by network centering around the interaction of WUS and CLV3. (6)

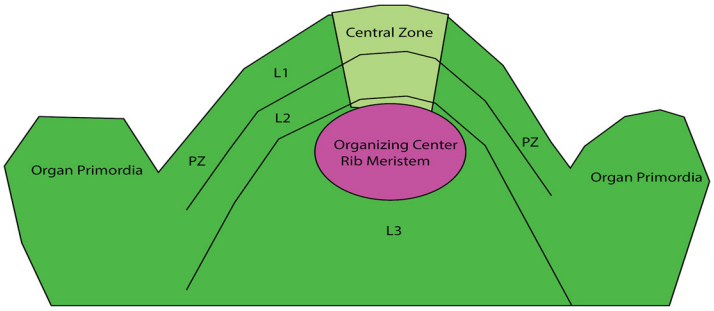

Fig. 0.1. Sections of the Shoot Apical Meristem

WUS is a homeodomain TF that mediates SAM dynamics in the plant *Arabidopsis thaliana*. WUS is composed of different domains with distinct functionality governing its behavior and effect on genes and proteins. (Fig. 0.2) (7) It binds to many targets across the genome through rules which remain to be fully understood, but one of the most important targets is *CLAVATA3 (CLV3*) (8).

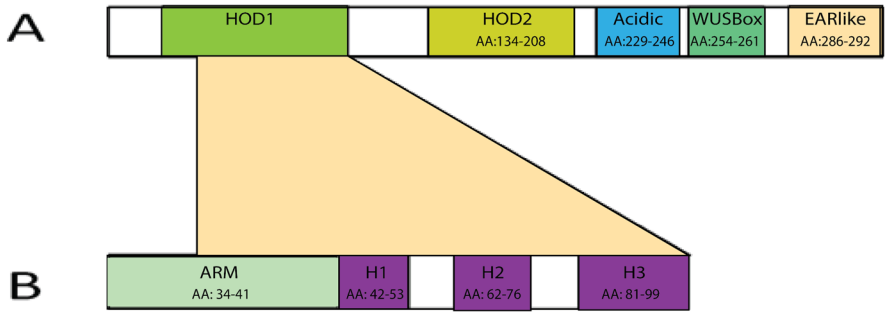

Fig. 0.2. Domains of the WUS protein.
(A) Domains of the WUS protein include HOD1, a homodimerization domain which handles DNA binding. HOD2 which is a second homodimerization domain which coordinates dimerization between proteins. The other domains are the Acidic domain which is linked with activation, the WUSBox which is linked with activation and nuclear retention. And the ERF-associated amphiphilic repression like (EARlike) domain which was linked to repression and export of the WUS protein from the nucleus. **(B)** Composition of the HOD1 domain: The unordered ARM positions WUS on the DNA, the third helix H3 binds the DNA in the major groove while the other two helices position the protein.

CLV3 is a signaling peptide. It interacts through CLV2, CLV1, and related receptors starting downstream cascades affecting many different targets (9).

CLV3 interaction with WUS takes place through the cis regulatory modules (CRM)s. The primary CRM in *CLV3* is known as CRM1 which is the main interaction site with WUS. CRM2 and CRM3 are other CRMs in the locus which have supplementary roles. CRM1 consists of 5 cis-elements; 950, 970, 997, 1007, and 1060. (Fig. 0.3) Of which 970 binds WUS which is the strongest in affinity. These cis-elements are the sites of direct interaction with WUS formed from what are known as TAAT cores consisting of TAAT nucleotide sequences and slight variations in surrounding sequence(8).

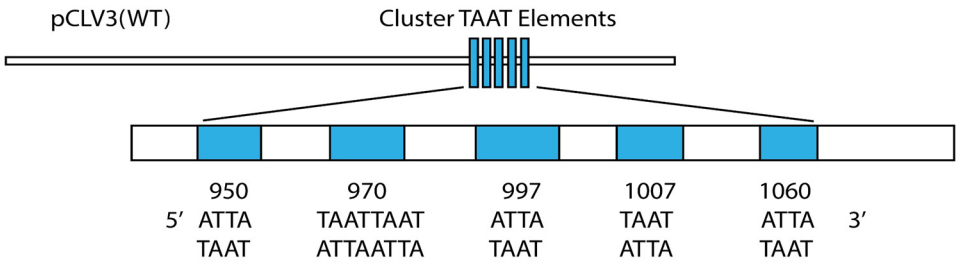

Fig. 0.3. The cis regulatory module of *CLV3*.
Cis elements 950, 970, 997, 1007, and 1060 make up the cis regulatory module (CRM1) of CLV3 and are composed of TAAT cores.

Together WUS and CLV3, along with other interactors, provide a balance which determines the fate of the SAM. WUS pushes stem cells into maintaining an undifferentiated state. CLV3 pushes cells toward differentiation and developing organs. Both are regulated in multiple ways by the other (Fig 0.4) (10). Through a signaling network centered around these interactions, the plant controls its structure and development. WUS protein activates *CLV3* through the CRM as a monomer and

represses it through the dimer. CLV3 regulates WUS in turn which is also regulated by effectors such as cytokinin and HAM proteins.

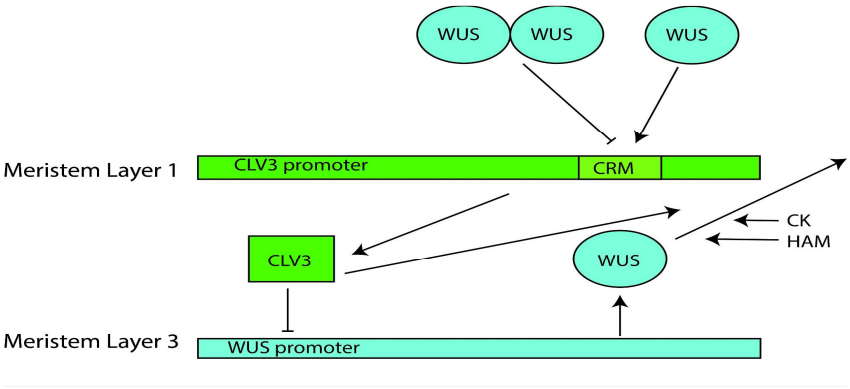

.

Fig. 0.4. The WUS/CLV3 circuit.
WUS and CLV3 regulate each other in multiple ways across the different layers of the meristem.

WUS is able to bind to targets not only as a monomer but as a dimer as well. Monomer binding has been associated with activation of the target while dimer binding has been associated with repression. With targets like *CLV3*, WUS is needed to activate it, so very low concentrations of WUS lead to low or no expression, whereas with a moderate amount of WUS, *CLV3* is activated. But too much WUS can lead to repression as WUS dimerizes (Fig. 0.5) (10). This nonlinear expression profile is known as the concentration dependent switch and is in stark contrast with the more simple on/off binary and concentration based linear models of expression (10). With the CRM, WUS can control *CLV3* and potentially other targets in a fine tuned and nonlinear manner beyond what is possible with traditional models of transcription factors (TF)s.

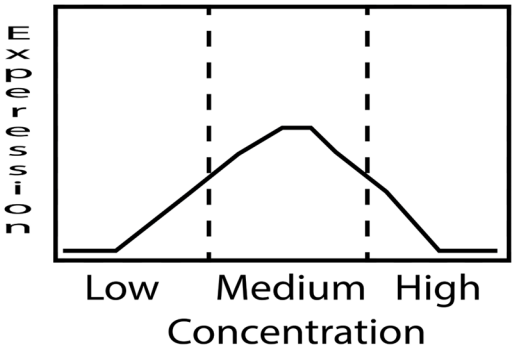

Fig. 0.5. Conceptual Graph of CLV3 Expression vs WUS Concentration. CLV3 expression is on the y axis and WUS concentration on the x axis. CLV3 expression is controlled by WUS in a nonlinear manner

Computational approaches to study the SAM

Composed of a multitude of cells interacting with each other through the activity and exchange of numerous molecular species, the SAM is a dauntingly complex system to observe, let alone understand quantitatively. Experiments sometimes cannot capture or change certain aspects of the system necessary to study properties such as the collective activity of the cis-elements.

A powerful complementary approach to solve these issues is the use of computational simulation of the SAM. There are a variety of strategies for simulating the SAM. They range from computationally expensive simulations which explicitly model molecules like the AMBER molecular dynamics package (11) to more abstract ordinary differential equation based simulations (12).

ODE Simulations

Ordinary differential equation (ODE) based models are systems of ODEs as the fundamental descriptor of their dynamics (12). ODEs relate the derivative to a function of one variable and are thus well suited for tracking temporal change of concentrations of

biomolecules or chemicals. A common approach in a biological signaling system is to have ODEs for each species with terms representing each process a species undergoes such as decay or production and use these to calculate the rate of change for the species concentration in timesteps, evolving the amount over time (Fig. 0.6) (12).

$$\frac{da}{dt} = p_a a - e_a a$$
$$\frac{db}{dt} = p_b b - e_b b$$
$$\frac{dc}{dt} = p_c c - e_c c$$

Fig. 0.6. An ODE Model of chemical dynamics.
A sample ODE system representing the dynamics of a 3 chemical species system. *P* terms represents production parameters, *e* represents the decay parameters while *a*, *b*, and *c* represent the amount of the 3 species.

The ODEs used in these simulations are usually too complicated to solve analytically so a numerical solver is used instead to calculate the change in each molecular species across timesteps.

One popular class of numerical solvers is known as the Runge-Kutta methods (13). The simplest of these methods is called the Euler Method. When applied to a situation relevant to this study i.e. the modeling of a species concentration in a cell, Euler approximates the concentration of the species in the next timestep by adding the slope at the current point/derivative at the current timestep multiplied by the timestep (13). For example, Given x_n and y_n are current points.

$y_{n+1} = y_n + hf(x_n,y_n)$

y_n = concentration at current step
y_{n+1} = concentration at next step
h = stepsize
$f(x_n,y_n)$ = function at the right hand side of the ODE evaluated at point n / slope of tangent to solution curve at point n.

By continuing to do this iteratively it is possible to numerically estimate the evolution of the species concentration over discrete time points.

A more accurate and stable version of Euler is known as the Runge-Kutta fourth order method (RK4)(13). The main difference with Euler is rather than 1 approximation of the slope, four are calculated for RK4 (Fig. 0.7B).

A

$$For \quad \frac{dy}{dt} = f(x,y), y(x_0) = y_0$$

$$y_1 = y_0 + hf\,(x_0, y_0)$$

B

$$For \quad \frac{dy}{dt} = f(x,y), y(x_0) = y_0$$

$$y_1 = y_0 + k$$

$$k_1 = hf\,(x_0, y_0)$$

$$k_2 = hf\left(x_0 + \frac{h}{2}, y_0 + \frac{k_1}{2}\right)$$

$$k_3 = hf\left(x_0 + \frac{h}{2}, y_0 + \frac{k_2}{2}\right)$$

$$k_4 = hf\,(x_0 + h, y_0 + k_3)$$

Fig. 0.7. Euler and RK4 numerical solver equations.
(A) The Euler method updates y for the next timestep by calculating the slope at the current time point. **(B)** The RK4 method updates to the next timestep by calculating 4 slopes. k1 = the same slope used in Euler. k2 = the slope at the midpoint of the timestep using k1 to step halfway. k3 = is another slope at the midpoint if you use k2 to step halfway. k4 = the slope at the endpoint if k3 is used to step to the end of the timestep.

The results are weighted and summed to the concentration then added like in the Euler method to advance to the next timestep.

An ODE based model of WUS/CLV3 interaction has been previously presented in (8). This provides a good starting point for building a more biologically relevant model of the SAM dynamics but lacks a critical portion of the system, having no particular means to simulate the dynamics of the *CLV3* CRM upon which the *WUS* concentration dependent switch relies.

Stochastic simulation methods and the hybrid model

The need to integrate CRM dynamics into the system may be filled by a more explicit model of molecular interaction. The Gillespie Algorithm is a stochastic simulation algorithm that generates probabilities for different events at each timestep based on conditions, then randomly picks from them to generate statistically correct trajectories (14) (Fig. 0.8). This makes the approach ideal for simulating the binding of WUS to the different cis-elements. Combined together hybrid ODE/Stochastic dynamics can form a multiscale model that accurately simulates both tissue, cell, and subcellular levels of the SAM.

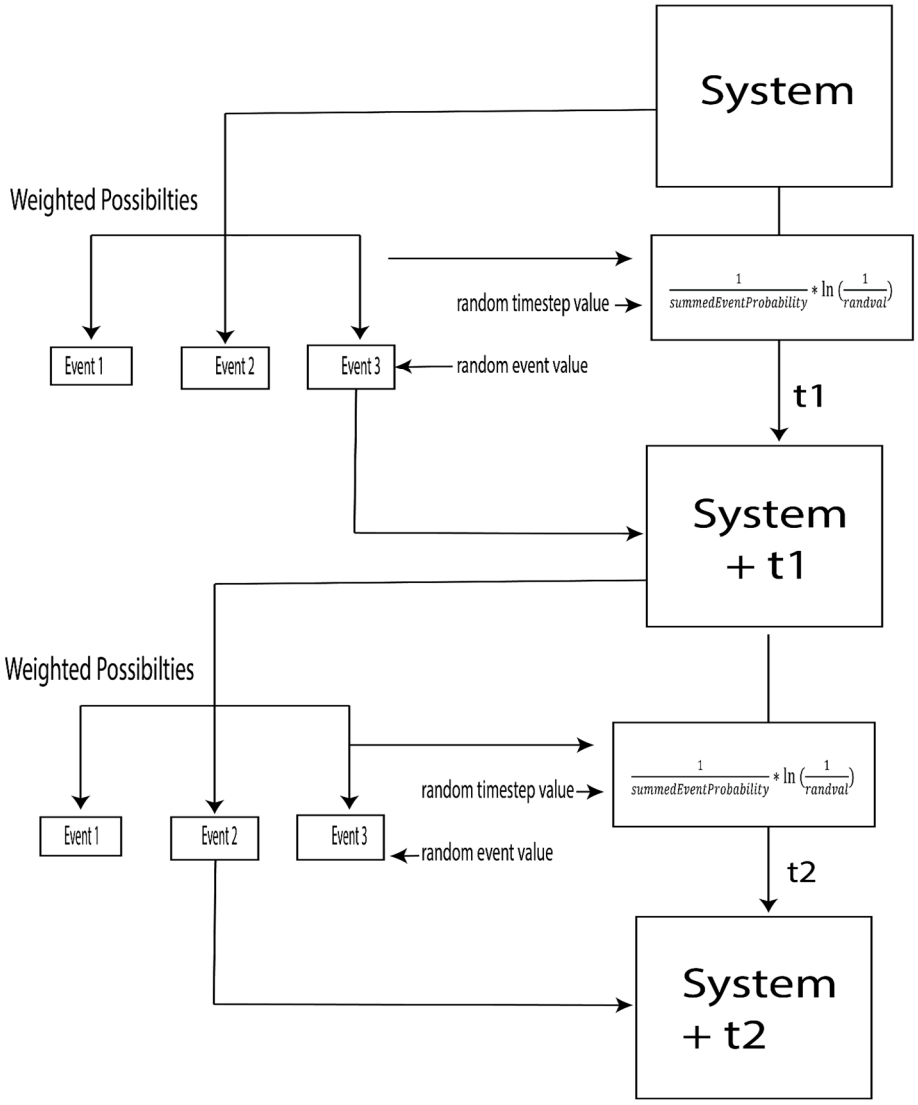

Fig. 0.8. Conceptual outline of the Gillespie algorithm.
In the Gillespie Algorithm probabilities for the different events and a random value are generated to select one of these events. Based on the summed probabilities and another random value; the timestep is generated. The system is then updated to the next timestep.

Bioinformatic analysis of WUS target data

The growing amount of datasets and the need to expand and test to see if findings in *CLV3* regulation hold for other targets, call for the application of bioinformatics methods. A straightforward technique is to simply scan for motifs and attempt to glean useful

patterns (15). A good starting point for this analysis would be to center efforts on TAAT core containing cis-elements that are known to be important for WUS binding to target genes (7).

HMM Analysis

A more exotic approach to analyzing sequence data compared to simply scanning for prespecified patterns would be to use a machine learning approach. Unlike the previous fixed motif technique, this approach would at least partially be based on generating motifs to look for from the data through a more systematic strategy. One strategy that has been used successfully is Hidden Markov Model (HMM) based classification (16). HMMs are statistical models that describe Markov processes, which are processes that describe sequences where event probabilities depend only on the previous event. Events are treated as a series of emissions by ‘hidden’ states. For example, Autumn can be seen as a hidden state emitting a sequence of days of weather; such as a rainy day, then a sunny day, then a muggy day, in a model of unknown seasons emitting weather (Fig. 0.9A). This can be built out to an entire model with starting probabilities, states with emission probabilities, and transition probabilities between these states. While genetic sequences are not perfectly Markov in nature (in that future sequence does not solely depend on current sequence), genes do show high dependency on their local surroundings and HMMs can be used as a way of classifying sequences by modeling them as emissions and types of sequences as states similarly to the previous seasons example (Fig. 0.9B) (16).

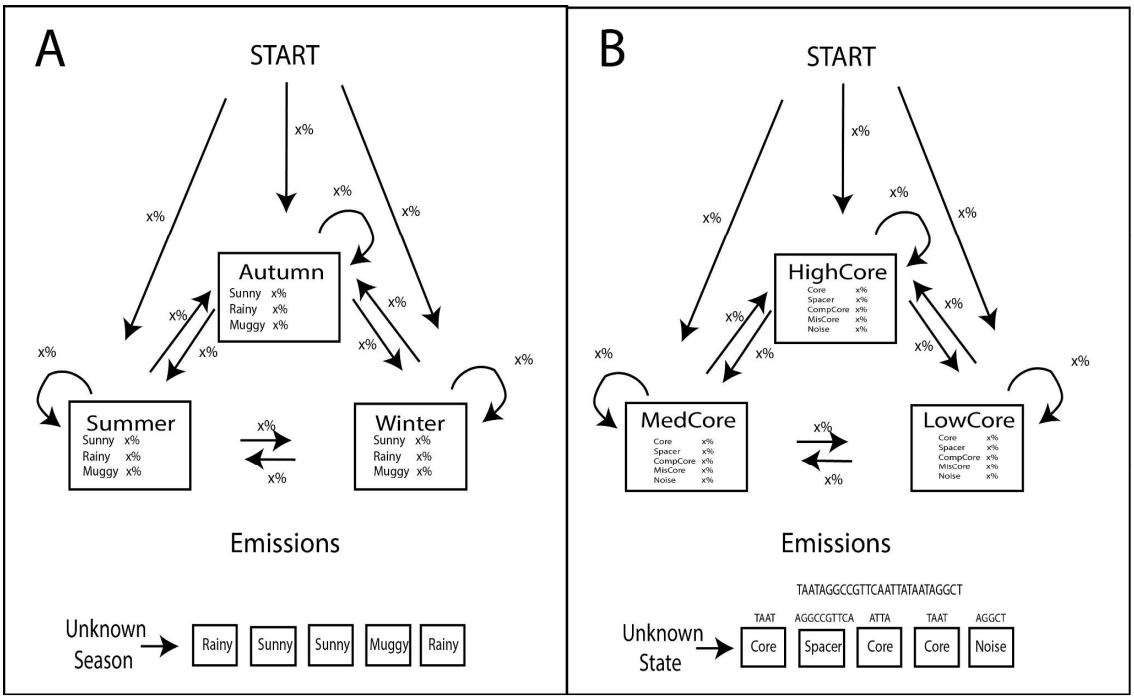

Fig. 0.9. Conceptual outline of an HMM model.
(A) Conceptual model of an HMM modeling a system of seasons with an unknown season emitting weather. The x% arrows emanating from Start indicate starting probabilities. The x% within the different states indicate emission probabilities. And the x% arrows traveling between the states indicate transition probabilities. **(B)** Conceptual model of an HMM modeling a system which transitions between types of gene sequences with an unknown type emitting a sequence.

Objectives

The goal of the present study is to use a combination of experimental and computational techniques to explain the mechanisms behind the WUS and CLV3 network from a multiscale perspective from subcellular to tissue level. The contribution of the different molecular and genetic factors will be more fully understood in context. Through this a comprehensive quantitative model of the WUS/CLV3 network, and the CRM's function in mediating the WUS concentration dependent switch will be developed. In Chapter 1, the *CLV3* CRM is investigated and how it gives rise to the concentration dependent switch and the role of the different cis-elements is developed. In Chapter 2, the non feedback

signaling model used to investigate the CRM in Chapter 1 is expanded to a coupled feedback model of fully dynamic WUS and CLV3 to get data on how the WUS components respond as well as how the system balances with its various parts and the contributions of the different parameters. Chapter 3 aims to describe the cis-element landscape around WUS targets and what goes into making up the structure of these targets. Various analyses of interactions and behavior of *CLV3* and WUS are conducted *in vivo* in Chapter 4 to gather data to test and more closely examine the concentration dependent switch and other mechanisms of the system at the tissue level.

References

1. S. Quijas, B. Schmid, P. Balvanera, Plant diversity enhances provision of ecosystem services: A new synthesis. Basic and Applied Ecology. 11, 582–593 (2010).

2. F. Chen, W. Dong, J. Zhang, X. Guo, J. Chen, Z. Wang, Z. Lin, H. Tang, L. Zhang, The Sequenced Angiosperm Genomes and Genome Databases. Front. Plant Sci. 0 (2018), doi:10.3389/fpls.2018.00418.

3. E. M. Engstrom, C. M. Andersen, J. Gumulak-Smith, J. Hu, E. Orlova, R. Sozzani, J. L. Bowman, Arabidopsis Homologs of the Petunia HAIRY MERISTEM Gene Are Required for Maintenance of Shoot and Root Indeterminacy. Plant Physiology. 155, 735–750 (2011).

4. K. F. X. Mayer, H. Schoof, A. Haecker, M. Lenhard, G. Jürgens, T. Laux, Role of WUSCHEL in Regulating Stem Cell Fate in the Arabidopsis Shoot Meristem. Cell. 95, 805–815 (1998).

5. W. Busch, A. Miotk, F. D. Ariel, Z. Zhao, J. Forner, G. Daum, T. Suzaki, C. Schuster, S. J. Schultheiss, A. Leibfried, S. Haubeiß, N. Ha, R. L. Chan, J. U. Lohmann, Transcriptional Control of a Plant Stem Cell Niche. Developmental Cell. 18, 841–853 (2010).

6. M. Perales, K. Rodriguez, S. Snipes, R. K. Yadav, M. Diaz-Mendoza, G. V. Reddy, Threshold-dependent transcriptional discrimination underlies stem cell homeostasis. Proceedings of the National Academy of Sciences. 113, E6298–E6306 (2016).

7. K. Rodriguez, M. Perales, S. Snipes, R. K. Yadav, M. Diaz-Mendoza, G. V. Reddy, DNA-dependent homodimerization, sub-cellular partitioning, and protein destabilization control WUSCHEL levels and spatial patterning. Proceedings of the National Academy of Sciences. 113, E6307–E6315 (2016).

8. R. K. Yadav, M. Perales, J. Gruel, T. Girke, H. Jönsson, G. V. Reddy, WUSCHEL protein movement mediates stem cell homeostasis in the Arabidopsis shoot apex. Genes Dev. 25, 2025–2030 (2011).

9. S. V. Nikolaev, A. V. Penenko, V. V. Lavreha, E. D. Mjolsness, N. A. Kolchanov, A model study of the role of proteins CLV1, CLV2, CLV3, and WUS in regulation of the structure of the shoot apical meristem. Russ J Dev Biol. 38, 383–388 (2007).

10. A. Plong, K. Rodriguez, M. Alber, W. Chen, G. V. Reddy, CLAVATA3 mediated simultaneous control of transcriptional and post-translational processes provides robustness to the WUSCHEL gradient. Nat Commun. 12, 6361 (2021).

11. D. A. Pearlman, D. A. Case, J. W. Caldwell, W. S. Ross, T. E. Cheatham, S. DeBolt, D. Ferguson, G. Seibel, P. Kollman, AMBER, a package of computer programs for applying molecular mechanics, normal mode analysis, molecular dynamics and free energy calculations to simulate the structural and energetic properties of molecules. Computer Physics Communications. 91, 1–41 (1995).

12. H. Jönsson, M. Heisler, G. V. Reddy, V. Agrawal, V. Gor, B. E. Shapiro, E. Mjolsness, E. M. Meyerowitz, Modeling the organization of the WUSCHEL expression domain in the shoot apical meristem. Bioinformatics. 21, i232–i240 (2005).

13. J. C. Butcher, A history of Runge-Kutta methods. Applied Numerical Mathematics. 20, 247–260 (1996).

14. C. V. Rao, A. P. Arkin, Stochastic chemical kinetics and the quasi-steady-state assumption: Application to the Gillespie algorithm. J. Chem. Phys. 118, 4999–5010 (2003).

15. C. E. Grant, T. L. Bailey, W. S. Noble, FIMO: scanning for occurrences of a given motif. Bioinformatics. 27, 1017–1018 (2011).

16. A. Krogh, Two methods for improving performance of an HMM application for gene finding. Cent. Biol. Seq. Anal. Phone. 45, 4525 (1997).

Chapter 1: Concentration-dependent transcriptional switching through a collective action of cis-elements

Abstract

Gene expression specificity of homeobox transcription factors has remained paradoxical. WUSCHEL activates and represses *CLAVATA3* transcription at lower and higher concentrations, respectively. We use computational modeling and experimental analysis to investigate the properties of the cis-regulatory module. We find that intrinsically each cis-element can only activate *CLAVATA3* at a higher WUSCHEL concentration. However, together, they repress *CLAVATA3* at higher WUSCHEL and activate only at lower WUSCHEL, showing that the concentration-dependent interactions among cis-elements regulate both activation and repression. Biochemical experiments show that two adjacent functional cis-elements bind WUSCHEL with higher affinity and dimerize at relatively lower levels. Moreover, increasing the distance between cis-elements prolongs WUSCHEL monomer binding window, resulting in higher *CLAVATA3* activation. Our work showing a constellation of optimally spaced cis-elements of defined affinities determining activation and repression thresholds in regulating *CLAVATA3* transcription provides a previously unknown mechanism of cofactor-independent regulation of transcription factor binding in mediating gene expression specificity.

Introduction

Spatiotemporal regulation of gene expression is critical for specifying different cell types during development (1–3). Eukaryotic gene regulation involves interactions among DNA sequences and proteins, many of which are transcription factors (TFs). Enhancers, the DNA sequences that bind a given TF or multiple TFs, can regulate transcription irrespective of their location in the gene (1, 3, 4). Since a given class of TFs binds similar

DNA sequences, how they achieve gene expression specificity has been the subject of intense investigation. One of the possible mechanisms to achieve specificity is the binding of cofactors that may unmask latent binding specificity of TFs as shown in the case of homeobox-mediated regulation in anterior-posterior body patterning in *Drosophila melanogaster* (5). Another mechanism involves the utilization of the cis-regulatory modules (CRMs), a subset of enhancers that contain cis-elements for one or more TFs, which have been shown to determine the expression of neighboring genes in a variety of organisms (4, 6–9). In general, the CRMs can be classified into homotypic, where they bind a given type of TF, or heterotypic, where they bind different TFs (10, 11). The heterotypic CRMs largely have been thought to mediate spatiotemporal regulation of gene expression through their ability to recruit different collections of TFs in space and time (10, 12, 13).

Both the homotypic and heterotypic CRMs have been shown to regulate spatiotemporal gene expression patterns in response to TF gradients. The earliest examples of homotypic CRMs have been described in the promoters of genes activated by the TFs that accumulate in a graded manner during early embryonic development in *Drosophila* (14–17). Classically, the French flag model proposed by Wolpert has been applied to explain the expression of genes by TF gradients. According to this model, the target gene expression is highest in places of the highest concentration of the TF (18). Analysis of multiple CRMs has identified three recurring properties: cis-element number, affinity, and cooperativity, which determine gene expression (16). Essentially, decreasing any of the three CRM properties reduces the mean expression while increasing any of the properties leads to overexpression (15, 16, 19, 20).

In *Arabidopsis* shoot apical meristems (SAMs), WUSCHEL (WUS) is a homeodomain TF expressed in the rib meristem (RM) (21, 22). WUS protein migrates into the overlying central zone (CZ), where it promotes stem cell fate by repressing differentiation and also activates its own negative regulator—*CLAVATA3* (*CLV3*) (23, 24) (Fig. 1.1, A to C). CLV3 encodes a secreted peptide that activates a receptor kinase pathway to restrict *WUS* expression (25, 26). WUS has also been shown to bind to the promoters of key differentiation-promoting TFs to repress transcription (27). How the same TF activates some genes, such as *CLV3*, and represses other genes in the same cells is largely unknown. However, a recent study has provided some clues to this regulation. Perales *et al*. (24) showed that WUS binds a CRM, a collection of five closely spaced cis-elements, in the *CLV3* enhancer region (Fig. 1.1D). The incremental deletion of cis-elements led to down-regulation of *CLV3* in the outer layers of the CZ and misexpression in the inner layers of the RM, suggesting that same cis-elements mediate activation and repression of *CLV3* at lower and higher WUS, respectively. Biochemical analysis revealed that WUS binds cis-elements as monomers at lower WUS concentrations and binds as dimers/multimers with increasing WUS concentrations, suggesting that dimerization/multimerization of WUS at higher levels may repress *CLV3* (Fig. 1.1E). The biochemical analysis also revealed that DNA promotes homodimerization (28, 29). Furthermore, increasing the affinity of one of the cis-elements decreased the dimerization threshold and led to the repression of *CLV3* in the CZ, supporting the hypothesis of affinity-based concentration-dependent activation-repression of transcription in maintaining *CLV3* expression over a window of WUS levels. This concentration-dependent switching of *CLV3* transcription is unique among the homotypic CRMs studied and forms an exception to the French flag model.

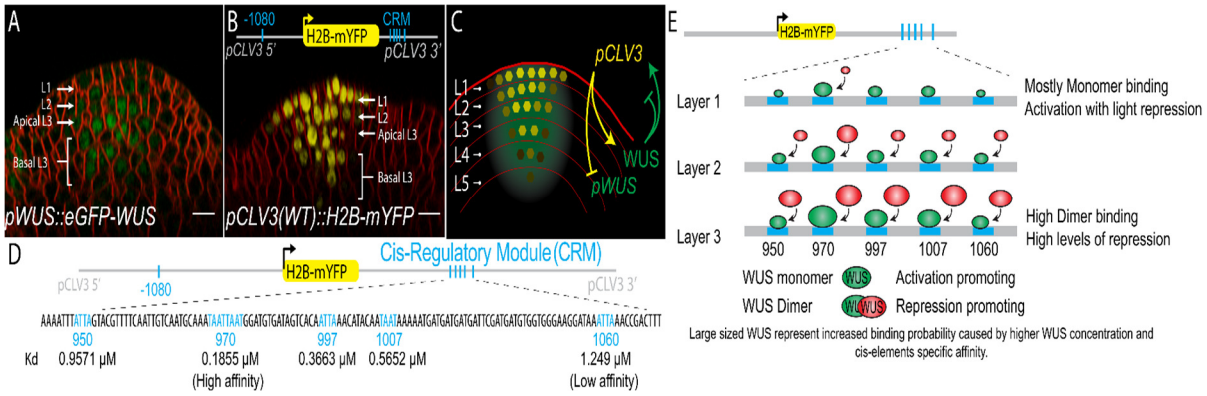

Fig. 1.1. CRM required for *CLV3* activation and repression.
Side views of wild-type (WT) meristems with the WUS protein reporter *pWUS::eGFP-WUS* **(A)** and CLV3 transcriptional reporter containing all five WT cis-elements within the 3′ CRM *pCLV3(WT)::H2B-mYFP* **(B).** Scale bars, 10 μm. **(C)** Side view of a SAM cartoon showing WUS protein distribution (green) and CLV3 (yellow), which form a regulatory feedback loop across cell layers. The *CLV3* CRM, a cluster of WUS binding cis-elements, interacts with the WUS concentration to repress and activate *CLV3*. CLV3 signals to WUS at both the posttranslational level, enriching the WUS protein, and the transcriptional level, repressing *WUS* expression. **(D)** Schematic of the *CLV3* gene including the location and K_d of WUS binding TAAT cis-elements (cyan) of the *CLV3* CRM. **(E)** Schematic of WUS monomer and dimer binding to the *CLV3* cis-elements depending on the WUS concentration gradient (across SAM cell layers) and the relative affinities of cis-elements.

Understanding how the concentration-dependent transcriptional switch is established requires understanding how the *CLV3* CRM functions as a unit. The complexity of the *CLV3* CRM regulation involving five cis-elements and the bidirectional relationship between *CLV3* and WUS can be challenging to untangle experimentally. The current experimental limitations cannot provide a direct real-time view of the actual WUS/*CLV3* molecular dynamics under precisely defined conditions. A multiscale computational model capable of simulating the binding and unbinding dynamics of WUS to all five cis-elements and *CLV3* transcription at the tissue level can be helpful in providing mechanistic insights into the WUS concentration–dependent functioning of the *CLV3* CRM.

Different approaches have been developed for studying TF binding dynamics. The thermodynamic models are usually based on the occupancy of the promoter by the TFs, the statistical weights of possible configurations, and the free energy (30–34). However, when multiple cis-elements with different affinities and their interactions are involved as observed in *CLV3* CRM, the number of possible configurations becomes large and it is not practical to use the thermodynamic approach. Instead, the stochastic simulation algorithm, i.e., Gillespie algorithm where the dynamics of WUS binding and unbinding to the cis-elements can be modeled as a series of probabilistic events occurring at random time steps determined, is ideal to explicitly model *CLV3* transcription.

We developed a stochastic model to simulate the WUS binding to the CRM in a single cell. The single-cell model was applied to simulate WUS binding cis-elements under different concentrations and compared the simulation output with the experimental data on tissue-level expression patterns of different cis-element mutants of *CLV3* to investigate the roles of WUS binding affinity, distance-dependent cooperativity among cis-elements, and RNA polymerase II (Pol II) recruitment in the transcription process. Subsequently the single-cell stochastic model was applied to multiple cells represented by unit spheres to develop a cell-based three-dimensional (3D) model representing the SAM. The 3D model was applied to further test the mechanisms identified in the single-cell model in generating the spatial patterns of *CLV3* expression.

Using a WUS gradient consistent with the experimental data, both computational models suggested a role for residence time limit (see Results for details) of WUS monomer binding to the individual cis-elements of different affinities, which have been shown to activate *CLV3* largely to a similar extent when acting alone. Beyond residence time limit, the aged WUS monomers fail to activate transcription and they are replaced with newly

synthesized WUS monomers to sustain *CLV3* activation. Our experimental observations showing a correlation between higher WUS turnover and increased *CLV3* activation support such a mechanism. When multiple cis-elements are involved, we found that the cooperative binding of WUS monomers and dimers is required to achieve correct *CLV3* activation patterns. The model simulations also suggested a nonhomogeneous cooperativity among cis-elements that depends on the intervening distance between cis-elements. The model prediction on distance-dependent cooperativity was tested in experiments by increasing the intervening distance between cis-elements, which revealed an increase in *CLV3* activation. The corresponding biochemical experiments revealed that an increase in intervening distance between cis-elements increased their affinity to WUS monomers but did not alter the concentration at which WUS monomers switch to form stable dimers/higher molecular weight complexes. These results show the importance of optimal spacing between cis-elements in determining the concentration range over which an appropriate number of WUS monomers and dimers populate on cis-elements in setting up the activation-repression thresholds. The 3D model that incorporates multiple cis-elements of different affinities that are spaced optimally allowed independent manipulation of the monomer and dimer cooperativity. Our simulations revealed that monomer cooperativity was critical for expression of *CLV3* at the lower WUS concentration, while the dimer cooperativity was critical for repression at the higher WUS concentration. Moreover, a balance of the monomer and dimer cooperativity levels was critical to achieve the wild-type *CLV3* expression at a WUS concentration range observed in experiments.

Results

Affinity and collective activity of multiple cis-elements determine *CLV3* expression

Incremental mutations of cis-elements within the CRM result in incremental down-regulation of *CLV3* expression in outer cell layers of the CZ and up-regulation in the inner cell layers of the RM, suggesting interaction among cis-elements (24). To understand the collective behavior of cis-elements, we first deduced the contribution of each cis-element within the CRM to the regulation of *CLV3* by analyzing the loss of binding mutations in each of the five cis-elements. Single loss of binding mutations in high-affinity cis-element 970 (Fig. 1.1D) led to drastic down-regulation in the outer layers of CZ (Fig. 1.2, A and B). On the other hand, independent loss of binding mutations in the four lower-affinity cis-elements led to a minor down-regulation in the L1 layer (Fig. 1.2, A and C). These results show that all five elements contribute to the *CLV3* expression, with the highest-affinity cis-element contributing maximally over the lower-affinity cis-elements *CLV3*. Moreover, our previous work shows that increasing the affinity of 970 cis-element alone down-regulated *CLV3* expression, revealing the critical role of affinity of cis-elements in regulating the *CLV3* expression (Fig. 1.2, A and D). These results suggest that each cis-element contributes to *CLV3* expression and their affinities are critical to achieving proper spatial regulation.

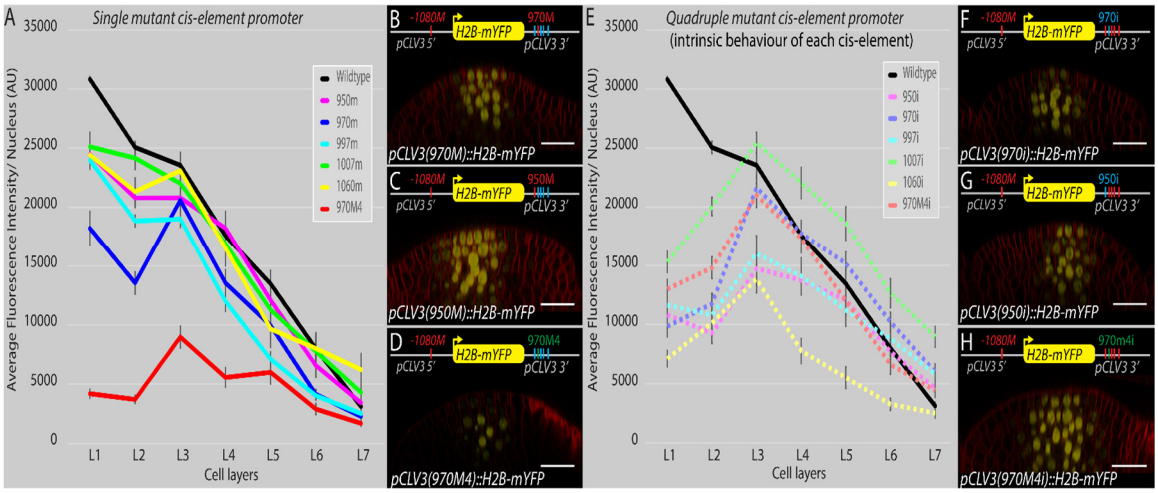

Fig. 1.2. The number of cis-elements and affinity influences the collective behavior of the CRM in regulating *CLV3* activation and repression.
Average fluorescence levels (mean ± SE) of H2B-mYFP in different cell layers of various *pCLV3::H2b-mYFP* promoter variants carrying a mutation in single cis-elements of the 3′ CRM **(A)**. AU, arbitrary unit. **(B to D)** Side views of WT meristems showing various mutant *pCLV3::H2B-mYFP* reporter expression patterns. Single cis-element mutants 970M **(B)** and 950M **(C)** and a higher-affinity mutant 970M4 **(D)**. Average fluorescence levels (mean ± SE) of H2B-mYFP in different cell layers of various *pCLV3::H2b-mYFP* promoter variants carrying mutations in four of the five cis-element mutants (quadruple mutants) **(E).** Side views of WT meristems showing various mutant *pCLV3::H2B-mYFP* reporter expression patterns. Quadruple mutant (mutants 950M, 997M, 1007M, and 1060M) referred to as 970 intrinsic (970i) **(F)**, (mutants 970M, 997M, 1007M, and 1060M) referred to as 950 intrinsic (950i) (**G**), and (mutants 950M, 997M, 1007M, and 1060M) referred to as 970M4 intrinsic (970M4i) (**H**). All cis-element mutations within the CRM in the 3′ region were generated in the mutant-1080 cis-element background. In all images, scale bars = 20 μm. **(A and E)** The error bars represent the SE (in all cases, *n* = 4 represents independent transformants).

Single cis-elements can only activate *CLV3* at a higher WUS level

The subtle changes observed upon mutating individual lower-affinity cis-elements ruled out a simple additive interaction in regulating *CLV3* expression. Therefore, to further understand the nature of interactions among cis-elements, we first determined the contribution of each one of the five cis-elements to *CLV3* expression, referred to as the intrinsic (i) behavior. We generated a library of five mutant *CLV3* reporters; each contained only one functional cis-element referred to as 970i, 997i, 1007i, 950i, and 1060i. The reporter expression analysis revealed a marked down-regulation of *CLV3*

expression in outer cell layers of CZ, including the higher-affinity cis-element 970i (Fig. 1.2, E and F). To test further the importance of affinities in influencing intrinsic behavior, we analyzed the expression of 970M4i (Fig. 1.2, E and H). The 970M4 cis-element is a mutation in 970 that binds WUS with three times higher affinity, and it has been shown to repress *CLV3* expression even at lower WUS in outer cell layers of CZ (*24*). The 970M4i reporter (Fig. 1.2, E and H) was expressed at a notably higher level than 970M4 (Fig. 1.2, A and D). To further test whether the reactivation of *CLV3* associated with 970M4i is functionally relevant, we examined its ability to complement *clv3-2* null mutants by expressing *CLV3* genomic version. The 970M4 mutants partially complement the SAM and the floral meristem (FM) phenotypes when compared to the wild-type *CLV3* promoter (Fig. 1.3). However, 970M4i was able to significantly better complement both the SAM and FM phenotypes, showing the reactivation of 970M4i (Fig. 1.3, F and L). Furthermore, both 970i (Fig. 1.3, E and K) and 970M4i (Fig. 1.3, F and L) complemented *clv3-2* to a similar extent despite binding WUS with different affinities. Consistent with this conclusion, all single cis-elements irrespective of large differences in their WUS binding affinities largely activated *CLV3* only in the inner layers of RM, where WUS accumulates at a higher level. However, cis-element affinity is important in the context of other functioning cis-elements in the CRM, as exemplified by the repression of 970M4. In summary, the affinity-dependent collective WUS binding to all five cis-elements is required for balancing activation and repression of transcription in regulating the spatial expression and levels of *CLV3*.

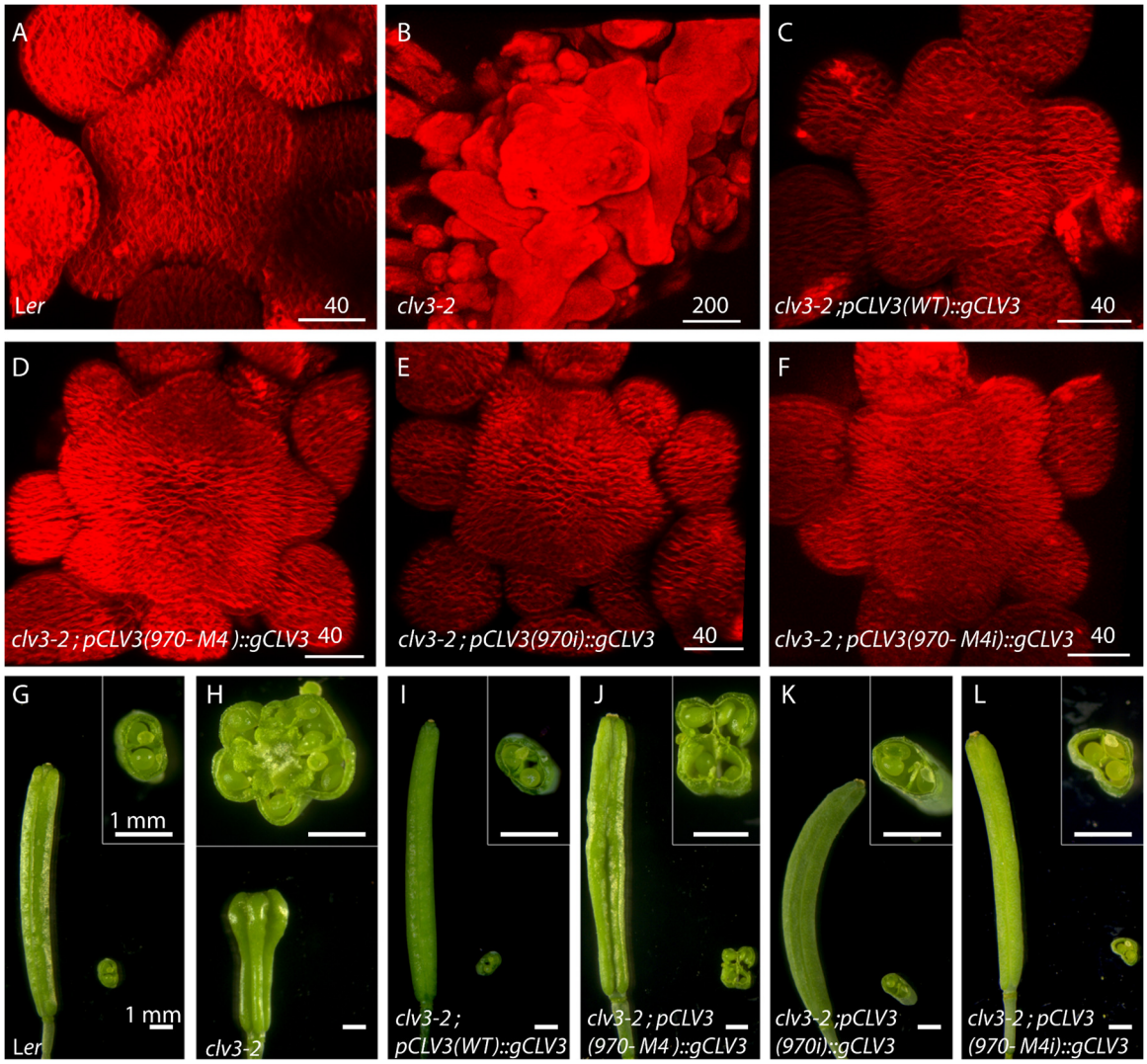

Fig. 1.3. Functional analysis reveals the importance of the collective behavior of the *CLV3* CRM. **(A to F)** Top views of 3D-reconstructed SAMs stained with plasma membrane dye FM4-64 (red). WT **(A)**, *clv3-2* **(B)**, and *clv3-2* complemented with WT genomic *CLV3* (*gCLV3*) expressed from the WT *CLV3* promoter [*pCLV3(WT)::gCLV3;clv3-2*] **(C)**, *CLV3* promoter carrying high-affinity 970M4 cis-element [*pCLV3(970M4)::gCLV3;clv3-2*] (D), CLV3 promoter carrying loss of binding mutation in 950, 997,1007, and 1060 [*pCLV3(970i)::gCLV3;clv3-2*] **(E)**, and *CLV3* promoter carrying high-affinity mutation 970M4 and loss of binding mutations in 950, 997, 1007, and 1060 [*pCLV3(970M4i)::gCLV3;clv3-2*] **(F)**. (**G** to **L**) Side views of intact siliques and cross section of sliced siliques. Insets show a higher-magnification view of the cross section of the sliced siliques. WT **(G)**, *clv3-2* **(H)**, and [*pCLV3(WT)::gCLV3;clv3-2*] **(I)**, [*pCLV3(970M4)::gCLV3;clv3-2*] **(J)**, [*pCLV3(970i)::gCLV3;clv3-2*] **(K)**, and [*pCLV3(970M4i)::gCLV3;clv3-2*] **(L)**. Scale bars (in micrometers) are given on individual panels in **(A)** to **(F)**, and the scale bars in **(G)** to **(L)** are 1 mm.

Description of a stochastic single-cell model of *CLV3* transcription

To investigate the mechanisms of interaction among five cis-elements, we developed a stochastic modeling framework to simulate the WUS binding to the *CLV3* CRM in a single cell, together with the RNA Pol II recruitment and *CLV3* mRNA synthesis (Fig. 1.4A). The model was applied to understand the mechanisms underlying the *CLV3* activation by the individual cis-elements that bind WUS with different affinities and the interactions among multiple cis-elements in regulating the *CLV3* expression together. The stochasticity was introduced by implementing the Gillespie algorithm (35) to simulate all possible WUS binding and unbinding events to form a monomer or dimer and recruitment of Pol II for activating *CLV3* transcription. A sufficiently long time was allowed for all the simulations to reach the steady state. The *CLV3* reporter analysis performed in the wild-type background uses a steady-state WUS gradient to quantify the effects of the number, affinity, and intervening distance between cis-elements on *CLV3* expression. Since the focus of this study is to analyze concentration-dependent binding of WUS to the *CLV3* CRM, the feedback regulation of CLV3 on WUS was disabled to maintain a constant WUS concentration gradient throughout simulations to match the reporter analysis. It was also assumed that WUS binding the *CLV3* CRM alone would not change the overall WUS concentration. The stochastic time step and index for the next occurring event were generated by following the original Gillespie algorithm based on the assumption that binding to one cis-element was independent of the other cis-elements unless cooperativity among cis-elements exists. The average amount of *CLV3* mRNA synthesized, at a fixed WUS concentration, from multiple simulations was

calculated. The model was then applied to measure the total amount of *CLV3* mRNA synthesized at different WUS concentrations.

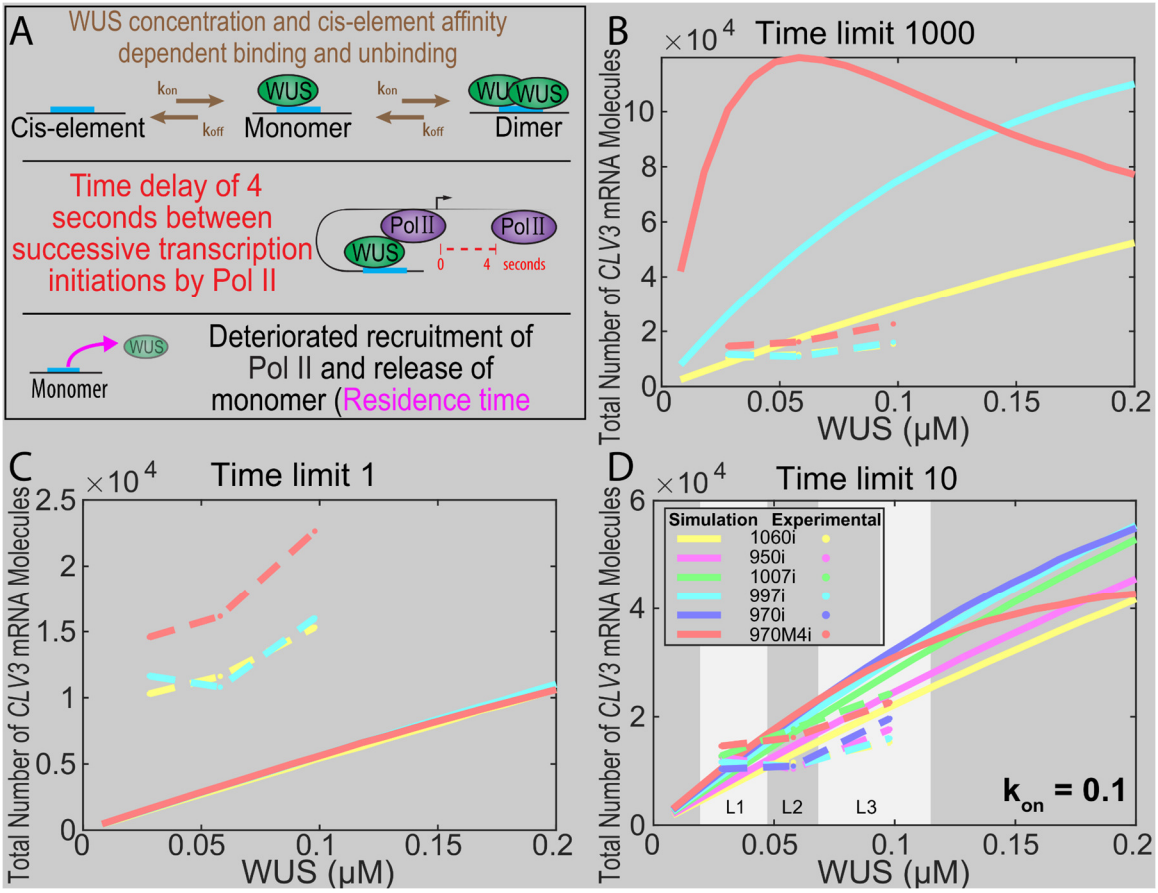

Fig. 1.4. WUS protein time limit on cis-elements determines the *CLV3* levels and domain of expression.
(**A**) WUS concentration–dependent binding [k_{on}WUS], k_{on} is the association rate, and cis-element affinity–dependent unbinding [$k_{off} = K_d k_{on}$] determine three possible WUS occupancy states: unbound (zero WUS), monomer bound (one WUS), and dimer bound (two WUS). We assume that only the monomer bound is able to recruit RNA Pol II. A 4-s gap between recruitment of successive Pol II molecules was estimated from the Pol II elongation rate and the size of Pol II footprint on the DNA. In addition, multiple rounds of Pol II recruitment by WUS monomer deteriorate the ability of WUS to recruit additional Pol II (residence time limit). (**B** to **D**) Single-cell model of WUS-mediated activation of *CLV3* from single cis-element promoters (four mutated and only one functional cis-element). **(B to D)** Scaled simulation results of highest-affinity (970M4i), intermediate-affinity (997i), and lowest-affinity (1060i) cis-elements with the residence time limit of 1000 s (similar expression pattern as without the time limit since the time limit is extremely large) **(B)**, 1 s **(C)**, or 10 s **(D)**. **(D)** All five cis-elements in addition to 970M4i and approximate WUS concentration range to reflect the corresponding WUS fold changes from L1, L2, and L3 layers.

Modeling WUS binding to the CRM

Our previous analysis revealed that each cis-element binds WUS at different concentrations as monomers first and then switches to forming dimers at increasing concentrations (24). Therefore, we first aimed to determine the binding and unbinding probabilities associated with each cis-element by reproducing the ratio of monomer- and dimer-bound cis-elements observed in electrophoretic mobility shift assay (EMSA) experiments (24). Since increasing the TF concentration decreases the search time of its binding to cis-elements (36), it was assumed that the probability of WUS binding to cis-elements increases with the increase in WUS concentration. In particular, the propensity of WUS binding to an empty cis-element or with a monomer is assumed to depend linearly on WUS concentration, i.e.,k_{on}^{M}[WUS], where k_{on}^{M} is the binding rate. Then, the unbinding propensity k_{off}^{M} of WUS associated with each cis-element is calculated as $k_{off}^{M} = K_d^M k_{on}^{M}$, where K_d^M, the dissociation constant, was quantified in our previous work (24). To test this assumption, we considered a wide range of WUS concentration that encompasses WUS monomer and dimer binding to each one of the five cis-elements observed in EMSA experiments (24). We first simulated WUS monomer binding to a single cis-element to determine k_{on}^{M}, a free parameter, such that proportions of bound monomers obtained in the model were similar to those observed in the EMSA experiments with WUS that lacked the C-terminal homodimerization domain (HOD). Since dimerization occurs through sequential recruitment of WUS to the WUS monomer-DNA complex, we next modeled the dimer formation by recruiting the second WUS molecule to a monomer. In the absence of the experimental values on binding affinity associated with the WUS dimerization, we chose K_d^D associated with the binding of the second WUS molecule to be the same as the one used to simulate monomer K_d^M. We

chose k_{on}^{D} for dimer binding such that proportions of monomer and dimer bound to the cis-elements matched the EMSA experiments with full-length WUS (24).

Modeling *CLV3* transcription

We considered the recruitment of Pol II as another stochastic event in the model. It has been shown that the transition from monomer binding to dimer binding could be correlated to the transcriptional switch from activation to repression of *CLV3*. Therefore, we assumed that monomer binding recruits Pol II to activate *CLV3* transcription, while the WUS dimers fail to recruit Pol II and activate *CLV3* transcription. We introduced a time delay between two successive Pol II recruitment events due to the size of the Pol II complex occupying the transcription start site. The time delay calculated based on an 80–base pair (bp) footprint of RNA polymerase and mRNA elongation rate, which is estimated to be 1.2 kb/min (37), was approximated as $80\ bp\ \times \frac{60s}{1200\ bp} = \ 4\ s$,It is also assumed that, after transcription initiation, the WUS monomer can unbind or bind another WUS molecule to form a dimer. Moreover, we considered the Pol II recruitment rate as an uncalibrated parameter and carried out perturbations to examine its effect on the transcriptional output. The model was calibrated over a wide range of WUS concentrations. We then applied the model to simulate WUS binding/unbinding to a single cis-element and Pol II recruitment to generate the intrinsic expression of *CLV3* at different WUS concentrations. By comparing the *CLV3* mRNA production with the experimental quantification of the *CLV3* expression in Fig. 1.2 (E to H), an optimal scale of WUS concentrations was obtained to capture the WUS gradient in different cell layers of the SAM. This optimal WUS concentration scale was used in all single-cell simulations

to investigate possible mechanisms controlling the intrinsic behavior of each cis-element in regulating the *CLV3* expression.

Mechanisms of the intrinsic behaviors of cis-elements in regulating *CLV3*

It has been observed that the transcriptional output depends on the affinity of cis-elements and the TF concentration (30, 32, 38–45). In general, a higher-affinity cis-element results in a longer TF occupancy than the lower-affinity cis-element at a given WUS concentration. Consequently, a longer TF occupancy leads to a higher mRNA production (46). Experiments reveal that WUS binds to 970M4i with approximately 21.4 times higher affinity than to the lowest-affinity cis-element 1060i. Therefore, a longer residence time of WUS on 970M4i was expected to produce much higher levels of *CLV3* than 1060i. However, our experiments revealed that, although five cis-elements bound WUS with different affinities, intrinsically (950i, 970i, 997i, 1007i, and 1060i mutants), they were able to similarly activate *CLV3* only in inner cell layers of RM where the WUS concentration is higher (Fig. 1.2, E to H). The initial attempt in modeling by assuming WUS occupancy based on affinities produced distinct *CLV3* expression patterns for the highest 970M4i cis-element and the lowest 1060i cis-element (Fig. 1.4B). 970M4i produced a much sharper increase in *CLV3* expression at the lower WUS concentration than did 1060i. With the increase in WUS concentration, 970M4i produced a lower amount of *CLV3* mRNA, which is expected because of the WUS dimerization, while 1060i continued to yield higher *CLV3* mRNA (Fig. 1.4B). Such markedly different *CLV3* expression patterns produced by 970M4i and 1060i were not consistent with experimental observations, suggesting that additional mechanisms may regulate the intrinsic activation behavior of cis-elements in addition to their affinities.

It has been noticed that for different types of TFs, including general control TF (GCN4) in yeast (47) and transcriptional coactivator NPR1 involved in systemic acquired resistance (SAR) in *Arabidopsis* (48), a higher turnover of TFs leads to a higher transcriptional activation. Furthermore, the transcriptional activation domains of GCN4 and other TFs have been shown to overlap with degradation domains, suggesting a possible correlation between transcriptional activation and TF turnover (47, 49). Moreover, transcription-dependent degradation has been shown for sterol regulatory element–binding protein (SREBP) family of TFs (50). These observations suggest that TFs when actively transcribing may get progressively modified (for example, phosphorylated) and become transcriptionally ineffective and marked for their degradation (47, 49). Although deep mechanistic links between WUS, protein phosphorylation, and protein destabilization machinery are still unknown, our earlier work suggests similarities between WUS and TFs described above. (i) The transcriptional regulatory domains [WUS-box and EAR-like (ethylene-responsive element binding factor associated amphiphilic repression) domains] function as degrons (51, 52). (ii) *CLV3* activated at the lower WUS concentration in the CZ can be repressed by enriching and stabilizing the WUS protein in the nucleus (24, 51). (iii) The dexamethasone (Dex)–mediated nuclear translocation of WUS by using the 35S::eGFP-WUS-GR system led to an immediate destabilization of the protein in the CZ within 6 hours (53). By 24 hours of Dex application, the protein was only detected in the nuclei of cells in the edge of the peripheral zone (PZ) and deeper cell layers of the RM. The *CLV3* activation and expansion into the PZ followed the centripetal pattern of rapid destabilization of the WUS protein [Fig. 1.5; (53)].

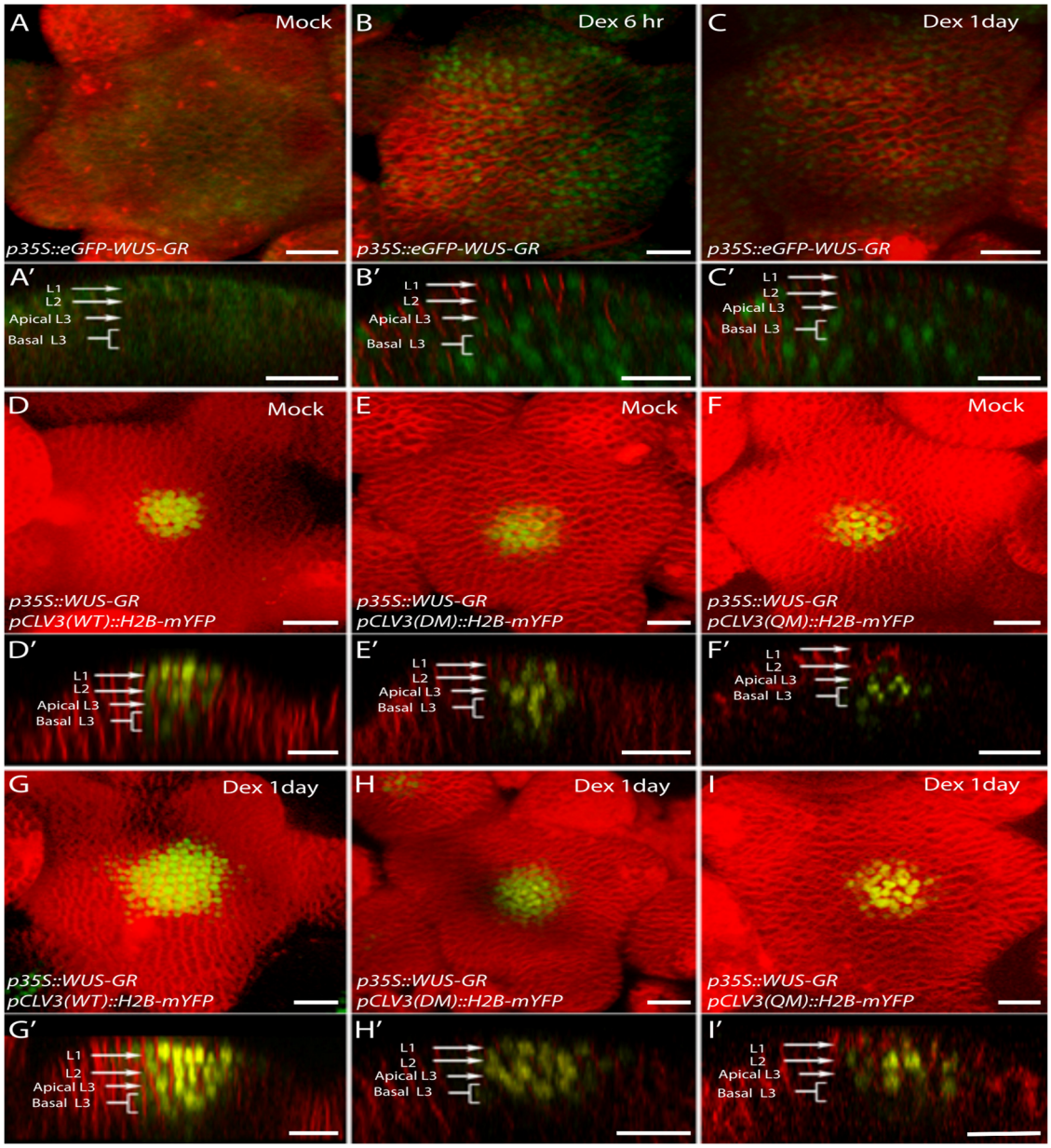

Fig. 1.5. The number of cis-elements determines the sensitivity of *CLV3* promoter to the dynamic changes in the WUS protein accumulation.
(**A to C**) SAMs showing WUS protein accumulation patterns (*p35S::eGFP-WUS-GR*) upon its Dex-induced nuclear translocation at 6 hours **(B)**, at 24 hours **(C)**, and upon mock treatment **(A)**. (**D** to **I**) *p35S::WUS-GR*–expressing SAMs showing *pCLV3::H2B-mYFP* reporter expression of WT *CLV3* promoter **(D)**, the double mutant promoter (970 and 997 mutants) **(E)**, and the quadruple mutant promoter (970, 997, 950, and 1060 mutants) **(F)** upon mock treatment. The *pCLV3* reporter expression of the corresponding genotypes after 24-hour Dex treatment is shown in **(G)** to **(I)**. **(A to I)** Three-dimensional reconstructed top views of SAMs and corresponding side views shown in **(A′)** to **(I′)**. Plasma membrane stain–FM4-64 (red), eGFP-WUS-GR (green), and H2B-mYFP (yellow). Scale bars, 20 μm.

Perhaps degradation of WUS decreases the dimer concentration or creates a dynamic WUS that works favorably with the Pol II binding limit to increase *CLV3* activation. Therefore, we considered an upper limit on the residence time of WUS beyond which WUS becomes inactive and fails to recruit Pol II, referred to as residence time limit in the model (Fig. 1.4A). The older/inactive WUS species need to be replaced with newly synthesized WUS monomers to maintain transcription. Therefore, we imposed the same WUS monomer residence time limit for all cis-elements. A markedly lower WUS monomer residence time limit substantially decreased *CLV3* expression for all cis-elements (Fig. 1.4C). Simulations with a balanced residence time limit were able to generate a similar intrinsic expression pattern of *CLV3* for all cis-elements. In particular, to generate similar expression patterns of 970M4i (highest affinity) and 1060i (lowest affinity) cis-elements, we chose the residence time limit to be 10 for all simulations involving multiple cis-elements discussed in the following sections (Fig. 1.4, B to D).

The *CLV3* CRM composition determines sensitivity to dynamic changes in WUS protein levels

The number of cis-elements may also determine the sensitivity of the *CLV3* promoter to WUS levels to regulate spatial expression of *CLV3*. To test this, we analyzed the response of the mutant promoters lacking several WUS binding cis-elements to *35S::eGFP-WUS-GR* system, upon 24 hours of Dex application, described in the previous section. The wild-type *CLV3* promoter with five functional cis-elements expressed at high levels and the promoter activity expanded into the PZ (Fig. 1.5, D and G). The mutant promoter lacking the two functional WUS binding cis-elements (970M and 997M)-*pCLV3(DM)::H2b-mYFP* is initially expressed in the deeper cell layers, and

the expression levels are below that of the wild-type promoter (Fig. 1.5E). The 24-hour Dex application was able to activate *pCLV3(DM)* in the CZ weakly but failed to expand into the PZ (Fig. 1.5H) (*n* = 8) when compared to the wild-type promoter, which revealed strong activation and radial expansion (Fig. 1.5G). The mutant promoter lacking four cis-elements (950M, 970M, 997M, and 1060M)-*pCLV3(QM)::H2b-mYFP* was expressed only in the deeper layers (Fig. 1.5F). After 24 hours of Dex application, the mutant promoter was mildly up-regulated in deeper layers; however, it failed to activate in the CZ and expand radially into the PZ (Fig. 1.5I). Together, rapid destabilization of WUS can lead to higher *CLV3* activation, which is maintained even at undetectable WUS protein levels, showing that all five cis-elements working together increase the sensitivity of *CLV3*.

Cooperativity among cis-elements regulates *CLV3* expression

Our experimental analysis showing different expression patterns of *CLV3* for single cis-elements and multiple cis-elements suggested an interaction among cis-elements within the CRM (24). The same study also showed that an increase in cis-element affinity (970M4) resulted in a decrease in dimerization threshold and repressed *CLV3* in outer cell layers of CZ where WUS accumulates at a lower level. These observations suggested that cis-element affinity is important in the context of the multiple cis-elements, possibly in inducing cooperative interactions among WUS dimers bound to multiple cis-elements within the CRM. To understand the multiple cis-element behaviors, we used the calibrated single-cell WUS binding model by extending it to include multiple cis-elements. Without any cooperative interactions among them, an increase in WUS concentration led to an increase in *CLV3* expression, which can be interpreted as a

linear combination of intrinsic behaviors of individual cis-elements, which is not consistent with the experimental analysis (Fig. 1.6A). Therefore, we introduced cooperativity among cis-elements into the model. First, we considered equal cooperativity among all cis-elements irrespective of the intervening distance. As the cooperativity increased, the *CLV3* expression decreased at the higher WUS concentration, which could be due to increased dimerization (Fig. 1.6B). Then, we chose appropriate values for parameters involved in the dimer cooperativity to obtain the highest activation of *CLV3* at a lower WUS concentration as observed in experiments. Next, we used the calibrated model with the chosen cooperativity parameters to simulate mutant *CLV3* consisting of different number of cis-elements. In particular, our experimental analysis showed a weaker down-regulation of *CLV3* upon mutating any one of the four lower-affinity cis-elements (950M, 997M, 1007M, and 1060M) for the low WUS concentration, compared to the highest affinity, i.e., 970 cis-element (970M) (Fig. 1.2, A to C). However, in the simulations with the calibrated equal dimer cooperativity, 950M was expressed at a much higher level than the wild type at the high WUS concentration (Fig. 1.6C), which was not consistent with the experimental observation, suggesting unequal cooperativity among those cis-elements in the CRM.

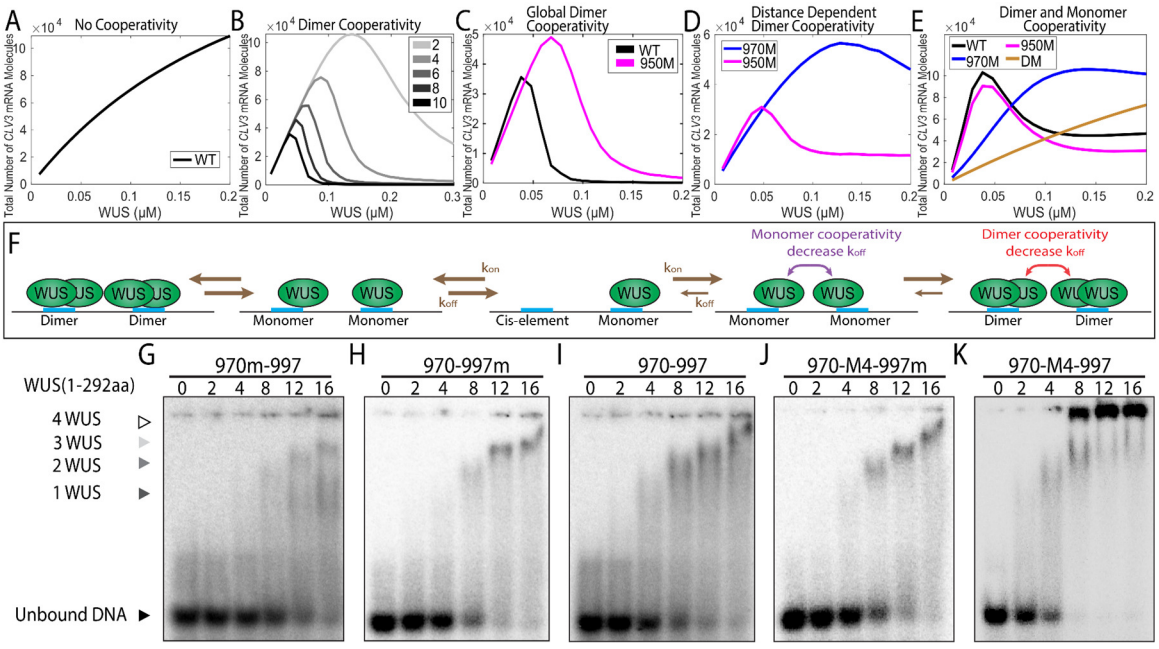

Fig. 1.6. Cooperativity among cis-elements regulates *CLV3* expression.
Average *CLV3* mRNA levels from single-cell simulations in response to WUS concentration without cooperativity **(A)**, at different strengths of dimer cooperativity **(B)**, when dimer cooperativity between every cis-element is considered **(C)**, when the dimer cooperativity depends on the intervening distance between cis-elements **(D)**, and when both WUS monomer and dimer cooperativity were considered **(E)**. **(F)** Binding and unbinding dynamics of WUS monomer and dimer on cis-elements. (**G to K)** Gel shift assay of increasing concentrations of full-length WUS 1 to 292 amino acids (aa)] to probes of similar length that cover the 970 and 997 cis-elements. Probes with loss of binding mutations to the TAAT elements in the 970 cis-element **(G)** and the 997 cis-element **(H)**. **(I)** Probe with WT copies of the 970 and 997 cis-elements. Probes that contain higher-affinity mutant 970M4 along with the mutant 997 **(J)** or WT 997 cis-element **(K)**. **(G to K)** Arrowheads denote higher-order WUS complexes: monomer (dark gray), dimer (light gray), and higher complexes (white). The unbound probe (black).

Next, we introduced unequal dimer cooperativity wherein the interaction between neighboring cis-elements was higher, and cooperativity decreased with increasing intervening distance (referred to as distance-dependent cooperativity). Similar kind of cooperativity was studied in thermodynamic models earlier (54). For simplicity, we simulated 970M and 950M expressions representing mutations in high- and low-affinity cis-elements, respectively. The model with distance-dependent dimer cooperativity was able to generate wild-type expression patterns. However, a similar expression behavior was observed for both 950M and 970M at lower WUS concentrations, which is

inconsistent with the experimental data (Fig. 1.6D). This suggested that the cis-element affinity influences interactions among cis-elements and the higher-affinity cis-element 970 interacts differently than the lower-affinity cis-elements in activating *CLV3* at lower WUS. Therefore, distance-dependent monomer cooperativity between cis-elements was considered. The monomer and dimer cooperativity were considered separately since one is responsible for activation and the other one is responsible for repression. Considering that the affinity plays a role when multiple cis-elements interact, the residence time limit associated with single cis-element was disabled. The additional WUS monomer cooperativity along with the dimer cooperativity between all cis-elements was able to generate expected wild-type and mutant (970M and 950M) cis-element behaviors at all WUS concentrations (Fig. 1.6E), showing the importance of both in regulating *CLV3* transcription.

The neighboring cis-elements influence WUS DNA-protein complex formation

To test predictions of model simulations on the possible cooperative behavior of cis-elements, we performed EMSA with increasing concentration of WUS on probes that contain two adjacent cis-elements. We considered the two adjacent cis-elements 970 and 997 because mutating these two cis-elements has been shown to down-regulate *CLV3* expression in outer cell layers of CZ and up-regulate expression in the inner layers of RM (24). Full-length WUS at lower concentration has been shown to bind as a monomer to single cis-elements, which shifts to a dimeric complex at the higher WUS concentration (24). We found that WUS bound the oligo that contains 970 and 997 cis-elements (Fig. 1.6I) at much lower concentrations than observed with the oligos of the same length that only contains one functional cis-element that is either the 970 (Fig.

1.6H) or 997 cis-element (Fig. 1.6G). In addition, the WUS shifted to form higher molecular weight complexes at much lower concentrations with the two functional cis-elements than one functional cis-element (Fig. 1.6I). To further test the nature of the protein and complex formation across multiple cis-elements, we tested the binding patterns of two WUS protein variants: WUS1-134 that only contained the DNA binding domain and lacked the centrally located HOD, and WUS1-208 that contains the centrally located HOD domain. Our earlier work has shown that these fragments bind cis-elements with comparable affinities to the full-length protein (24). With increasing concentration of WUS1-134, a gradual switch from monomeric to the higher molecular complex was observed, which is expected as previous work has shown that the DNA binding domain also participates in dimerization (24, 29). With WUS1-208, at the same protein concentration range, we observed a faster shift from the monomer form into the higher molecular weight complex. Testing these two protein versions on a probe containing only one functional 970 cis-element revealed higher molecular complex formation at a much higher concentration (24). These results suggest that the second dimerization domain may facilitate interaction between WUS molecules bound to the adjacent cis-elements in promoting higher molecular WUS complex formation.

The distance between cis-elements is critical for *CLV3* expression

The cooperativity observed in gel shift assays suggests that the neighboring cis-elements increase WUS binding, possibly through protein-protein interaction facilitated by the second HOD (HOD2). To test the influence of spacing between cis-elements without reducing the number or affinity, we duplicated the sequence between neighboring cis-elements. The increased distance might reduce the interaction of WUS

bound to neighboring cis-elements without affecting the intrinsic binding to each independent cis-elements. Therefore, we duplicated the intervening sequence between 970-997 and 997-1007 (double space around 997) *pCLV3(DS-997)::H2B-mYFP*. Increasing the distance between neighboring cis-elements led to increased *CLV3* expression in all cell layers, and an increase in the deeper layers was much higher than in the outer cell layers of CZ (Fig. 1.7, A to C). These results suggest that the distance between cis-elements is more critical for the repression of *CLV3*, likely through the formation of large WUS complexes across neighboring cis-elements. To test whether the increased distance between 970 and 997 cis-elements alters the binding dynamics, we analyzed WUS binding to the oligo with duplicated sequences that doubled the distance between 970 and 997 (970--997). The full-length WUS protein could bind the oligo (970--997) at lower WUS (Fig. 1.7, D and E). However, the transition from lower molecular weight complexes to higher molecular weight complexes occurred over a much wider WUS concentration range. Therefore, the increase in *CLV3* expression in all cell layers seen in DS-997 could be explained by the larger WUS concentration range over which it remains as a lower molecular weight complex, showing that, in addition to the affinity of the cis-elements, the intervening distance is important in regulating the *CLV3* expression.

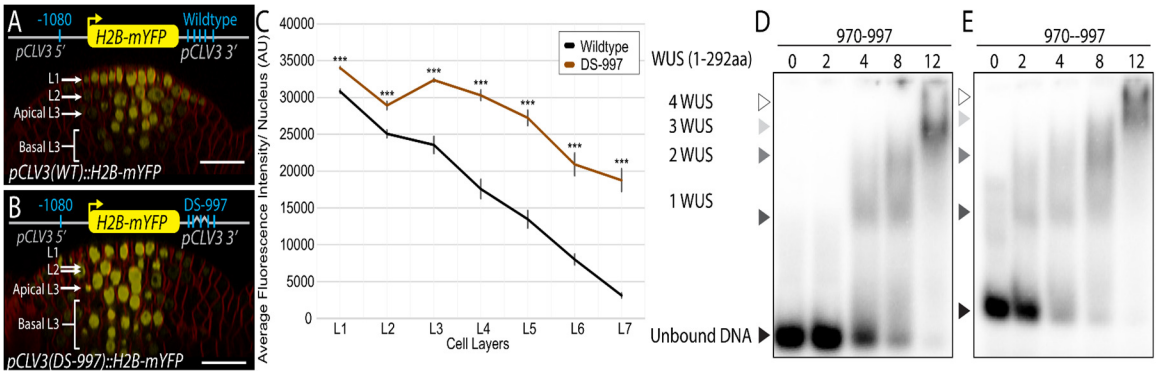

Fig. 1.7. Spacing between cis-elements is critical for *CLV3* repression.
Side view of SAM showing the WT *pCLV3::H2B-mYFP* expression (**A**) and mutant *CLV3* reporter containing duplicated sequence to the left (5′) and right (3′) of the 997 cis-element (double sequence around 997—DS-997) (**B**). Scale bars, 20 μm. (**C**) Average H2B-mYFP fluorescence intensity (mean ± SE) in 10 centrally located nuclei/cell layers quantified from four independent transformants of WT and DS-997 (n = 4). ***P < 0.001. EMSAs showing increasing concentrations of full-length WUS (1 to 292 amino acids) bound to the probe containing the 970 and 997 cis-elements with WT intervening sequence (**D**) or a duplicated intervening sequence (**E**).

Description of a 3D cell–based model of *CLV3* transcription

The single-cell model provided insights into the WUS binding dynamics with individual cis-elements, Pol II recruitment, and minimum cooperativity mechanisms required for *CLV3* expression. However, the single-cell model can only provide average expression behavior at given WUS concentrations, without considering the tissue spatial organization and the stochasticity associated with individual cells within layers of the SAM under a broader range of WUS concentrations. Therefore, we expanded our scope of study by developing a 3D multicellular model to capture the tissue-level spatial dynamics.

The 3D model could help quantify the establishment of the *CLV3* expression pattern throughout the tissue by simulating the stochastic single-cell model in individual cells simultaneously at different WUS concentrations. The 3D model was constructed on the basis of the framework used in our previous work (27) combined with new biological data

and mechanisms identified by using the stochastic single-cell model. The computational domain consisted of a 3D matrix of unit spheres organized in a half-dome shape, corresponding to cells within the SAM from the L1 to L7 layers. At the tissue level, a spatial gradient of WUS proteins across different layers, which captured a similar fold change from deeper layers to outer layers observed in experiments (Fig. 1.8C), was introduced and maintained at this fixed concentration throughout each simulation (Figs. 1.1A and 1.8C). In individual cells, the single-cell stochastic model was applied to simulate WUS binding with cis-elements by using the local WUS concentrations to regulate *CLV3* transcription. The same mechanisms identified by the single-cell stochastic model were implemented under wild-type and multiple cis-element mutant conditions. Each simulation was allowed to run long enough to achieve the steady-state behavior, and the parameters used in the simulations are listed in Fig. 2.15.

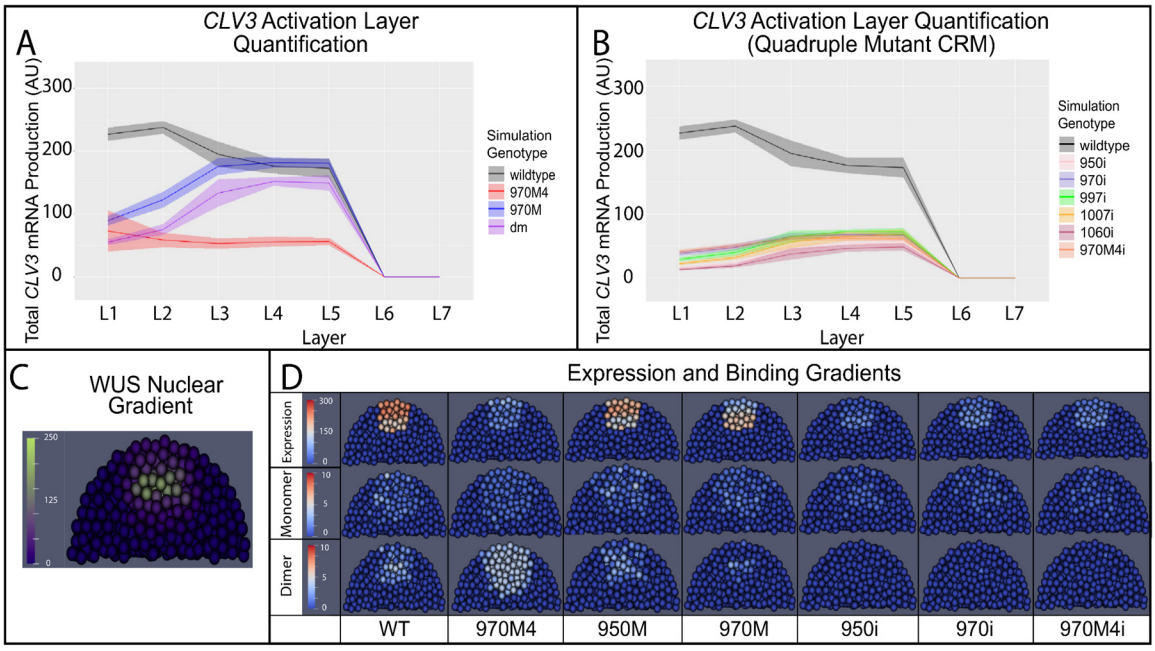

Fig. 1.8. Simulated *CLV3* dynamics and WUS protein complexes in the 3D SAM model. **(A)** Levels of *CLV3* (mean = line, SD = shaded area) activation in WT system and system with selected mutated cis-elements. **(B)** Levels of *CLV3* gene activation (mean = line, SD = shaded area) in WT system and system carrying all possible combinations of quadruple mutants (reflects intrinsic behavior of each functional cis-element). Line indicates mean *CLV3* in different cell layers. Shaded area indicates SD of activation among the cells in a given cell layer. L1 to L7 indicate the layers of the SAM from outermost CZ to inner layers of the RM. **(C)** Spatial distribution of nuclear-localized WUS. **(D)** Median longitudinal sections of simulated SAMs showing WUS monomer (middle), WUS dimer (bottom), and *CLV3* expression (top) in WT and system carrying various mutant cis-elements 970M4, 950M, 970M, 950i, 970i, and 970M4i.

Analysis of *CLV3* expression and WUS complexes captured by the 3D model

Using a biologically relevant WUS gradient (Fig. 1.8C), *CLV3* simulations were generated under a variety of different conditions, including wild type, four cis-elements (970M), three cis-elements (DM), and single cis-element (e.g., 970i). The behaviors of several cis-element mutants are shown in Fig. 1.8 (A and B). *CLV3* expression in wild type was generally higher than in other mutants, similar to the experimental data shown in Fig. 1.2A. In particular, wild-type *CLV3* activation was highest in the L1 layer and lowest in the inner layers of RM. 970M showed a higher expression in the inner layers of RM than in the outer L1 layer. Of particular interest was 970M4, in which the affinity was

strengthened over the default 970 affinity, expressed at a lower level in all cell layers. When simulating the mutants with a single functional cis-element in the CRM, e.g., 950i, 970i, 997i, 1007i, and 1060i, the *CLV3* expression was detected in only the inner layers of RM. Other than the minor difference in the magnitude, all single cis-element mutants expressed only in the inner cell layers (Fig. 1.8B), similar to the experimental results. Simulations also showed an impairment in the spatial patterns of *CLV3* expression as more cis-elements were deleted. For example, the deletion of a single lower-affinity cis-element 950 (950M) had a relatively minimal effect on *CLV3* activation (Fig. 1.8D). In contrast, deletion of the higher-affinity cis-element 970 (970M) shifted *CLV3* expression to the inner layers (Fig. 1.8D). The more drastic shift in *CLV3* expression into deeper layers occurred when deleting four cis-elements (e.g., 950i or 970i) regardless of their WUS binding affinity (Fig. 1.8D). Therefore, the cooperativity mechanism identified by the single-cell stochastic model was able to generate the expected *CLV3* expression behavior in the 3D model.

Bimolecular fluorescence complementation (BiFC) assays in plants expressing split enhanced green fluorescent protein (eGFP)–WUS constructs expressed from the native *WUS* promoter revealed very few fluorescent positive cells in the L3 and L2 layers of SAMs. These results show that WUS dimerizes in cells that accumulate higher levels of WUS, supporting the correlation observed in biochemical analysis. However, the observed dimerization in BiFC assays does not distinguish between DNA-bound WUS complexes and unbound complexes. Moreover, it likely represents WUS complexes with cis-elements of many target genes (27). Therefore, we used the 3D model to visualize the spatiotemporal distributions of WUS complexes including monomers and dimers on

the *CLV3* promoter across cell layers in SAMs (Fig. 1.8D). A higher concentration of WUS monomers in the outer layers of CZ and higher dimers in the inner layers of RM were observed for the wild-type and lower-affinity cis-element 950M. Deleting the 970 cis-element showed lower levels of WUS monomers in the outer layers of CZ and lower levels of dimers in the inner layers of RM (Fig. 1.8D). This suggested that the higher-affinity cis-element exerts a stronger influence on *CLV3* transcription, but it was not sufficient to completely activate in the outer layers of the CZ or repress the inner layers of RM on its own, showing that cis-elements interact with each other in maintaining specific amounts of WUS monomer and dimer complexes in different layers in regulating *CLV3* expression. The 970M4 results resolved the seemingly paradoxical expression patterns of this mutant. A massive amount of WUS dimers in all layers can explain a marked reduction of *CLV3* expression. In contrast, both monomers and dimers accumulated at a lower level when only one cis-element was functional, showing that WUS failed to populate at higher levels on cis-elements likely due to the lack of cooperativity. Overall, the 3D model simulations showed the spatial distributions of WUS complex formation at a quantitative level in different cell layers of SAMs. The WUS complex formation could be correlated to WUS concentration in different cell layers and the affinity-dependent cooperative behavior of cis-elements in expressing *CLV3* in the CZ.

Effect of cooperativity on the spatial patterns of *CLV3* transcription

The experimental evidence suggested that the cooperativity among cis-elements is critical to achieving proper spatial patterns of *CLV3* expression. To better understand the role of cooperativity in the robust regulation of *CLV3* expression quantitatively, we

imposed different levels of cooperativity between monomers or dimers for both wild-type and mutant conditions. A complete removal of cooperativity led to a higher *CLV3* expression in the inner cell layers of RM and a lower expression in outer cell layers of CZ under all conditions (Fig. 1.9A). In contrast, increasing cooperativity led to *CLV3* down-regulation (Fig. 1.9C), showing that strength of cooperativity influences *CLV3* expression. Our experimental analysis shows that increasing the cis-element affinity (970M4) leads to down-regulation of *CLV3* expression, which could be due to a higher cooperativity among cis-elements leading to the repression. To test this hypothesis, we removed cooperativity from 970M4, which led to an increase in *CLV3* expression, and the pattern of expression resembled that of wild type (Fig. 1.9A). These results show the importance of cooperativity in modulating *CLV3* expression, which in turn depends on the cis-element affinity.

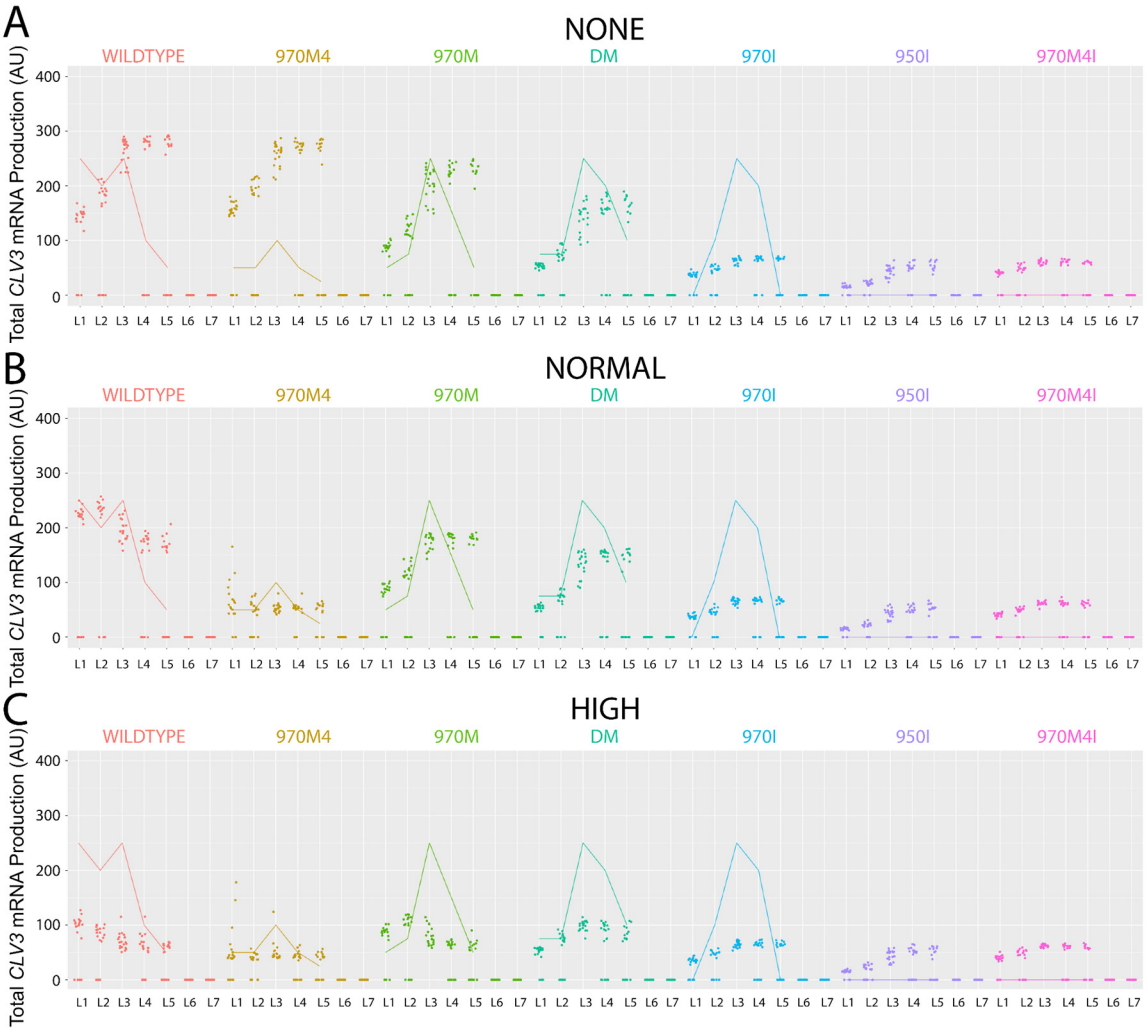

Fig. 1.9. Cooperativity levels influence *CLV3* activation.
CLV3 activation level of WT *CLV3* CRM and mutant *CLV3* CRMs under various cooperativity levels. **(A)** No cooperativity: simulations had no cooperativity between cis-elements. **(B)** Normal cooperativity: normal cooperativity values (0.01 monomer cooperativity, 0.2 dimer cooperativity) used in the default simulations. **(C)** High cooperativity: simulations with 10× the cooperativity of the default values in the simulation, i.e., 0.001 monomer cooperativity and 0.02 dimer cooperativity. Dots are simulation values for a cell. Lines are corresponding average expression values from experimental studies. Colors represent different mutants.

Our experimental analysis also showed that decreasing the number of cis-elements leads to a decrease in *CLV3* expression in outer cell layers of CZ and an increase in inner cell layers of RM, suggesting that the number of cis-elements may also aid in inducing cooperativity. Consistent with the requirement of multiple cis-elements in

mediating cooperativity, the effects of cooperativity levels on *CLV3* expression diminished with the deletions of multiple cis-elements (Fig. 1.9).

As shown above, removing the overall cooperativity that includes both the monomer and dimer cooperativity leads to the internalization of *CLV3*, which is not entirely consistent with the in vivo observed overall increase of *CLV3* expression even in the outer cell layers of *pCLV3(DS-997)* (Fig. 1.7, B and C). Removing the overall cooperativity that also included the monomer cooperativity might have caused the down-regulation of *CLV3* in outer cell layers of CZ. Therefore, we perturbed monomer and dimer cooperativity independently. At a constant dimer cooperativity, increasing monomer cooperativity alone led to a gradual increase in *CLV3* expression in outer cell layers and expression maxima shifted to outer cell layers (Fig. 1.10A). In contrast, increasing the dimer cooperativity alone led to an overall decrease in *CLV3* expression, which was more pronounced in the inner layers of RM and a shift in the expression maxima to the outer layers of CZ (Fig. 1.10B). This suggests that *CLV3* expression is regulated through a balance between dimer and monomer cooperativity mediating the repression and activation, respectively. These simulation results could also help us to understand the experimental data, in which the increased expression of *CLV3* in all cell layers observed upon doubling the distance (DS-997) could be attributed to lower dimer cooperativity leading to derepression. Together, these results show that cooperativity plays a critical role in regulating *CLV3* expression when all five cis-elements are functional.

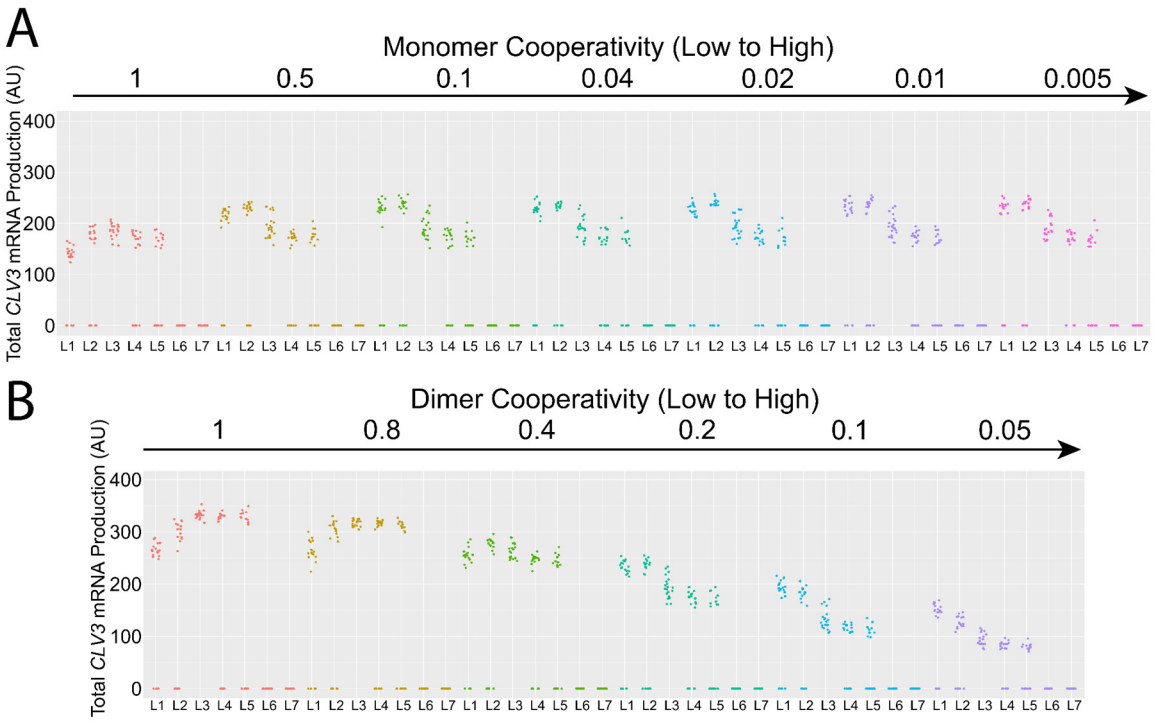

Fig. 1.10. Independent perturbations of the monomer or dimer cooperativity.
The effect of changes in monomer cooperativity (from 1 to 0.005) and dimer cooperativity (from 1 to 0.05) on *CLV3* activation. The direction of the arrows indicates an increase in cooperativity. In row **(A)**, dimer cooperativity was held constant at 0.2, while monomer cooperativity was varied (1 to 0.005). In row **(B)**, monomer cooperativity was held at 0.01 and dimer cooperativity was varied (1 to 0.05). A complete table of changes in monomer and dimer cooperativity is presented in fig. S6. The individual graphs represent the *CLV3* activation in different cell layers (L1 to L7) of simulated SAMs under the cooperativity levels noted for each simulation. The dots represent the values of the *CLV3* signal for individual simulated cells.

Discussion

A homotypic cluster of five cis-elements with different WUS binding affinities regulates levels and spatial expression of *CLV3*. WUS has been shown to activate and repress *CLV3* at lower and higher levels, respectively. Our work reveals that the relative affinities of each element, the number of cis-elements, and intervening distance contribute to the collective effect. Moreover, the collective activity of the CRM arises not only because of the individual affinity but also because of cooperative binding of multiple neighboring cis-

elements to WUS. WUS was previously shown to form a mixture of monomers, dimers, and oligomers in solution over a wide concentration range (24). Moreover, DNA/cis-elements have been shown to promote dimerization or multimerization of WUS over a small two- to fourfold increase in the WUS level.

Our biochemical analysis presented here reveals that two adjacent cis-elements can increase the binding sensitivity of WUS at lower levels than the single cis-elements, suggesting that the cis-elements cooperate in increasing the binding probability of WUS monomers, which could contribute to boost activation. Our biochemical work also shows that the two cis-elements working together allows the formation of higher-order WUS complexes at lower WUS levels, which depends on the second HOD (Fig. 1.6, J and K). This suggests that the second HOD may allow interaction of WUS species bound to the adjacent cis-elements in forming higher-order complexes. WUS has two dimerization domains, one of which is near the DNA binding domain and the other is found outside the DNA binding domain (24). The second dimerization domain may allow protein-protein interaction across neighboring cis-elements, which then allows cooperative binding across the cis-elements. Our analysis also reveals that cis-element affinity plays a critical role in inducing cooperativity across cis-elements. The increased affinity of 970M4 cis-element contributed to higher cooperativity, leading to the repression of *CLV3*. However, such repression requires other functional cis-elements in the CRM, showing that the collective behavior arises as a result of the number of cis-elements and the WUS binding affinities. The collective behavior of a low-affinity homotypic CRM has been shown to be critical in a recent study of the *Drosophila* SHAVENBABY locus. Increasing the binding affinity of one of the cis-elements resulted in a strong ectopic activation, suggesting that low-affinity homotypic CRMs may lead to higher specificity

(9). Our work showing the importance of the number of cis-elements in regulating gene expression agrees with the fundamental concept of having multiple cis-elements organized in a constellation leading to gene expression specificity. However, the *CLV3* CRM regulation differs from other homotypic CRMs such as SHAVENBABY locus where *CLV3* expression is regulated through a concentration-dependent activation-repression switching mechanism. The C terminus of WUS has been shown to bind at least three proteins: HAIRYMERISTEM (55), SHOOT-MERISTEMLESS (56), and TOPLESS (57). Earlier analysis shows that the C terminus of WUS is not required for the regulation of DNA binding affinity and dimerization (24) and DNA binding specificity (29). Therefore, we suggest that WUS binding to the *CLV3* CRM is a cofactor-independent mechanism that depends on the organization of cis-elements in the CRM. Besides *CLV3*, WUS has been shown to activate and repress several hundred genes (27). Our bioinformatics search for “TAAT” core-containing cis-element clusters (see the Chapter 3 for details of the algorithm) identified multiple clusters in 152 of 154 WUS up-regulated genes and 298 of 303 WUS down-regulated genes. This resource should guide future in vivo analysis to refine our understanding of the relationship between CRMs and gene expression specificity.

Our analysis also shows that the interaction between cis-elements in promoting higher molecular WUS complexes also depends on the distance between cis-elements. Increasing the distance between cis-elements unexpectedly decreased the WUS detection threshold, suggesting that distance may also play a role in sensing WUS concentration through an unknown mechanism. This might increase the probability of WUS monomer binding to adjacent cis-elements. However, the stabilization of WUS into a higher molecular weight complexes still occurred at the same WUS levels as observed

with the wild-type distance. Thus, the increase in *CLV3* expression observed upon increasing the distance could be due to increased activation and not entirely due to the reduced repression. Together, our results show that the cis-element affinity plays a dominant role in *CLV3* repression, while it appears that the system can withstand an increase in intervening distance in forming higher WUS complexes.

The computational model developed in this study allows us to recreate and, in a sense, verify the plausibility of our mechanistic explanations of experimental results. It was possible to quantify properties that are very difficult to obtain through experimental means such as the residence time of WUS on cis-elements to calibrate the model and visualization of concentration-dependent ratios of WUS monomer and dimer/higher-order complexes on the *CLV3* cis-elements. The upper limit on the residence time of WUS was critical to explain individual cis-element behaviors that differ in their binding affinities. Our experimental analysis shows that a higher WUS turnover leads to a higher *CLV3* activation, suggesting that older WUS species may become ineffective and may unbind. The nuclear export of WUS has been shown to play a crucial role in regulating the WUS nuclear concentration (51). It has also been shown that a nuclear export signal is required for WUS degradation in the cytoplasm. Perhaps the older WUS molecules that unbind are exported and degraded in the cytoplasm, which may create space for newly synthesized WUS that moves into the outer layer of CZ to bind cis-elements to sustain *CLV3* activation. CLV3 has been shown to offset nuclear export of WUS, which forms an additional feedback mechanism in regulating the nuclear concentration (51). Whether CLV3 levels also independently determine residence time of WUS by influencing its unbinding from cis-elements perhaps by regulating the WUS protein modifications remains to be explored. Nevertheless, a seamless connection involving

WUS binding, unbinding, export, and degradation could lead to a robust maintenance of *CLV3* transcription. However, the current model assumes a constant WUS gradient and is limited to exploring the mechanisms underlying the *CLV3* expression without considering the feedback regulations of CLV3 signaling on WUS. Our recent study developed a model involving both transcriptional and posttranslational regulations of WUS by the CLV3 signaling (51). This model used a generic function of WUS concentration to represent the *CLV3* transcription. The model perturbations revealed that the dual control of *WUS* transcription and nuclear levels by the CLV3 signaling when coupled to the WUS concentration–dependent transcriptional activation and repression of *CLV3* leads to a robust maintenance of the WUS protein gradient. Our results show that the cis-element mutant reporter 970i was markedly reset into the outer layers of CZ in the *clv3* null mutants complemented with the 970i genomic construct. Perhaps this is due to the effects of altered CLV3 signaling on the expression and nuclear accumulation of WUS establishing a new gradient. In the future, coupling the 3D stochastic model of *CLV3* transcription developed here with the CLV3 signaling model of the regulation of WUS transcription and the WUS protein dynamics should allow assessment of the influence of different properties of the *CLV3* CRM, including the number of cis-elements in regulating the robustness of the WUS gradient.

Methods

Experimental design

Plants were grown under continuous light as described earlier in (24). Imaging was performed on the Zeiss 880 AIRYSCAN upright under a 40× objective. eGFP-WUS was excited at 488 nm and collected with filter 495 to 550 nm. Histone 2B modified yellow

fluorescent protein (H2B-mYFP) was excited at 514-nm filtered with main beam splitter (MBS) 458/514/561/633 and collected with band-pass (BP) filter 495 to 550 nm. FM4-64 was excited at 561 nm and collected with BP 570 to 620 nm.

Statistical analysis

The means, *N*, and *P* values are included within each dataset.

References

1. M. Levine, Transcriptional enhancers in animal development and evolution. Curr. Biol. 20,R754–63 (2010).

2. C.-T. Ong, V. G. Corces, Enhancer function: new insights into the regulation of tissue-specific gene expression. Nat. Rev. Genet. 12, 283–293 (2011).

3. F. Spitz, E. E. M. Furlong, Transcription factors: from enhancer binding to developmental control. Nat. Rev. Genet. 13, 613–626 (2012).

4. J. Banerji, S. Rusconi, W. Schaffner, Expression of a beta-globin gene is enhanced by remote SV40 DNA sequences. Cell. 27, 299–308 (1981).

5. M. Slattery, T. Riley, P. Liu, N. Abe, P. Gomez-Alcala, I. Dror, T. Zhou, R. Rohs, B. Honig, H. J. Bussemaker, R. S. Mann, Cofactor binding evokes latent differences in DNA binding specificity between Hox proteins. Cell. 147, 1270–1282 (2011).

6. G. Struhl, K. Struhl, P. M. Macdonald, The gradient morphogen bicoid is a concentration-dependent transcriptional activator. Cell. 57, 1259–1273 (1989).

7. W. D. Fakhouri, A. Ay, R. Sayal, J. Dresch, E. Dayringer, D. N. Arnosti, Deciphering a transcriptional regulatory code: modeling short-range repression in the Drosophila embryo. Mol. Syst. Biol. 6, 341 (2010).

8. R. Joshi, J. M. Passner, R. Rohs, R. Jain, A. Sosinsky, M. A. Crickmore, V. Jacob, A. K. Aggarwal, B. Honig, R. S. Mann, Functional specificity of a Hox protein mediated by the recognition of minor groove structure. Cell. 131, 530–543 (2007).

9. J. Crocker, N. Abe, L. Rinaldi, A. P. McGregor, N. Frankel, S. Wang, A. Alsawadi, P. Valenti, S. Plaza, F. Payre, R. S. Mann, D. L. Stern, Low affinity binding site clusters confer hox specificity and regulatory robustness. Cell. 160, 191–203 (2015).

10. B. P. Berman, Y. Nibu, B. D. Pfeiffer, P. Tomancak, S. E. Celniker, M. Levine, G. M. Rubin, M. B. Eisen, Exploiting transcription factor binding site clustering to identify cis-regulatory modules involved in pattern formation in the Drosophila genome. Proc. Natl. Acad. Sci. U. S. A. 99, 757–762 (2002).

11. A. P. Lifanov, V. J. Makeev, A. G. Nazina, D. A. Papatsenko, Homotypic regulatory clusters in Drosophila. Genome Res. 13, 579–588 (2003).

12. S. Small, A. Blair, M. Levine, Regulation of even-skipped stripe 2 in the Drosophila embryo. EMBO J. 11, 4047–4057 (1992).

13. Y. T. Ip, R. E. Park, D. Kosman, E. Bier, M. Levine, The dorsal gradient morphogen regulates stripes of rhomboid expression in the presumptive neuroectoderm of the Drosophila embryo. Genes Dev. 6, 1728–1739 (1992).

14. W. Driever, C. Nüsslein-Volhard, The bicoid protein is a positive regulator of hunchback transcription in the early Drosophila embryo. Nature. 337, 138–143 (1989).

15. J. Gaudet, S. E. Mango, Regulation of organogenesis by the Caenorhabditis elegans FoxA protein PHA-4. Science. 295, 821–825 (2002).

16. J. Jiang, M. Levine, Binding affinities and cooperative interactions with bHLH activators delimit threshold responses to the dorsal gradient morphogen. Cell. 72, 741–752 (1993).

17. S. Rowan, T. Siggers, S. A. Lachke, Y. Yue, M. L. Bulyk, R. L. Maas, Precise temporal control of the eye regulatory gene Pax6 via enhancer-binding site affinity. Genes Dev. 24, 980–985 (2010).

18. L. Wolpert, Positional information and the spatial pattern of cellular differentiation. J. Theor. Biol. 25, 1–47 (1969).

19. J. Jiang, D. Kosman, Y. T. Ip, M. Levine, The dorsal morphogen gradient regulates the mesoderm determinant twist in early Drosophila embryos. Genes Dev. 5, 1881–1891 (1991).

20. D. S. Parker, M. A. White, A. I. Ramos, B. A. Cohen, S. Barolo, The cis-regulatory logic of Hedgehog gradient responses: key roles for gli binding affinity, competition, and cooperativity. Sci. Signal. 4, ra38 (2011).

21. K. F. Mayer, H. Schoof, A. Haecker, M. Lenhard, G. Jürgens, T. Laux, Role of WUSCHEL in regulating stem cell fate in the Arabidopsis shoot meristem. Cell. 95, 805–815 (1998).

22. H. Schoof, M. Lenhard, A. Haecker, K. F. X. Mayer, G. Jürgens, T. Laux, The Stem Cell Population of Arabidopsis Shoot Meristems Is Maintained by a Regulatory Loop between the CLAVATA and WUSCHEL Genes. Cell. 100, 635–644 (2000).

23. R. K. Yadav, M. Perales, J. Gruel, T. Girke, H. Jönsson, G. V. Reddy, WUSCHEL protein movement mediates stem cell homeostasis in the Arabidopsis shoot apex. Genes Dev. 25, 2025–2030 (2011).

24. M. Perales, K. Rodriguez, S. Snipes, R. K. Yadav, M. Diaz-Mendoza, G. V. Reddy, Threshold-dependent transcriptional discrimination underlies stem cell homeostasis. Proc. Natl. Acad. Sci. U. S. A. 113, E6298–E6306 (2016).

25. S. E. Clark, R. W. Williams, E. M. Meyerowitz, The CLAVATA1 gene encodes a putative receptor kinase that controls shoot and floral meristem size in Arabidopsis. Cell. 89, 575–585 (1997).

26. U. Brand, J. C. Fletcher, M. Hobe, E. M. Meyerowitz, R. Simon, Dependence of Stem Cell Fate in Arabidopsis on a Feedback Loop Regulated by CLV3 Activity. Science. 289,
617–619 (2000).

27. R. K. Yadav, M. Perales, J. Gruel, C. Ohno, M. Heisler, T. Girke, H. Jönsson, G. V. Reddy, Plant stem cell maintenance involves direct transcriptional repression of differentiation program. Mol. Syst. Biol. 9, 654 (2013).

28. C. Koppermann, Crystal Structure of the WUSCHEL Homeodomain. Thesis, Universität zuKöln, https://d-nb.info/1153121050/34 (2017).
197
29. J. Sloan, J. P. Hakenjos, M. Gebert, O. Ermakova, A. Gumiero, G. Stier, K. Wild, I. Sinning, J. U. Lohmann, Structural basis for the complex DNA binding behavior of the plant stem cell regulator WUSCHEL. Nat. Commun. 11, 2223 (2020).

30. J. Reinitz, S. Hou, D. H. Sharp, Transcriptional Control in Drosophila. Complexus. 1, 54–64 (2003).

31. M. A. Shea, G. K. Ackers, The OR control system of bacteriophage lambda. A physical-chemical model for gene regulation. J. Mol. Biol. 181, 211–230 (1985).

32. X. He, M. A. H. Samee, C. Blatti, S. Sinha, Thermodynamics-based models of transcriptional regulation by enhancers: the roles of synergistic activation, cooperative binding and short-range repression. PLoS Comput. Biol. 6 (2010).

33. D. Chu, N. R. Zabet, B. Mitavskiy, Models of transcription factor binding: sensitivity of activation functions to model assumptions. J. Theor. Biol. 257, 419–429 (2009).

34. M. S. Sherman, B. A. Cohen, Thermodynamic state ensemble models of cis-regulation. PLoS Comput. Biol. 8, e1002407 (2012).

35. D. T. Gillespie, A general method for numerically simulating the stochastic time evolution of coupled chemical reactions. J. Comput. Phys. 22, 403–434 (1976).

36. J. Swift, G. M. Coruzzi, A matter of time - How transient transcription factor interactions create dynamic gene regulatory networks. Biochim. Biophys. Acta Gene Regul. Mech. 1860, 75–83 (2017).

37. T. O'Brien, J. T. Lis, Rapid changes in Drosophila transcription after an instantaneous heat shock. Mol. Cell. Biol. 13, 3456–3463 (1993).

38. G. K. Ackers, A. D. Johnson, M. A. Shea, Quantitative model for gene regulation by lambda phage repressor. Proc. Natl. Acad. Sci. U. S. A. 79, 1129–1133 (1982).

39. H. G. Garcia, R. Phillips, Quantitative dissection of the simple repression input-output
function. Proc. Natl. Acad. Sci. U. S. A. 108, 12173–12178 (2011).

40. J. Gertz, E. D. Siggia, B. A. Cohen, Analysis of combinatorial cis-regulation in synthetic and genomic promoters. Nature. 457, 215–218 (2009).

41. E. Segal, T. Raveh-Sadka, M. Schroeder, U. Unnerstall, U. Gaul, Predicting expression patterns from regulatory sequence in Drosophila segmentation. Nature. 451, 535–540 (2008).

42. R. P. Zinzen, C. Girardot, J. Gagneur, M. Braun, E. E. M. Furlong, Combinatorial binding predicts spatio-temporal cis-regulatory activity. Nature. 462, 65–70 (2009).

43. R. Amit, H. G. Garcia, R. Phillips, S. E. Fraser, Building enhancers from the ground up: a synthetic biology approach. Cell. 146, 105–118 (2011).

44. E. Davidson, The Regulatory Genome (Academic Press, 2006).

45. H. G. Garcia, A. Sanchez, J. Q. Boedicker, M. Osborne, J. Gelles, J. Kondev, R. Phillips, Operator Sequence Alters Gene Expression Independently of Transcription Factor Occupancy in Bacteria. Cell Rep. 2, 150–161 (2012).

46. C. R. Lickwar, F. Mueller, S. E. Hanlon, J. G. McNally, J. D. Lieb, Genome-wide protein–DNA binding dynamics suggest a molecular clutch for transcription factor function. Nature. 484, 251–255 (2012).

47. J. R. Lipford, G. T. Smith, Y. Chi, R. J. Deshaies, A putative stimulatory role for activator turnover in gene expression. Nature. 438, 113–116 (2005).

48. S. H. Spoel, Z. Mou, Y. Tada, N. W. Spivey, P. Genschik, X. Dong, Proteasome-mediated turnover of the transcription coactivator NPR1 plays dual roles in regulating plant immunity. Cell. 137, 860–872 (2009).

49. F. Geng, S. Wenzel, W. P. Tansey, Ubiquitin and proteasomes in transcription. Annu. Rev. Biochem. 81, 177–201 (2012).

50. A. Sundqvist, J. Ericsson, Transcription-dependent degradation controls the stability of the SREBP family of transcription factors. Proc. Natl. Acad. Sci. U. S. A. 100, 13833–13838 (2003).

51. A. Plong, K. Rodriguez, M. Alber, W. Chen, G. V. Reddy, CLAVATA3 mediated simultaneous control of transcriptional and post-translational processes provides robustness to the WUSCHEL gradient. Nat. Commun. 12, 1–13 (2021).

52. S. A. Snipes, K. Rodriguez, A. E. DeVries, K. N. Miyawaki, M. Perales, M. Xie, G. V. Reddy, Cytokinin stabilizes WUSCHEL by acting on the protein domains required for nuclear enrichment and transcription. PLoS Genet. 14, e1007351 (2018).

53. K. Rodriguez, M. Perales, S. Snipes, R. K. Yadav, M. Diaz-Mendoza, G. V. Reddy, DNA-dependent homodimerization, sub-cellular partitioning, and protein destabilization control WUSCHEL levels and spatial patterning. Proc. Natl. Acad. Sci. U. S. A. 113, E6307–E6315 (2016).

54. R. Sayal, J. M. Dresch, I. Pushel, B. R. Taylor, D. N. Arnosti, Quantitative perturbation-based analysis of gene expression predicts enhancer activity in early Drosophila embryo. Elife. 5 (2016).

55. Y. Zhou, X. Liu, E. M. Engstrom, Z. L. Nimchuk, J. L. Pruneda-Paz, P. T. Tarr, A. Yan, S. A. Kay, E. M. Meyerowitz, Control of plant stem cell function by conserved interacting transcriptional regulators. Nature. 517, 377–380 (2015).

56. Y. H. Su, C. Zhou, Y. J. Li, Y. Yu, L. P. Tang, W. J. Zhang, W. J. Yao, R. Huang, T. Laux, X. S. Zhang, Integration of pluripotency pathways regulates stem cell maintenance in the Arabidopsis shoot meristem. Proc. Natl. Acad. Sci. U. S. A. 117, 22561–22571 (2020).

57. M. Kieffer, Y. Stern, H. Cook, E. Clerici, C. Maulbetsch, T. Laux, B. Davies, Analysis of the transcription factor WUSCHEL and its functional homologue in Antirrhinum reveals a potential mechanism for their roles in meristem maintenance. Plant Cell. 18, 560–573 (2006).

58. B. Senay-Aras, W. Chen. Stochastic Cis-elements Binding Model. https://zenodo.org/badge/latestdoi/349283086 (2022).

59. A. Do, MeristemBasic_p. https://zenodo.org/badge/latestdoi/501822165 (2022).

60. A. Do, BasicCisElementAnalyzer. https://zenodo.org/badge/latestdoi/498280124 (2022)

61. M. R. Roussel, R. Zhu, Validation of an algorithm for delay stochastic simulation of transcription and translation in prokaryotic gene expression. Phys. Biol. 3, 274–284 (2006).

62. E. Azpeitia, A. Wagner, Short Residence Times of DNA-Bound Transcription Factors Can Reduce Gene Expression Noise and Increase the Transmission of Information in a Gene Regulation System. Frontiers in Molecular Biosciences. 7 (2020).

63. P. S. Gutierrez, D. Monteoliva, L. Diambra, Cooperative binding of transcription factors promotes bimodal gene expression response. PLoS One. 7, e44812 (2012).

64. U. Brand, M. Grünewald, M. Hobe, R. Simon, Regulation of CLV3 expression by two homeobox genes in Arabidopsis. Plant Physiol. 129, 565–575 (2002).

Chapter 2: The Coupled Feedback Meristem Model

Abstract

A computational multiscale model was developed which simulates WUS/CLV3 intercellular signaling at tissue scale and WUS binding to *CLV3* cis-elements at the subcellular level. This model was compared to the earlier model which simulated *CLV3* expression dynamics on a fixed WUS protein gradient, presented in Chapter 1. The expression of the *CLV3* species in this model were depressed compared to the previous model except for 970M4 where the effect of CLV3 on WUS appeared to feedback on *CLV3* expression raising it higher. Perturbations on individual parameters of the model were implemented to show their effects on an otherwise WT background. This mostly showed the model and connections between the species behaving as expected. The contribution of monomer cooperativity and dimer cooperativity in this model also remained the same as it was in the previous model. Work is in progress to simulate and analyze the resetting of CLV3 expression to the outer layers in *clv3-2* complemented mutants

Introduction

In Chp1 the computational SAM model was presented which generates data on the properties of the CRM and how the different cis-elements contribute directly to expression on a fixed WUS background. The model has been extended by changing the previously fixed WUS background to being fully dynamic where the WUS species in the SAM fully affect *CLV3* expression and are, in turn, affected by the CLV3 species allowing feedback between the two. Practically the WUS species are now controlled by

ODE equations and updated across the interval of the simulation along with the CLV3 species. This extended coupled feedback model like the previous model has its underlying codebase for the data processing portion forked from a previous model by (1) but with new dynamics and various other changes including the addition of a subcellular stochastic system. This model will help to show the effects of the CRM in a wider context as well as demonstrate how the different WUS species contribute to the network and hopefully help to quantify the dynamics behind specific phenomenon witnessed in experimental studies such as the resetting of the *CLV3* pattern, where in specific situations *CLV3* expression recovers to a more wildtype distribution in the SAM even though the CRM is missing one or more cis-elements (2). The non feedback model and feedback model correspond to different wet lab experimental setups. The non feedback model corresponds to tracking a transformed construct of WT and mutated cis-elements within the CRM driving a fluorescence (H2b-mYFP) marker gene in wild-type background. Whereas the feedback model corresponds to an experiment which can track the underlying dynamics of the SAM network with mutations on the *CLV3 promoter* driving the expression of functional *CLV3* introduced into *clv3* (*clv3-2*) null mutants (Fig. 2.1). Because of this the behavior of species under the same parameter settings while often consistent is not necessarily identical across both models and should be examined independently.

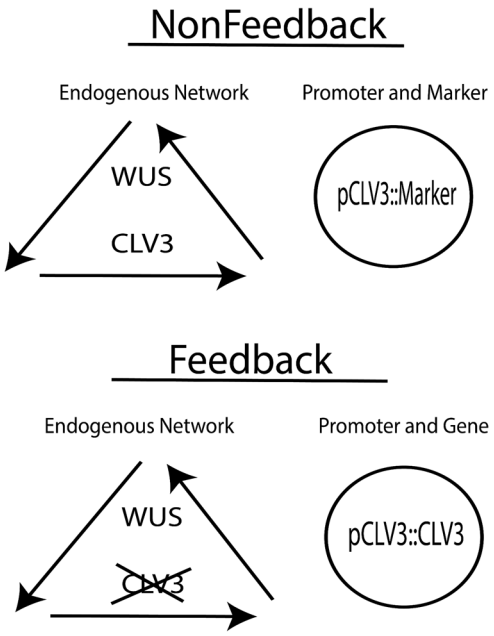

Fig. 2.1. Experimental setup corresponding to the non feedback vs feedback meristem model. The non feedback model corresponds to a construct driving a marker in a wildtype background plant. The feedback model corresponds to a construct driving a *CLV3* gene complementing a *clv3-2* mutant background.

The feedback model consists of two distinct portions, the subcellular binding system from Chp1 which operates stochastically and an expanded (relative to the non feedback model) ODE protein/RNA signaling system which operates deterministically. The protein system consists of the proteins and RNA species which are produced and decay and diffuse through the SAM. The species the system tracks are *WUS RNA*, WUS protein in the nucleus and cytoplasm, *CLV3 RNA*, CLV3 peptide, Cytokinin, Cytokinin receptor, and Cytokinin complexed receptor.

The subcellular system models the direct interaction of the *CLV3 gene* with WUS in the nucleus. The *CLV3* gene is modeled as a segment (CRM) of 5 WUS-binding cis-elements that contain the TAAT core sequence in the gene known as 950, 970, 997, 1007, and 1060. The binding of WUS to *CLV3* CRM is controlled stochastically with

events (binding, unbinding, RNA polymerase (PolII) recruitment, etc) probabilistically occurring based on the state of the system. These factors include bound neighbors, WUS concentration etc. The different states of the cis-element can be empty, monomer, or dimer bound. Through the different patterns of WUS binding to these segments, the system can achieve a fine tuned control of the *CLV3* target greater than seen in earlier simpler models of expression systems (3).

While ODE systems are commonly used in modeling biochemical scenarios (4) the addition of Chp1's stochastic subcellular model brings several advantages over a plain ODE system. ODE systems are most suited for modeling large bulk mixed systems which are very different from the situation of proteins binding to limited genome sequences. The direct modeling of binding allows visualization of the explicit molecular dynamics and patterns of WUS complexes formed on the binding sequence itself and biologically relevant data can be gathered from these observations. A stochastic system is also capable of capturing the variability of individual runs rather than the average behavior captured by ODE systems model. A more comprehensive description of the simulation system can be found in the Methods section.

Calibration data for the model

Ultimately the coupled feedback model as an extension of the non feedback model uses the same parameters and values as applicable. And its parameters are ultimately derived from or tuned to available experimental data. Specifically, the affinities of the *CLV3* CRM cis-elements are derived from EMSA binding studies (2). The binding

patterns showing the ratio of cis-element/WUS bound states were used to derive the K_D values of the cis-elements.

The non feedback model is calibrated to data from (2) and other studies measuring the signals of *pCLV3::H2B-mYFP* reporters carrying various mutant cis-elements in WT background. Expression data was collated from SAM confocal images which showed expression across cell layers for different mutants. Work is currently being undertaken to produce similar data for the feedback simulations by conducting studies of mutant and wild-type *pCLV3::CLV3genomic*.

Results

The coupled feedback model was compared against the non feedback model from Chp1 by graphing the concentration of the different species (*CLV3* RNA for example) In individual cells on the y axis and SAM layer on the x axis across different mutants (Fig 2.2-2.4). The same *CLV3* CRM mutants used in Chp1 are used here and are described in Methods. The trend across the *CLV3* expression was that they were generally lower than in the non feedback model save for a few exceptions such as the synthetic higher affinity mutant-*970M4* and the lower affinity mutant-*950i* (Fig. 2.2). The reactive WUS protein of the feedback model was able to increase significantly in concentration and accumulated in a broader spatial domain, (Fig. 2.3) pushing *CLV3* mRNA species concentration down. The cis-element mutant expression levels remained generally the same relative to each other. The peptide levels of CLV3 were very similar to its non feedback counterpart though slightly lower (Fig. 2.2B). On the other hand *CLV3* m*RNA* levels in the outer layer tend to fall across the different mutants (Fig. 2.2A and C) as now

responsive WUS (as opposed to the WUS in the non feedback model) is purged from the outer layers due to the presence of CLV3 and the gradient shifts to the interior of the SAM (Fig. 2.3B).

Resetting of the CLV3 gradient where expression was higher in the feedback than its non feedback counterpart was seen in *970M4* and possibly the inner layers of *950i* (Fig. 2.2).

The WUS species, while increased from the non feedback model in the feedback model, remained remarkably similar across the different mutants. Meanwhile the dimers expanded across the inner layers of several mutants as would be expected with the increased WUS (Fig. 2.4).

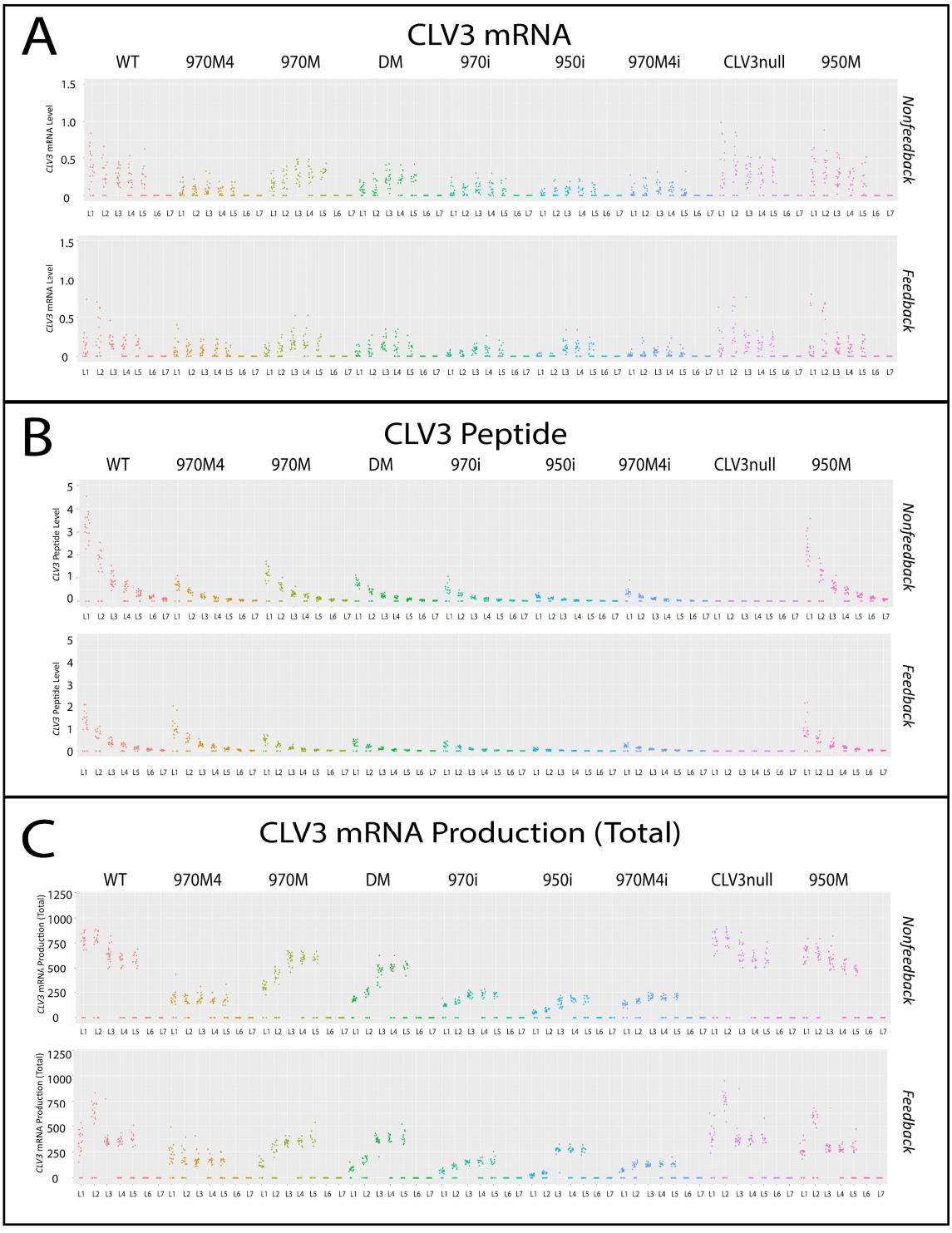
A
CLV3 mRNA
WT
970M4
970M
DM
970i
950i
970M4i
CLV3null
950M
CLV3 mRNA Level
Nonfeedback
Feedback
B
CLV3 Peptide
CLV3 Peptide Level
C
CLV3 mRNA Production (Total)

Fig. 2.2. Comparison of expression in the non feedback model vs the feedback model: CLV3 Species.
(A) CLV3 RNA: Amount of CLV3 RNA at the end of the simulation. Amount is on the y axis. Layer is on the x axis. Genetic background is specified on top of the graph. Non feedback graph is on the top. Feedback graph is on the bottom. **(B)** CLV3 Peptide amount. **(C)** Total RNA production over the course of the simulation.

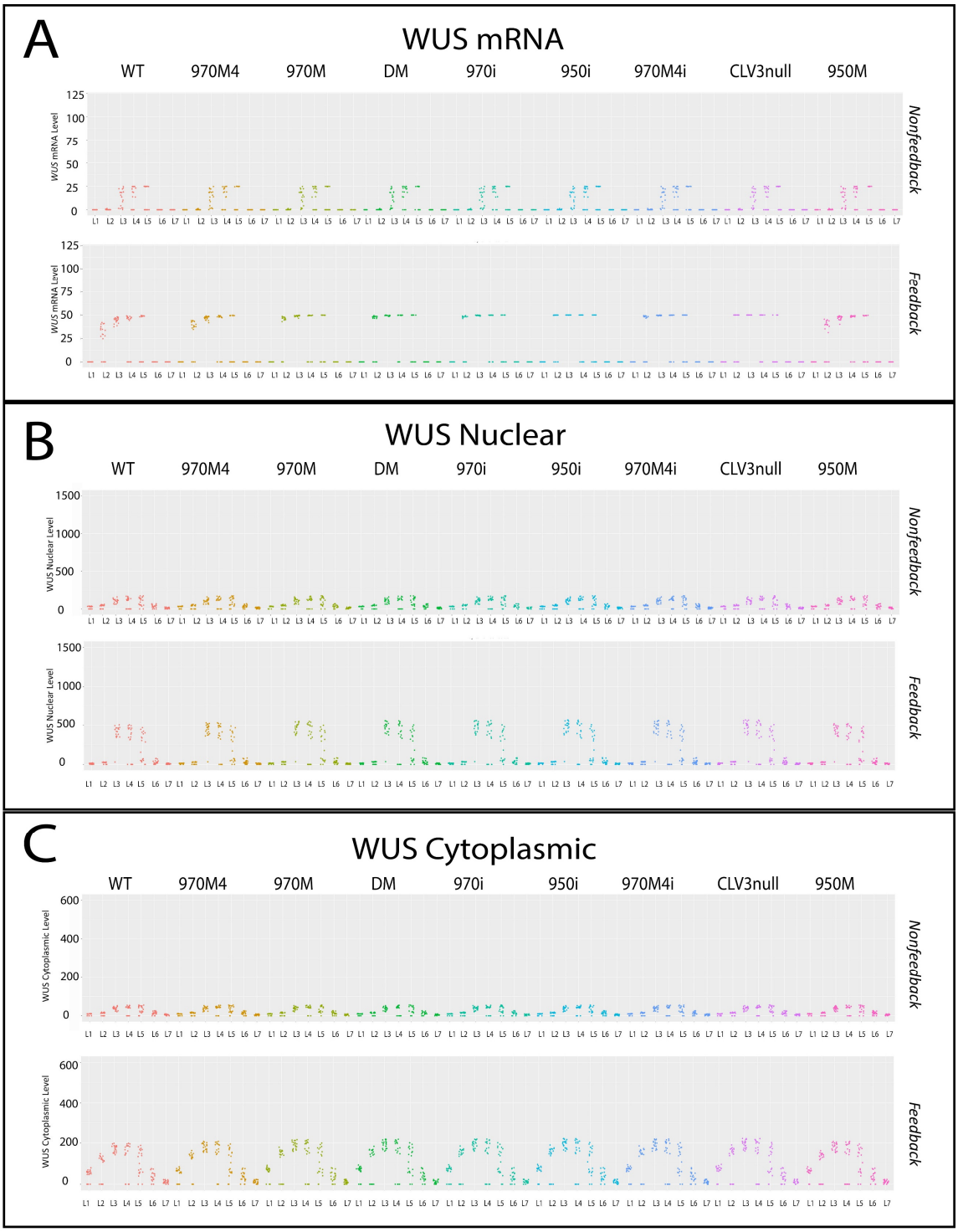

Fig. 2.3. Comparison of expression in the non feedback model vs the feedback model. WUS Species.
(A) WUS RNA amount **(B)** WUS Nuclear amount **(C)** WUS Cytoplasmic amount..

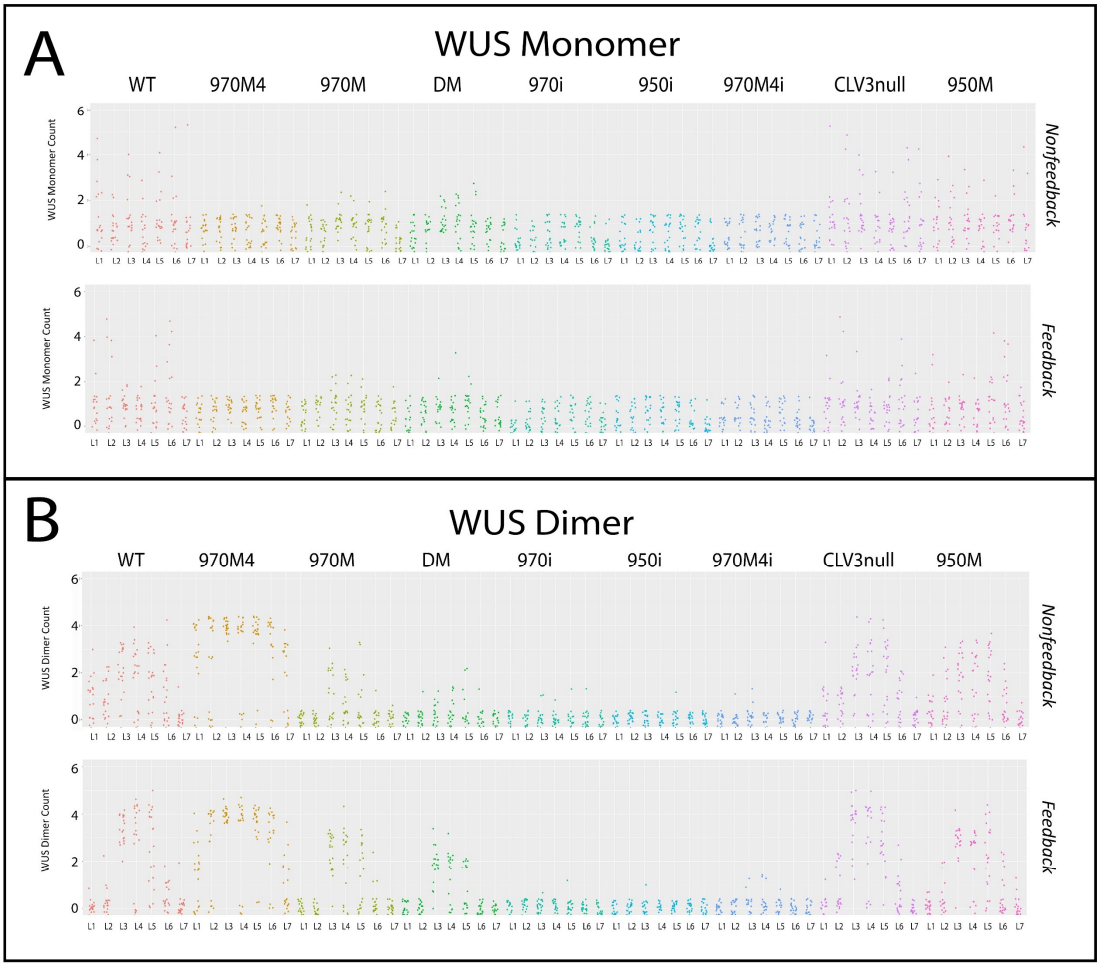

Fig. 2.4. Comparison of expression in the non feedback model vs the feedback model. Monomer and Dimer.
(A) Monomer amount. **(B)** Dimer amount

Perturbations of the coupled model

Several perturbations were performed on the coupled feedback model to see what effect the different parameters would have on the system and how the different species would respond to different changes in conditions. These perturbations are to *WUS RNA*

production and degradation, WUS Nuclear export and WUS Nuclear/CLV3 interaction, WUS Cytoplasmic diffusion, the WUS saturation value for *CLV3 RNA*, and the CLV3 peptide production. These parameters were picked to alter the system in distinct ways without too much overlap. The results are shown in Fig. 2.5 to 2.11. While not a comprehensive survey on how all parameters would contribute to the model under all circumstances, they can give an idea of the role and contribution of different aspects of the model and how the system functions in a wider context.

The perturbations consisted of running simulations with a single parameter in question in otherwise WT conditions at a default level and at ½ and 2x relative to the default level. The effect of the perturbations was then visualized by graphing the major species of the simulation in plots with the concentration/amount in the y-axis and layer of the SAM in the x-axis for all three levels. The species tracked are Pol Bind (equivalent to total RNA produced), *CLV3 RNA*, CLV3 Peptide, WUS Monomer, *WUS RNA*, WUS Nuclear, WUS Cyto, and WUS Dimer. Fig. 2.5-2.11 follow the same format.

The *WUS RNA* production parameter as the name suggests drives the rate of *WUS RNA* production (Fig 2.5). Lowering the rate 1/2x brings the level of polymerase binding down in the outer layers and up in the inner layers. *CLV3 RNA* is affected in the same fashion. CLV3 peptide is lowered in the outer layers. For 2x the gradients for the CLV3 species are similar though more defined/slightly higher in the outer layers. The WUS species (*RNA*, Nuclear, and Cytoplasmic) decreased in level at 1/2x and increased in 2x particularly in the inner layers. WUS Dimer decreased noticeably from the inner layers at 1/2x.

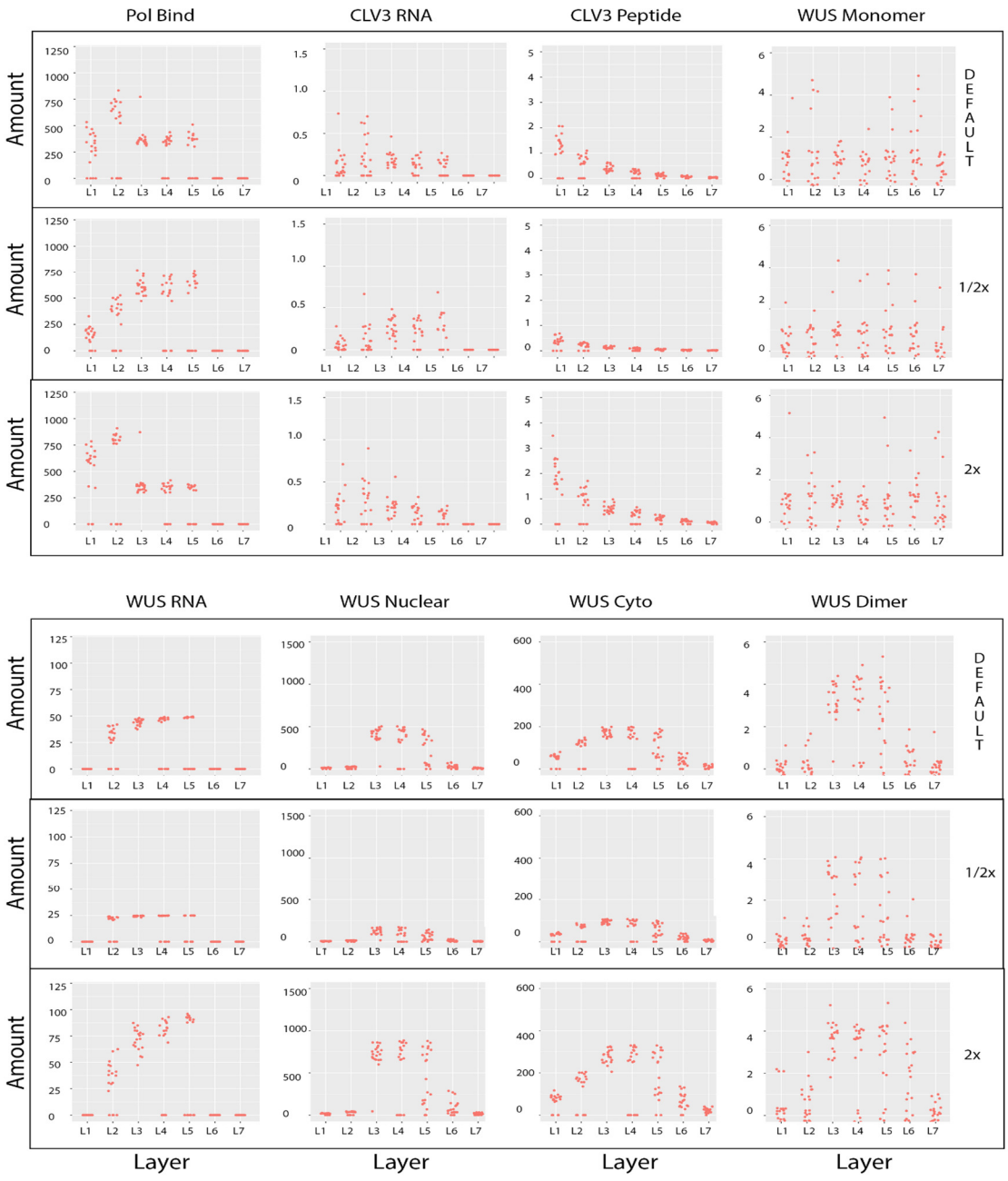

Fig. 2.5. WUS RNA Production perturbation effects.
Species type at the top. Amount of species is on the y axis. Meristem layer is on the x axis. First row is default parameters. Second row is 1/2x perturbation of selected parameter. Third row is 2x perturbation of selected parameter.

WUS RNA Degradation had the opposite effect of *WUS RNA* Production with 2x corresponding to the Production perturbation 1/2x effects and vice versa.

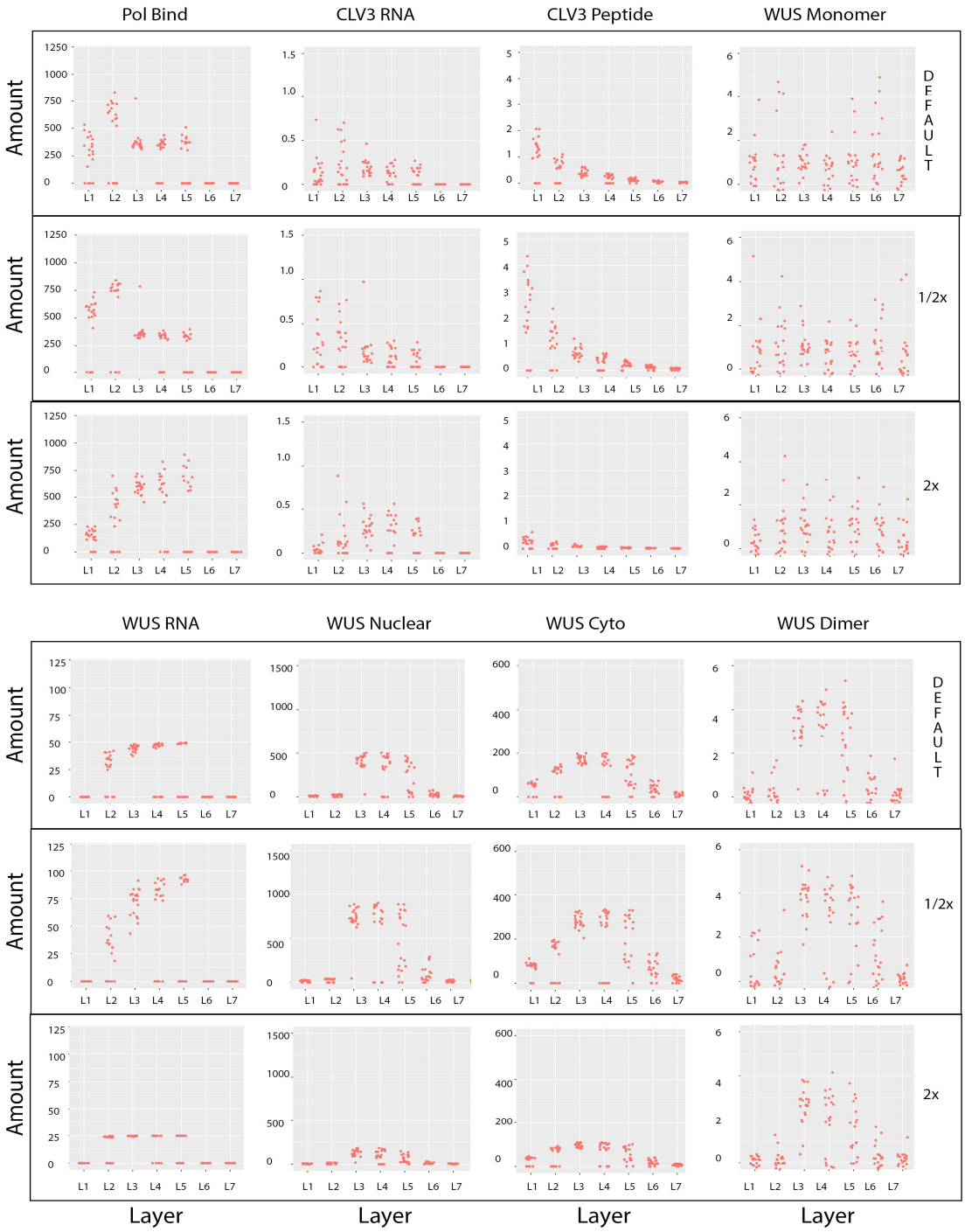

Fig. 2.6. WUS RNA Degradation perturbation effects.
Species type at the top. Amount of species is on the y axis. Meristem layer is on the x axis. First row is default parameters. Second row is 1/2x perturbation of selected parameter. Third row is 2x perturbation of selected parameter.

WUS Nuclear export had a noticeable effect mostly in the 2x perturbation. The effects were similar to lowering *WUS RNA* production with the exception that the RNA production wasn't affected.

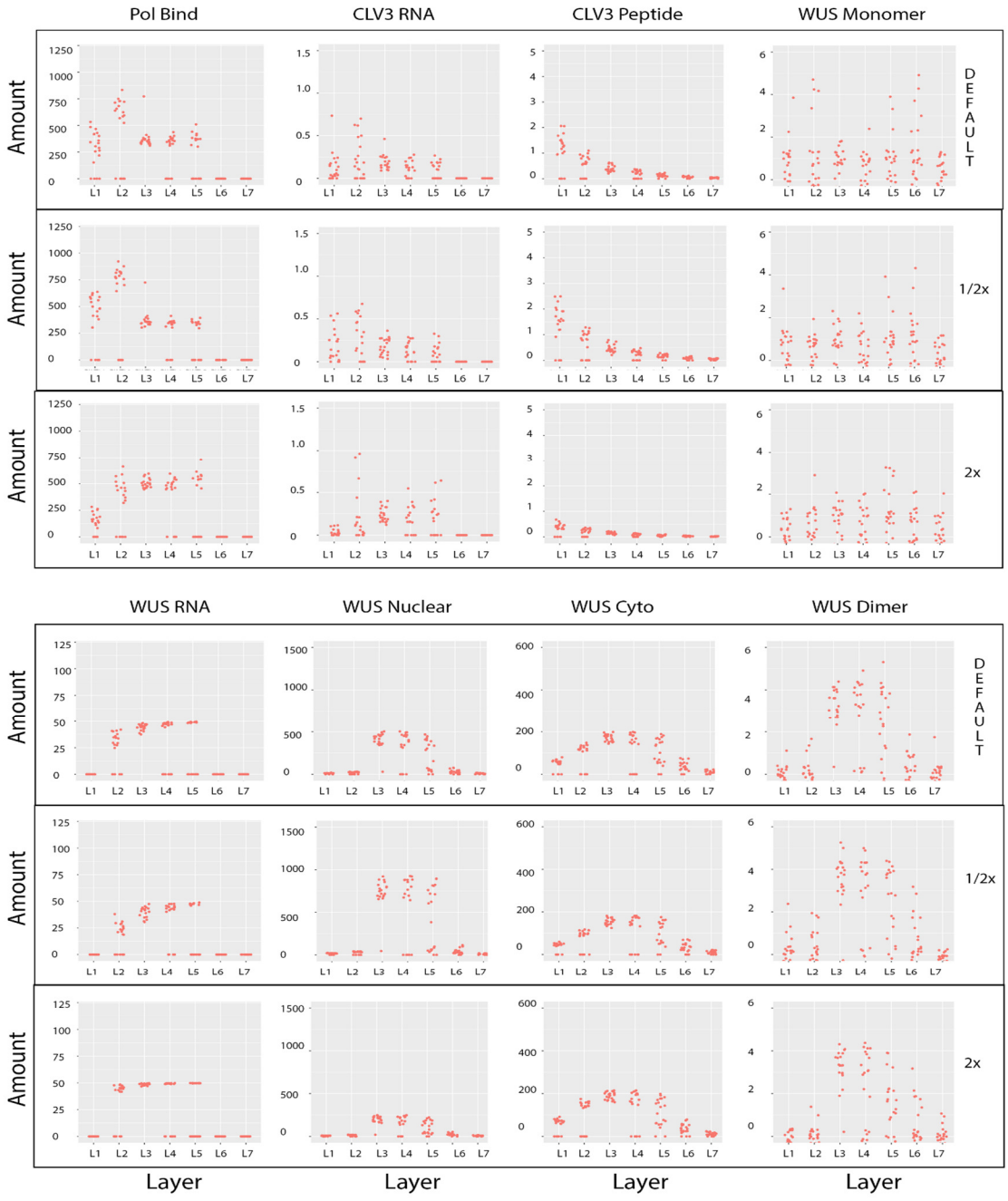

Fig. 2.7. WUS Nuclear Export Perturbation.
Species type at the top. Amount of species is on the y axis. Meristem layer is on the x axis. First row is default parameters. Second row is 1/2x perturbation of selected parameter. Third row is 2x perturbation of selected parameter.

WUSNuc CLV3 interaction perturbations had all major species expression patterns remain very similar to each other across the perturbation interval of 1/2x to 2x in the cells quantified.

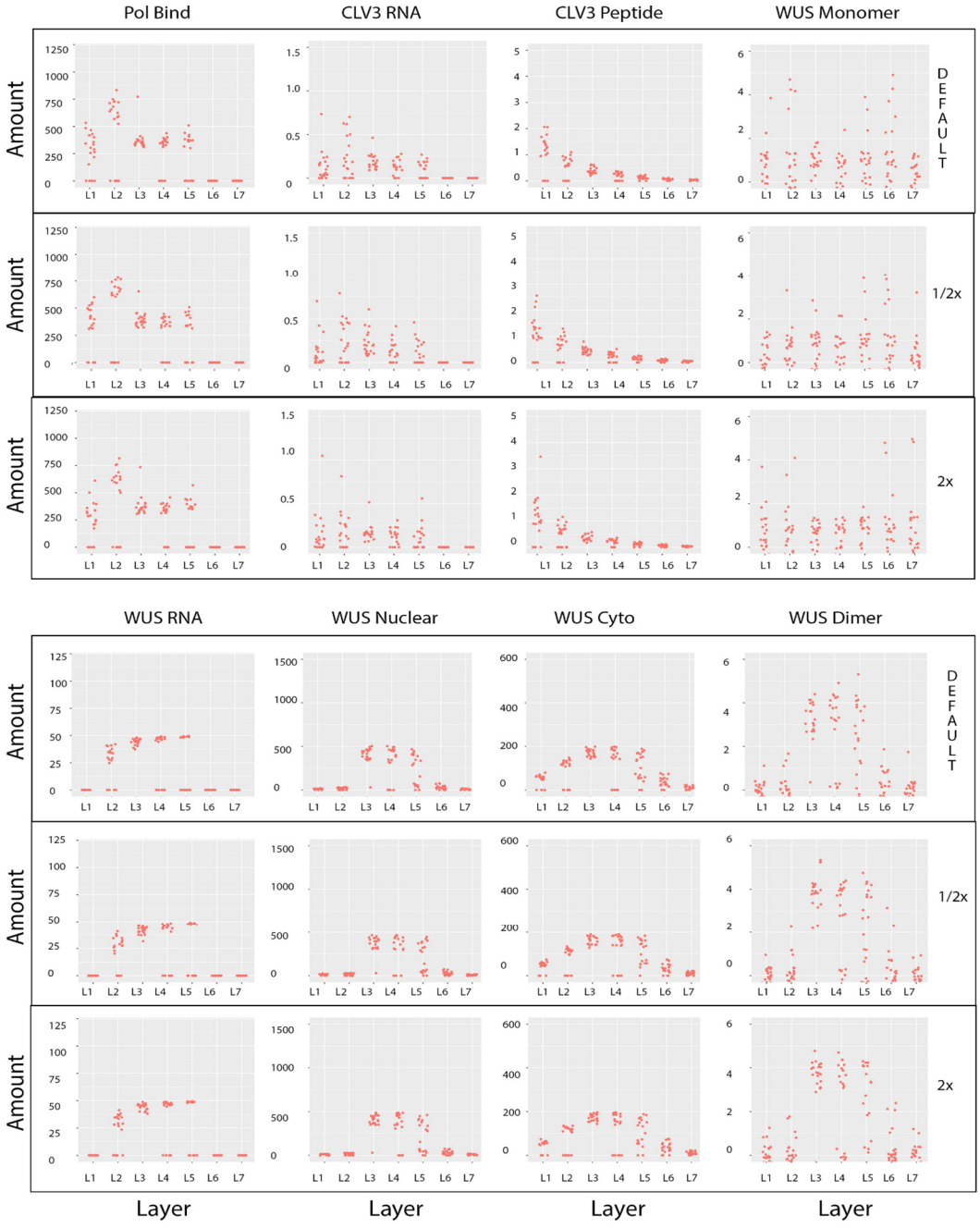

Fig. 2.8. WUS Nuclear/CLV3 Interaction perturbation effects.

WUS Cyto Diffusion effects were mostly significant when perturbing to 2x which lowered polymerase binding in the outer layers and lowered nuclear and cytoplasmic WUS.

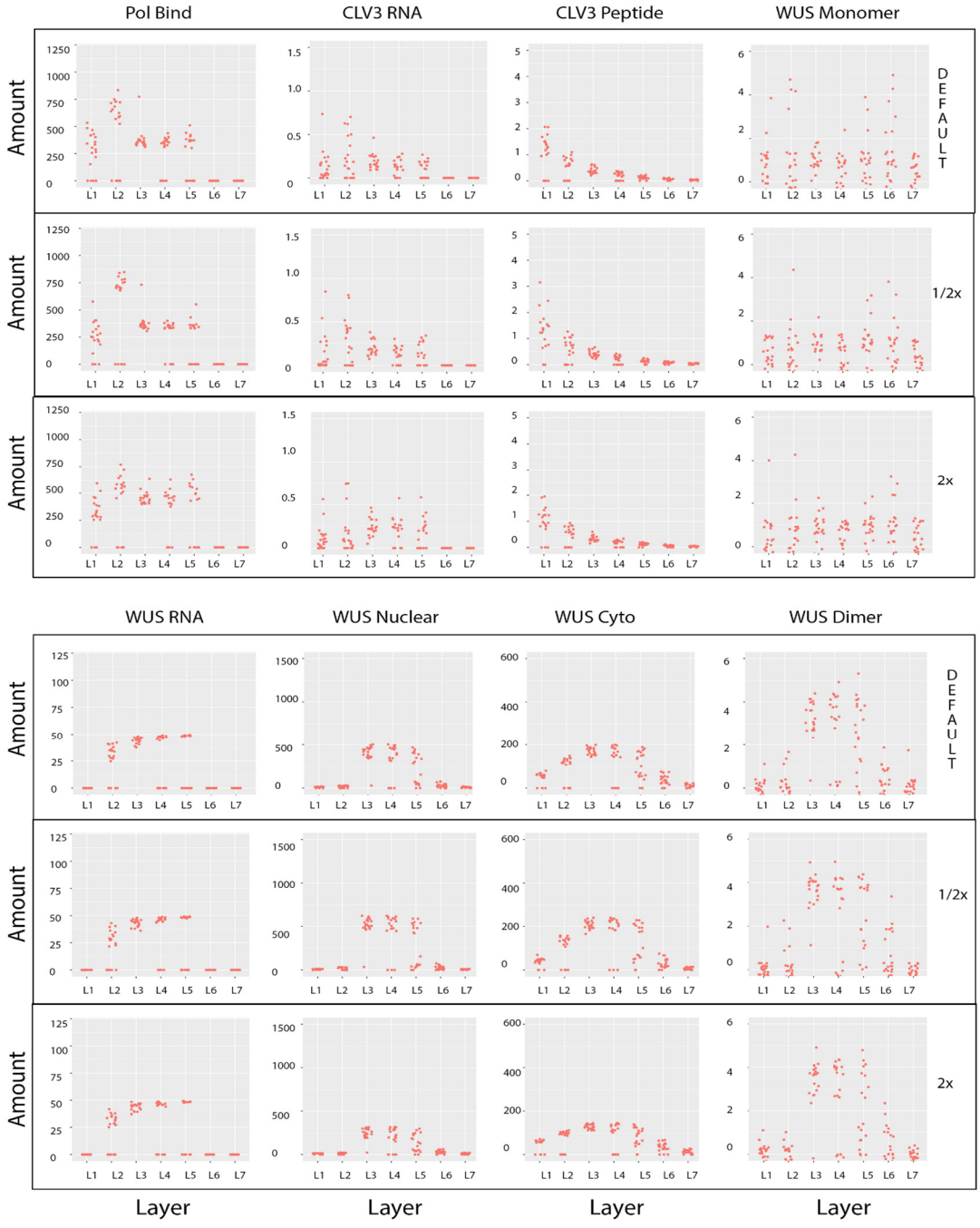

Fig. 2.9. WUS Cytoplasmic Diffusion perturbation effects.

CLV3 RNA WUS Saturation is the threshold of WUS that has the maximum effect on the system. Any higher WUS has no additional effect. Increasing this parameter lowers the effect of WUS. Perturbations in this parameter had slight effects at 1/2x. At 2x polymerase binding was lowered in the outer layers but increased in the inner layers. *CLV3 RNA* was lowered in the outer layers and CLV3 peptide was lowered as well. *WUS RNA* production was increased along with slightly increased WUS protein showing the indirect effect the lowered CLV3 was having.

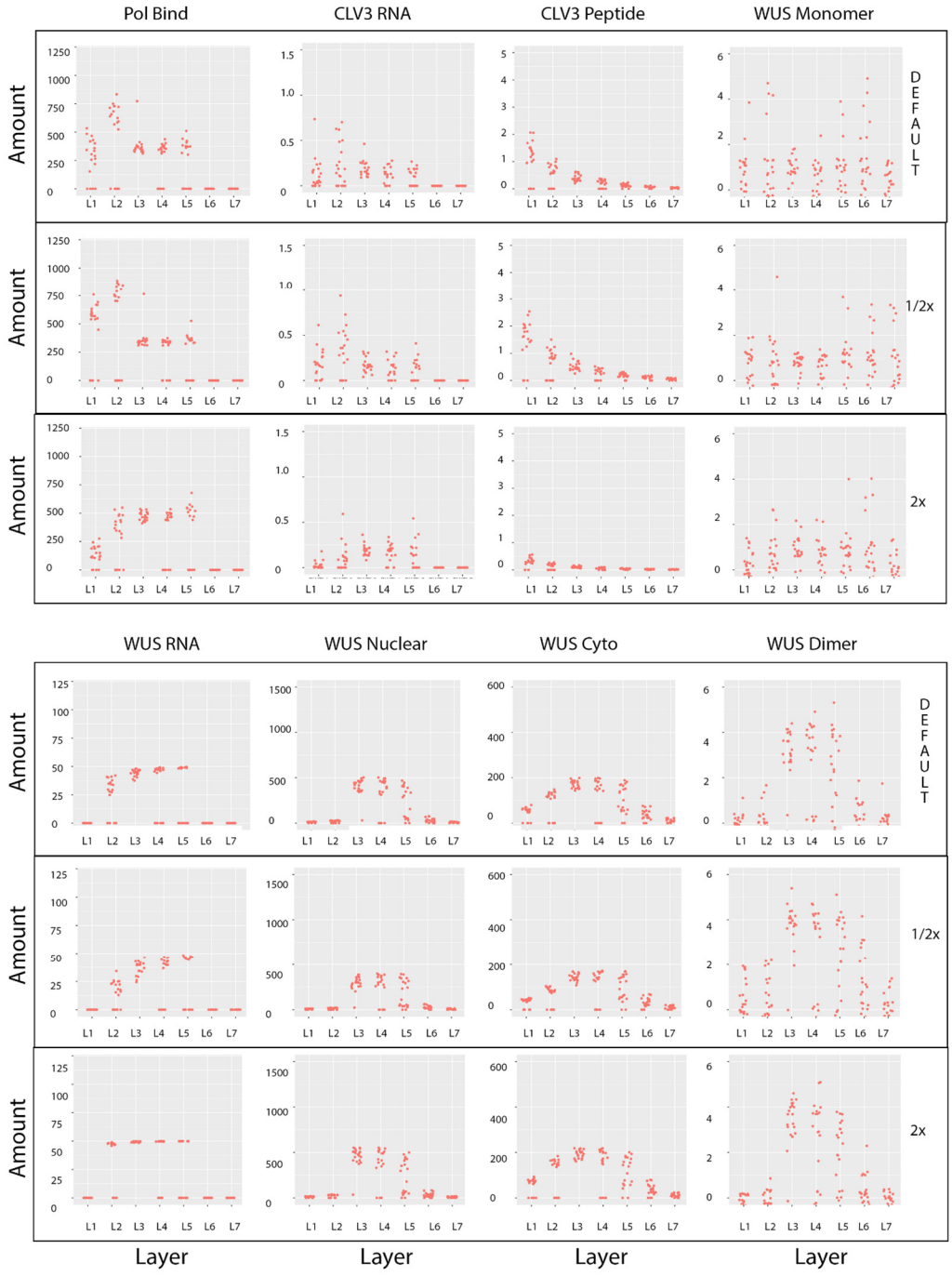

Fig. 2.10. CLV3/WUS Saturation perturbation effects

For CLV3 Peptide production only relatively small differences between the perturbations were noticed.

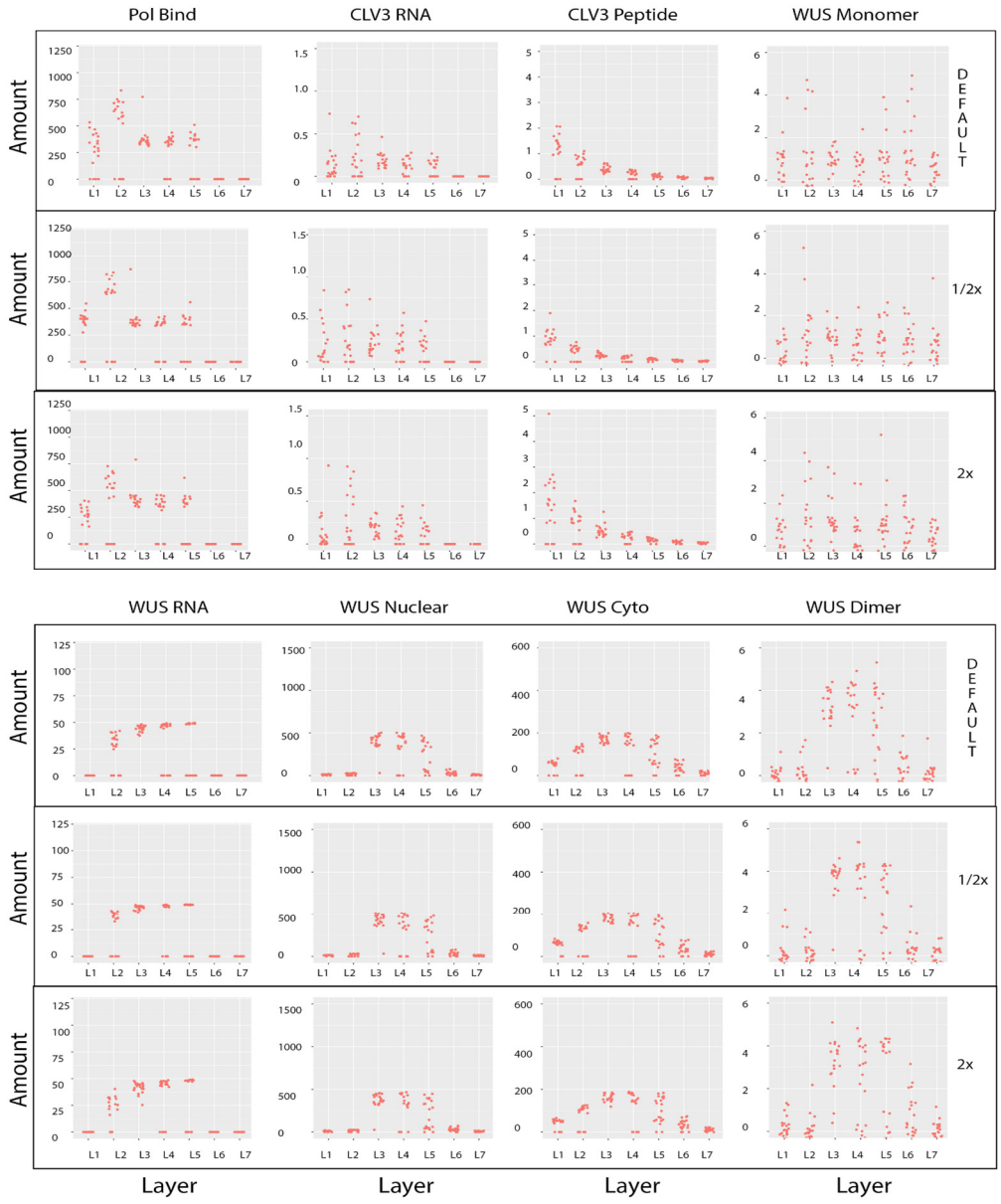

Fig. 2.11. CLV3 peptide production perturbation effects.

Cooperativity in the Coupled Feedback Model

Similar to Chp1, in the non feedback model, the cooperativity of the coupled feedback model was tested with a variety of combinations of monomer and dimer cooperativity. Monomer cooperativity was varied from 1 to 0.005 and dimer cooperativity varied from 1 to 0.05. A lower number means higher cooperativity where the monomer/dimer more strongly reduces its neighbor's chance to unbind. The number corresponds to the percentage neighboring WUS's chances to unbind are reduced (0.05 means unbinding reduced to 5%). As seen in Fig. 2.12, increasing monomeric cooperativity led to slight increases in RNA production at higher dimer cooperativity in the outer layers. Dimer cooperativity on the other hand tended to push the inner layers down while leaving the outer layers more elevated. Like the non feedback model the feedback model sees the monomeric cooperativity affecting the levels of production while the dimeric cooperativity affects the shape of the graph.

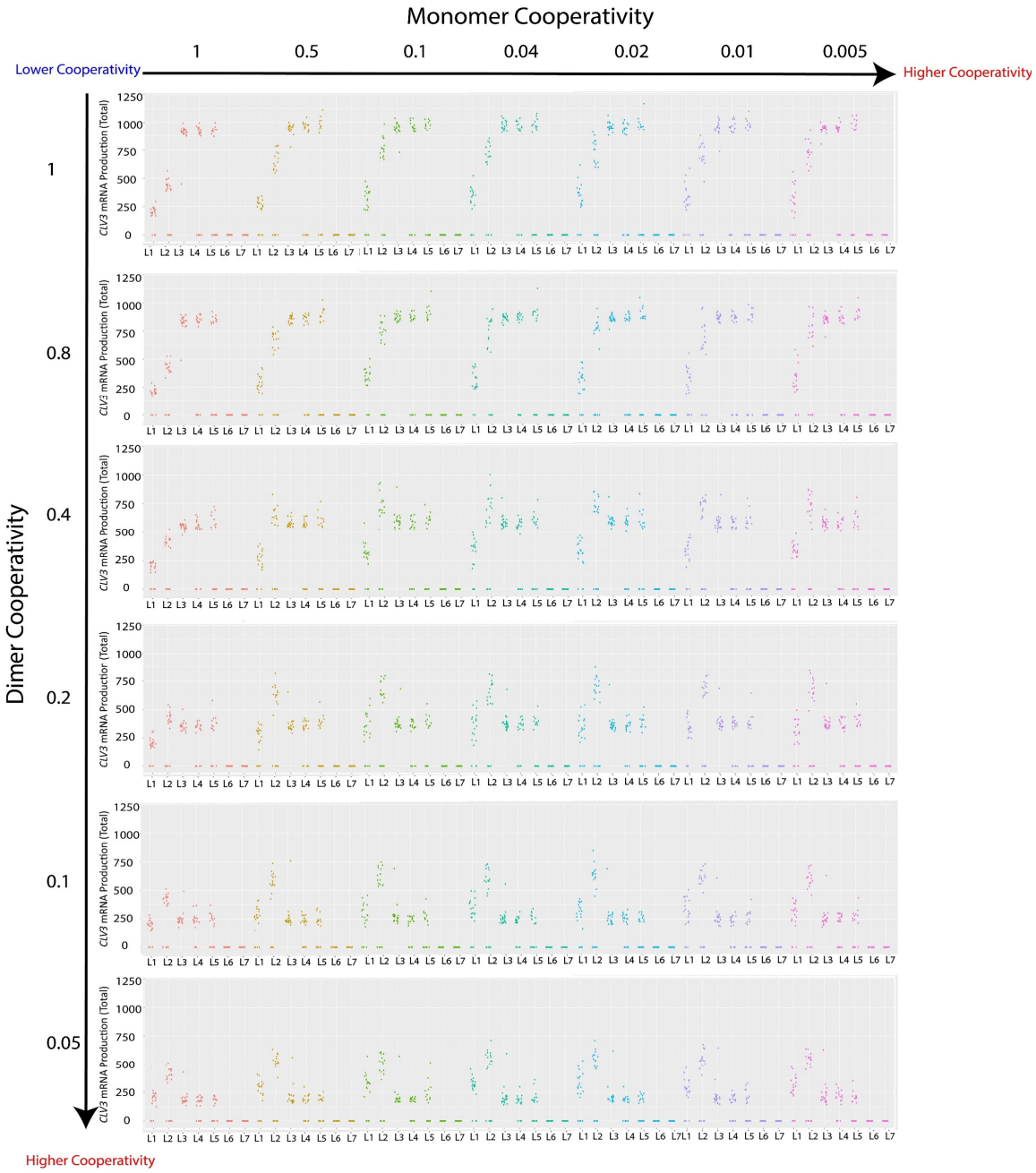

Fig. 2.12. Independent perturbations of the monomer or dimer cooperativity.
The effect of changes in monomer cooperativity (from 1 to 0.005) and dimer cooperativity (from 1 to 0.05) on CLV3 activation. The direction of the arrows indicate an increase in cooperativity. The result for each combination of monomer and dimer cooperativity value is represented by the graph at their intersection. The individual graphs represent the CLV3 activation in different cell layers (L1 to L7) of simulated SAMs under the cooperativity levels noted for each simulation. The dots represent the values of the CLV3 signal for individual simulated cells.

Discussion

The next step after laying out the behavior of the CLV3 CRM and the nature of the concentration dependent mechanism which controls its expression is to determine how it fits into the overall WUS/CLV3 signaling network and how the plant maintains the balance between all the interdependent species. Although the feedback model is still being refined and does not match up completely with preliminary experimental data it has still given a more complete picture about how WUS Species affect targets and are affected in a variety of mutant conditions.

When comparing the CLV3 expression of mutants with less and less cis-elements (from WT to *970M* to *DM* to *970i* for example) the results are similar to the non feedback model with expression retreating to the inner layers (Fig. 2.2C). The major difference between the non feedback and feedback model is the lowering of the CLV3 species except in certain mutants such as *970M4* and *950i*. What is observed in *970M4* may be signs of the system resetting where lower CLV3 leads to increased WUS which ends up at least partially restoring some *CLV3* expression to a level higher than might be expected from the non feedback model.

The increase in feedback model expression is seen in *950i* which is an especially weak mutant and *970M4* which is an especially strong mutant. In *970M4* this is possibly due to the CLV3 reducing the excessively large amount of WUS that would otherwise reduce expression. In the case of *950i* this mutant is so weak, WUS that would normally repress expression in other mutants becomes activating in the inner layers creating CLV3. The chain of events where CLV3 affects WUS which feeds back into an effect on CLV3 is the

mechanism by which resetting is believed to occur. However preliminary experimental results show resetting across all mutants in corresponding wet lab studies complementing *clv3-2* mutants, so the model may need further adjustment to increase the strength of the effect.

Perturbing the different species in the model mostly went as expected and showed the interaction pathways between the species working as designed. Lowering *WUS RNA* production lowered the concentration of all WUS species (Fig. 2.5). Increasing WUS Nuclear Export lowered *CLV3* production in the outer layers (Fig. 2.7). In other cases the perturbation effects were more muted than expected. Adjusting WUS Nuclear/CLV3 interaction for example had little change across all the species whether perturbing to 1/2x or 2x (Fig 2.8). It is possible that in the parameter space the range of perturbation for this particular parameter is not significant. For other parameters such as 2x increased *WUS RNA* production not leading to 2x WUS Cytoplasmic across all layers, this is due to other factors like the model parameters of the simulated SAM not having production in the outer layers. Perturbations have been only systematically carried out in wild-type so far but eventually mutant studies may allow more insight into how the species respond and contribute to the evolution of the system in non-WT situations.

The contribution of cooperativity and by extension monomers and dimers to shaping expression appears to be the same between feedback and non feedback models. Though the RNA expression patterns in the feedback model are different, increasing monomer cooperativity leads to an increase in expression in both models. And

increasing dimer cooperativity, shapes the graph by pushing the inner layers down in relation to the outer layers. The role of monomers and dimers does not change which is expected as there wouldn't be any reason for them to do so in the switch to the feedback system.

The smaller than expected increase from increasing monomer cooperativity is probably due to the nature of the WUS gradient in the current system setup. In outer layers WUS is too diffuse under most conditions to support high expression, in the inner layers it is too densely concentrated. In effect there is too narrow of a window to see a more pronounced effect of monomer cooperativity across multiple layers.

Methods

The Coupled Model

The feedback model can be seen as an extension of the non feedback model presented in Chp1. The CLV3 dynamics of the non feedback model was coupled to WUS dynamics which not only affect but are now affected by the CLV3 dynamics. Fig. 2.13 provides an overall schematic of the data flow of the model. The base data processing structure is carried over from an earlier model (1) but with new dynamics. The model can be divided into 4 major parts as annotated in the figure. In Fig. 2.13A, input from the commandline is read in and some initial setup functions are started. In Fig. 2.13B, the model file which contains the vast majority of the information about the species, reactions, and parameter values which define the simulation as well as the Init file which defines the initial state of the cells in the simulation are read in. Fig. 2.13C involves the setup of the numerical solver which handles the updating of the cell states throughout the running of the

simulation as well as reading in the parameter file with parameters for the solver. Fig. 2.13D, contains the setup for and the main simulation loop which is where the simulation runs its time course. Finally output to the results file and printing out debug information takes place during and after the simulation loop. Simulations are run for the same time as the non feedback model.

.

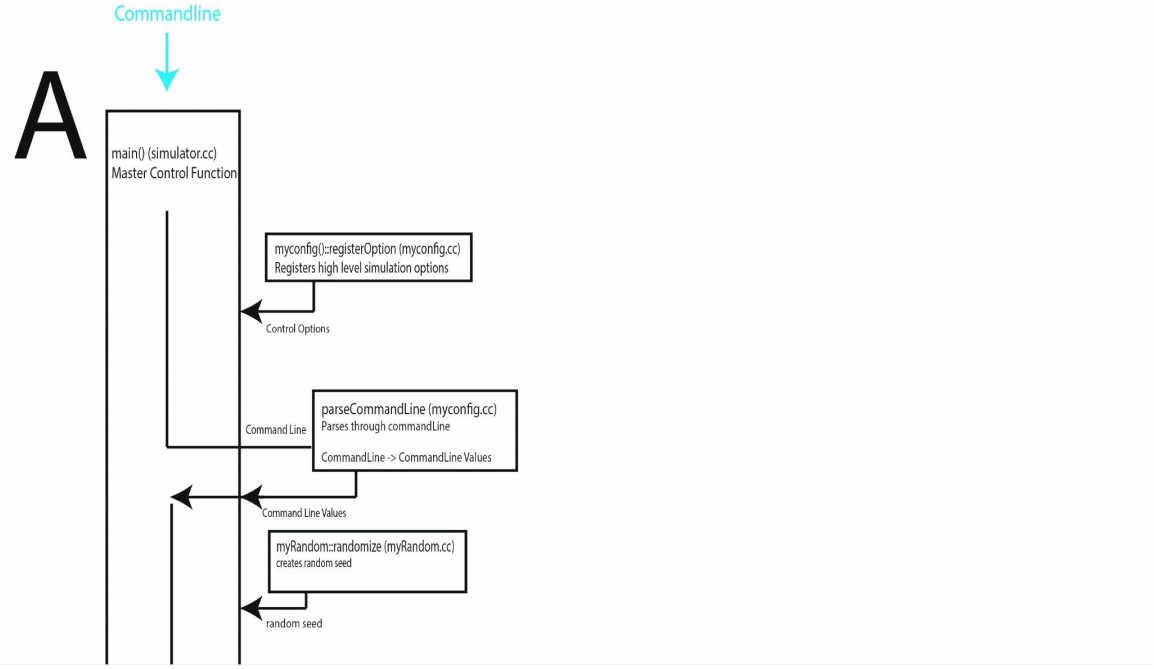
A
Commandline
main() (simulator.cc)
Master Control Function
myconfig()::registerOption (myconfig.cc)
Registers high level simulation options
Control Options
Command Line
parseCommandLine (myconfig.cc)
Parses through commandLine
CommandLine -> CommandLine Values
Command Line Values
myRandom::randomize (myRandom.cc)
creates random seed
random seed

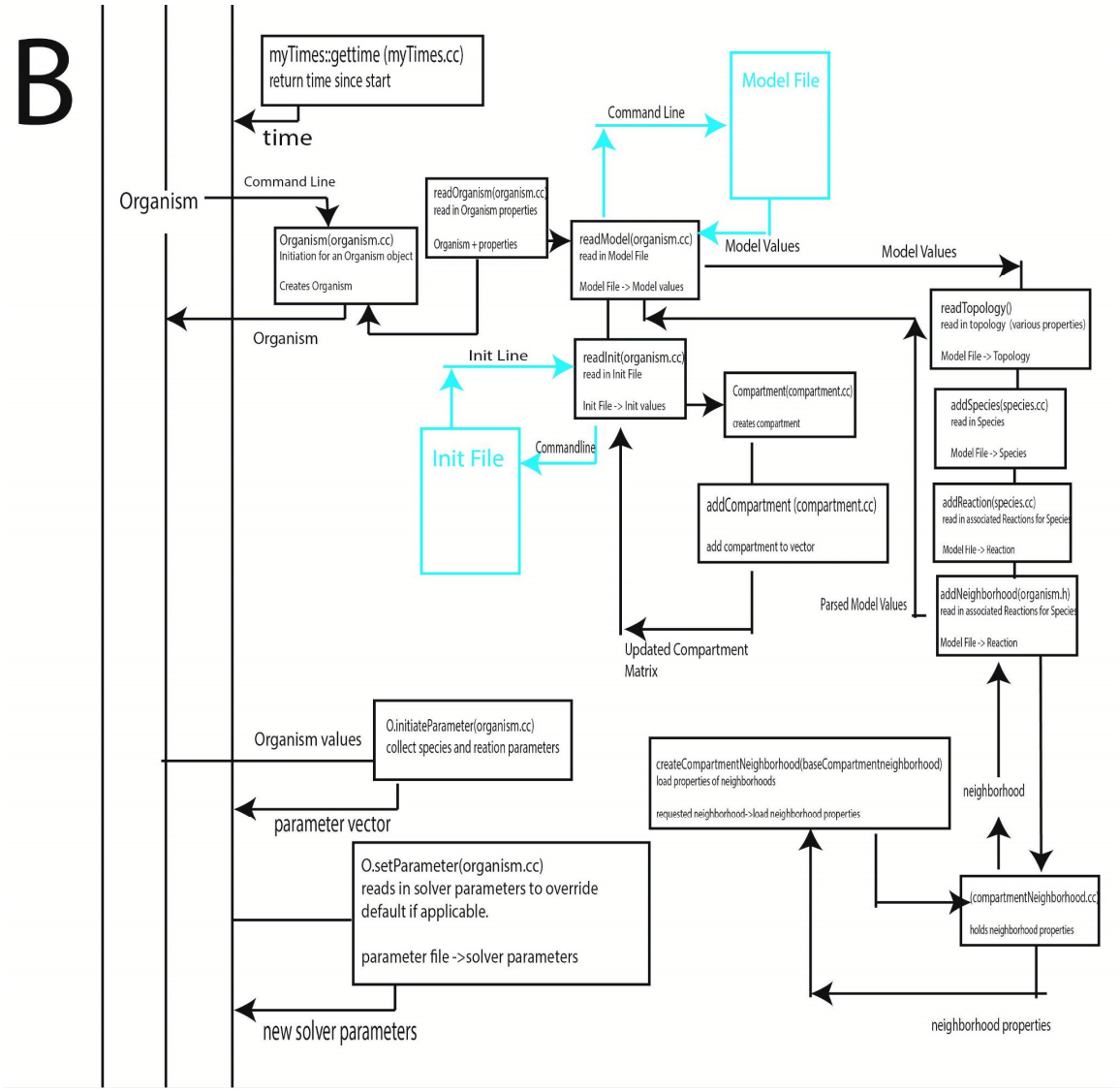
B
myTimes::gettime (myTimes.cc)
return time since start
time
Organism
Command Line
Organism(organism.cc)
Initiation for an Organism object
Creates Organism
Organism
readOrganism(organism.cc)
read in Organism properties
Organism + properties
Command Line
Model File
readModel(organism.cc)
read in Model File
Model File -> Model values
Model Values
Model Values
readTopology()
read in topology (various properties)
Model File -> Topology
Init Line
readInit(organism.cc)
read in Init File
Init File -> Init values
Compartment(compartment.cc)
creates compartment
addSpecies(species.cc)
read in Species
Model File -> Species
Init File
Commandline
addCompartment (compartment.cc)
add compartment to vector
addReaction(species.cc)
read in associated Reactions for Species
Model File -> Reaction
Parsed Model Values
addNeighborhood(organism.h)
read in associated Reactions for Species
Model File -> Reaction
Updated Compartment
Matrix
Organism values
O.initiateParameter(organism.cc)
collect species and reation parameters
parameter vector
createCompartmentNeighborhood(baseCompartmentneighborhood)
load properties of neighborhoods
requested neighborhood->load neighborhood properties
neighborhood
O.setParameter(organism.cc)
reads in solver parameters to override
default if applicable.
parameter file ->solver parameters
new solver parameters
compartmentNeighborhood.cc
holds neighborhood properties
neighborhood properties

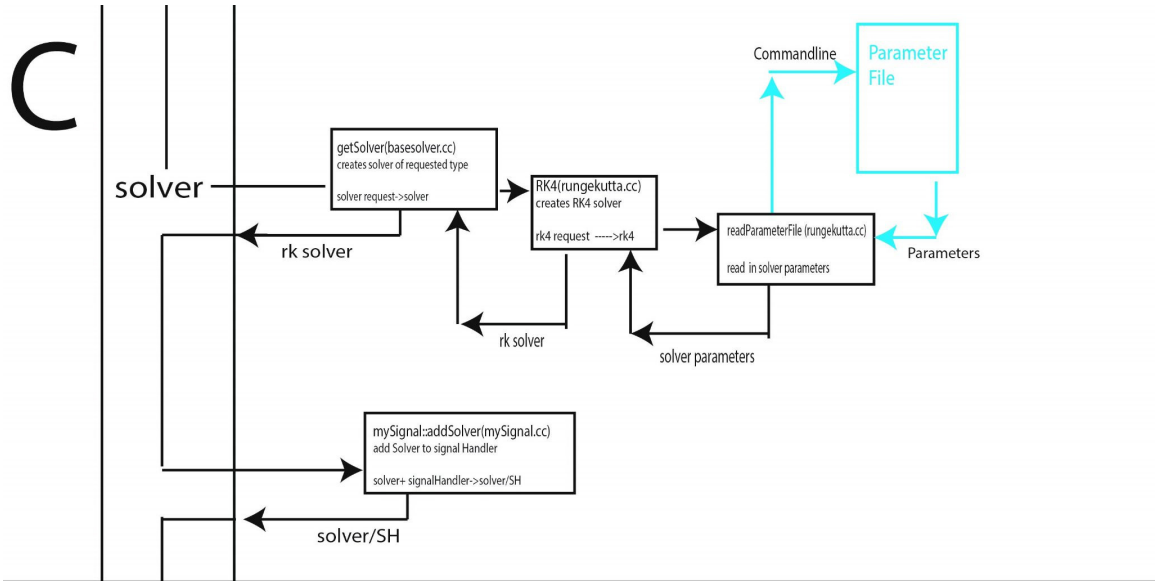
C
solver
getSolver(basesolver.cc)
creates solver of requested type
solver request->solver
rk solver
RK4(rungekutta.cc)
creates RK4 solver
rk4 request ----->rk4
rk solver
readParameterFile (rungekutta.cc)
read in solver parameters
solver parameters
Commandline
Parameter File
Parameters
mySignal::addSolver(mySignal.cc)
add Solver to signal Handler
solver+ signalHandler->solver/SH
solver/SH

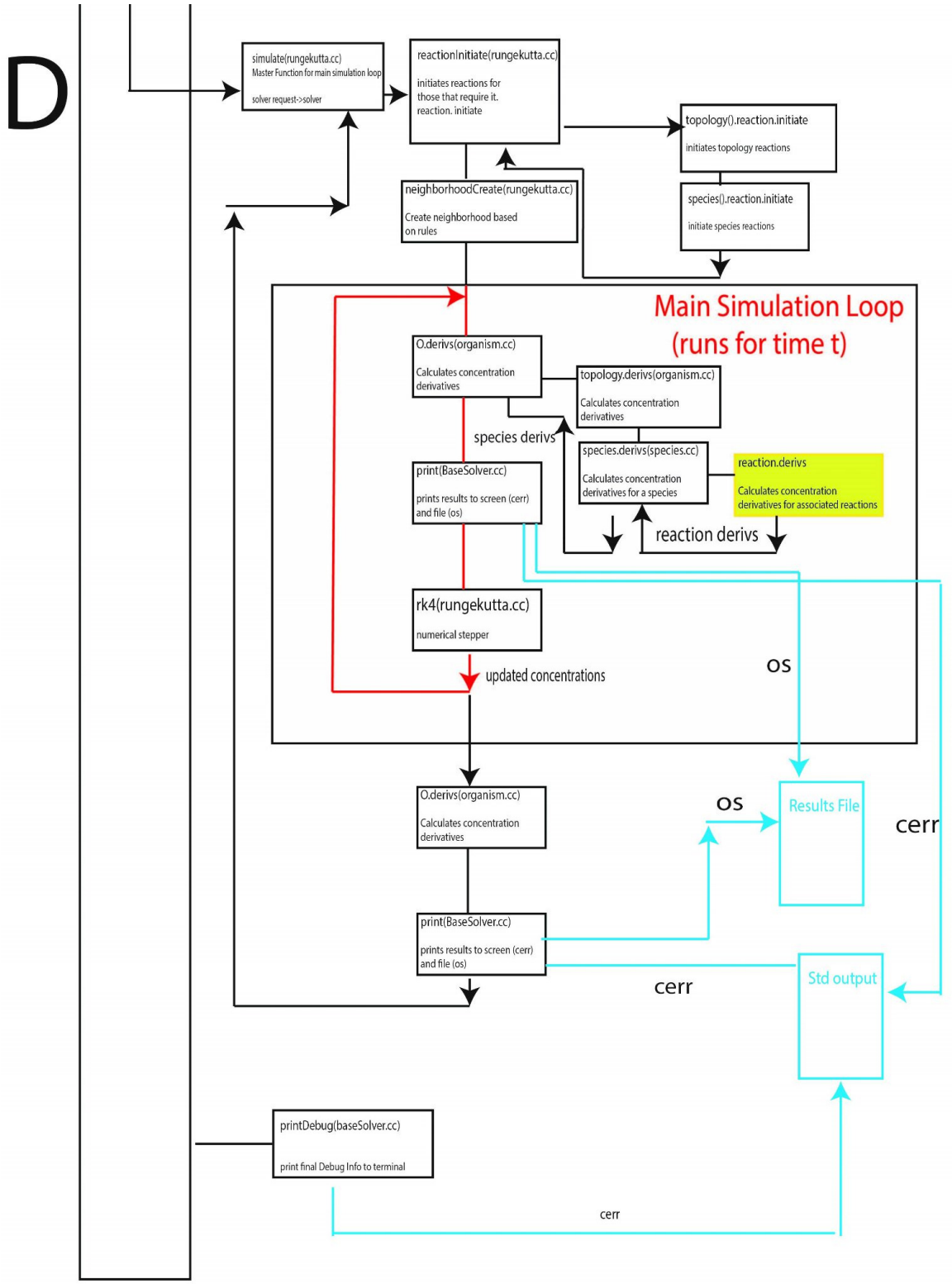
D
simulate(rungekutta.cc)
Master Function for main simulation loop
solver request->solver
reactionInitiate(rungekutta.cc)
initiates reactions for those that require it. reaction. initiate
topology().reaction.initiate
initiates topology reactions
species().reaction.initiate
initiate species reactions
neighborhoodCreate(rungekutta.cc)
Create neighborhood based on rules
Main Simulation Loop (runs for time t)
O.derivs(organism.cc)
Calculates concentration derivatives
topology.derivs(organism.cc)
Calculates concentration derivatives
species derivs
species.derivs(species.cc)
Calculates concentration derivatives for a species
reaction.derivs
Calculates concentration derivatives for associated reactions
reaction derivs
print(BaseSolver.cc)
prints results to screen (cerr) and file (os)
rk4(rungekutta.cc)
numerical stepper
updated concentrations
os
O.derivs(organism.cc)
Calculates concentration derivatives
os
Results File
cerr
print(BaseSolver.cc)
prints results to screen (cerr) and file (os)
cerr
Std output
printDebug(baseSolver.cc)
print final Debug Info to terminal
cerr

Fig. 2.13. Data flow outline of the Feedback Model
Programmatic diagram of the feedback model. **(A)** Initial set up of the model functions. **(B)** Loading the main model parameters and initial values of the system. **(C)** Setting up the numerical solver and loading the solver parameters. **(D)** Running the simulation loop and generating output.

The Protein and RNA dynamics of the simulation evolve in a deterministic stepwise manner over a predetermined time. The dynamics are controlled by a set of ODEs for each species tracked in the simulation and are shown in Fig. 2.14. The equations and by extension the behavior of each of the species are controlled by the species variables and a set of parameters as shown in Fig. 2.15. The ODEs update the species concentration at each time step evolving the concentrations in the cells over the simulation. The system tracks several species. These are as follows.

WUSRNA: Represents the transcribed RNA of the *WUS* gene. The equation of *WUSRNA* is created and decayed by the terms indicated in Fig 2.14. Generation is limited to a region in the interior of the SAM bounded by *underL1Thickness* and *WUSRNAbarrier* on the z axis and *wusRNASourceWidth* on the x/y axis. *WUSRNA* is necessary to generate WUS protein.

WUS Protein: WUS protein is generated in the cytoplasm of simulated cells. WUS protein comes in two forms which are tracked as separate species. WUSNuc and WUSCyto.

WusNuc: WUSNuc represents the fraction of WUS protein confined to the nucleus of the cell and capable of directly interacting with the DNA of the target *CLV3*. WUSNuc is imported from the cytoplasmic WUS, decays, and can be exported back out into the cytoplasm. WUSNuc affects the production of CLV3 and WUSCyto by being exported. WUSNuc export is modified in cells greater than 7.5 units away from the central base of the SAM.

WUSCyto: WUSCyto is the fraction of WUS protein located in the cytoplasm of the cell. It is the protein that is directly produced from the *WUSRNA* species. It cannot affect

CLV3 directly but can be exported to surrounding cells. WusCyto is produced through *WUSRNA* and decays. WusCyto influences WusNuc by being imported to the nucleus.

CLV3RNA: *CLV3 RNA* represents the RNA of the *CLV3 gene*. It is produced in a cylindrical region governed on the x and y axis by *clv3sourcewidth* and on the z-axis by *clv3 barrier*. Its production is controlled stochastically and influenced by nuclear WUS and it also decays. *CLV3RNA* influences the production of the species CLV3Peptide

CLV3Peptide: This species represents the CLV3 peptide in the system. CLV3 affects both the production of *WUSRNA* and the export of WUSCyto. CLV3 production is modified if it is in layers other than L1.

The feedback system also implements the CK effector of WUS through the species. CK ligand, CK receptor, and CK complex.

CK ligand: The CK ligand influences the production of the CK complex along with the CK receptor by binding together. It is produced in a spherical region defined by *ckLIProdDiameter*.

CK receptor: The CK receptor is an effector field that occupies a spherical region defined by *ckRISourceDiameter*. It combines with CK ligand to create the CK complex.

CK complex: CK complex represents the portion of the CK system which actively influences WUS. IE cytokinin interacting with one of its receptors. It is created from and decays back to CK ligand and receptor. CK complex influences the degradation of cytoplasmic WUS.

A

WUS RNA CONDITION: if (distanceFromCentralAxis <= wusRnaSourceWidth (AND) distanceFromCentralBase < underL1Thickness (AND) distanceFromCentralBase > WUSRNAbarrier)

$$WUSRNA : contribution = \frac{\overset{Production}{wusRnaSourceModP(wusRnaSource)}}{1 + \frac{clv3var}{clv3wusRnaP}^{clv3wusRnaNexp}}$$

wusRNAsource=1 wusRNAsourceP=10

$$WUSRNADegradation : contribution- = \overset{Degradation}{wusRnaDegP} * wusRNAvar$$

B

$$WUSCytoplasmic : contribution = \overset{Production}{wusRNAvar(wusRNAtransP)} - \frac{\frac{\overset{Degradation}{wusCytoDegP*wusCyto}}{1+\frac{clv3var}{clv3IwusCytoP}^{clv3IwusCytoNexp}}}{ckvar * wusCytoICkP + 1} - \overset{Import}{wusCytoINucP} * wusCytoVar + \overset{Export}{wusPIFromNuc}$$

$$WUSCytoplasmicDiffusion : +- Diffusion$$

CLV3 Regulated Diffusion: if neighbor is
L2 and main cell is L1 or neighbor is L3 and main cell is L2

$$Diffusion = \frac{Diffusion}{1+(\frac{clv3var}{diffparam1})^{*}diffparam2}$$

C

WUSNUC Export Condition: if (distanceFromCentralBase GT 7.5) outerLayerExportMod EQ wusNucOuterLayerExportP

$$WUSNuclear : contribution = \overset{Production}{wusRNAvar(wusRNAtransP)} - \frac{\overset{Degradation}{(wusNucDeg)wusNucVar}}{1 + (\frac{wusNucVar}{wusNucStabP})^2} + \overset{Import}{wusPFromCyto} - (\frac{\frac{\overset{Export}{wusNucVar*wusNucICytoP}}{1+outerLayerExportMod*\frac{clv3var}{clv3IwusNucP}^{clv3IwusNucNexp}}}{(ckvar)wusNucICkP + 1}) \quad (5)$$

D

CKLgand Condition: if (distanceFromGradientCenter < ckLIProdDiameter)

$$CKLigand : contribution = \overset{Production}{(ckLIProdP * ckLISourceP)}(2.718^{ckLISpatialMod})$$

$$CKLigandDegradationandExport/Import : contribution+ = \overset{Degradation}{(ckLIDegP * ckLigandVar(-1)} - \overset{Association}{(newAssCk)} + \overset{Disassociation}{(newDissCk)}$$

$$CKLigandDiffusion : +- Diffusion$$

E

$$CKComplex : contribution = \overset{Association}{(newAssCk)} - \overset{Disassociation}{(newDissCk)} - \overset{Degradation}{ckCIDegP(ckCvar)}$$

F

CK Receptor Condition: if (distanceFromGradientCenter < ckRISourceDiameter)

$$CKReceptor : contribution = \overset{Production}{ckRIProdP} + \overset{Disassociation}{newDissCk} - \overset{Association}{newAssCk} - \overset{Degradation}{ckRIDegP} * ckRvar$$

$$CKDIS : newDissCk = ckRIComplexDissP * ckRIckComplexVar;$$

$$CKASS : newAssCk = ckRIComplexAssP * ckRVar * ckRILigandVar;$$

G

$$CLV3Peptide : contribution = (clv3RnaSource * clv3PeptideProdP)$$

$$CLV3PeptideDegradation : contribution- = clv3PeptideDegP * clv3Pvar$$

Peptide Effect Condition: if (distanceFromCentralBase<8.5)

$$CLV3PeptideEffectiveness : contribution = contribution * innerLayerEffectiveness$$

$$CLV3PeptideDiffusion : +- Diffusion$$

H

CLV3 Condition: if (distanceFromCentralAxis<=clv3SourceWidth AND zvar>=clv3Barrier)

$$CLV3Activation : contribution = clv3Creation$$

$$CLV3Degradation : clv3Decay = clv3Var * clv3DecayParameter;$$

Fig. 2.14. Equation system of the Feedback Model.
Equations for the simulated species of the feedback model. **(A)** WUS RNA equations **(B)** WUS Cytoplasmic equations. **(C)** WUS Nuclear equations **(D)** CK Ligand equations. **(E)** CK Complex equations **(F)** CK Receptor equations. **(G)** CLV3 Peptide equations. **(H)** CLV3 RNA equations.

A

WUS RNA
Wus RNA Dynamics
1 #WusRNASource (WUS RNA Production Rate)
5 #wusRnaSourceModP (WUS RNA Production Parameter)
0.1 #WusRnaDegP (WUS Degradation Rate)
1 #clv3wusRnaP (WUS RNA/CLV3 Interaction Parameter)
2 #Clv3wusRnaNexp (WUS RNA/CLV3 Interaction Exponent)
3.0 #wusRnaSourceWidth (WUS RNA Width of Expression Domain)
8.5 #underL1Thickness (Expression Domain Top Height)
5.5 #wusRnaBarrier (Expression Domain Bottom Height)
0 #wusRna_Freeze (Freeze WUS RNA Dynamics)
0 #WusRna_X (cell x coordinate)
1 #WusRna_Y (cell y coordinate)
2 #WusRna_Z (cell z coordinate)
8 #clv3var (CLV3 peptide reference: Location not concentration value)

B

WUS Nuclear
WUS Nuc Dynamics
0 # wusRNAtransP (WUS Nuclear Translation Rate)
0.5 #wusNucDegP (WUS Nuclear Degradation Rate)
7 #clv3IWusNucP (WUS Nuclear/CLV3 Interaction Parameter)
2 #clv3IWusNucNexp (WUS Nuclear/CLV3 Interaction Exponent)
0.1 #wusPfromCyto (WUS Import to Nucleus)
0 #wusNuc_Freeze (Freeze WUS Nuclear Dynamics)
0.4 #wusNucICkP (WUS Nuclear/Cytokinin Interaction Parameter)
1.0 #wusNucOuterLayerExportP (Outer Layer export parameter (0 disables CLV3 Effect on L1 export))
100 #wusNucStabP (WUS Nuclear Self Stabilization Parameter)
0 #wusn_X (cell x coordinate)
1 #wusn_Y (cell x coordinate)
2 #wusn_Z (cell x coordinate)
4 #wusRNAvar (WUS RNA Reference)
8 #clv3var (CLV3 Peptide Reference)
6 #WusNuc_WusCyto (WUS Cytoplasmic Reference)
18 #ckvar (Cytokinin Complex Reference)

C

WUSCyto Cytoplasmic
wUSCyto Dynamics
3.5 #wusRnaTransP (WUS Cytoplasmic Translation Rate)
0.1 #wusCytoDegP (WUS Cytoplasmic Degradation Rate)
0.5 #wusCytoINucP (WUS Import to Nucleus)
10 #clv3IwusCytoP (WUS Cytoplasmic/CLV3 Interaction Parameter (Degradation))
2 #clv3IwusCytoNexp (WUS Cytoplasmic/CLV3 Interaction Exponent (Degradation))
0 #wusCyto_Freeze (Freeze WUS Cytoplasmic Dynamics)
0.4 #wusCytoICkP (WUS Cytoplasmic/Cytokinin Interaction Parameter)
4 #wusRNAvar (WUS RNA Reference)
5 #wusCyto_WusNuc (WUS Nuc Reference)
8 #clv3var (CLV3 Peptide Reference)
18 #ckvar (Cytokinin Complex Reference)
WusC Diffusion
0.2 #wusCyto_diffusionP (WUS Cytoplasmic Diffusion Parameter)
1 #wusCyto_diffparam1 (Diffusion Modification Parameter)
5 #wusCyto_diffparam2 (Diffusion Modification Parameter)
0 #WusRna_X (cell x coordinate)
1 #WusRna_Y (cell y coordinate)
2 #WusRna_Z (cell z coordinate)
8 #clv3var (CLV3 peptide reference: Location not concentration value)

D

CkLigand
CkLigand Dynamics
1 #ckLISourceP (Cytokinin Ligand Production Rate)
3 #ckLIProdP (CkL Production Parameter)
0.1 #ckLIDegP (CkL Degradation Rate)
5 #ckL_GradientCenterHeight (Height of CkL gradient)
14 #ckLIProdDiameter (Diameter of CkL gradient)
0 #ckL_x (cell x coordinates)
1 #ckL_y (cell y coordinates)
2 #ckL_z (cell z coordinates)
CkL Diffusion 1 0
0.5 #ckL_diffusionP (ckL diffusion rate)

E

CkComplex
ckComplex Dynamics
0.1 #ckCIDegP (ck Complex Degradation Rate)
0 #ckC_x (cell x coordinates)
1 #ckC_y (cell y coordinates)
2 #ckC_z (cell z coordinates)

F

Cytokinin Receptor
Cytokinin Receptor Dynamics
1 #ckR_SourceP (CkR Production)
3 #ckRISourceDiameter (Diameter of CkR gradient)
5 #ckR_GradientHeight (Height of CkR gradient)
3 #ckRIProdP (CkR production rate)
0.1 #ckRIDegP (CkR Degradation)
0.1 #ckRIComplexAssP (CkR Binding Rate)
0.1 #ckRIComplexDissP (CkR Unbinding Rate)
4 #ckR_GradXaxe (ckR Gradient x dimension)
4 #ckR_GradYaxe (ckR Gradient y dimension)
3 #ckR_GradZaxe (ckR Gradient z dimension)
0 #ckR_x (cell x coordinates)
1 #ckR_y (cell y coordinates)
2 #ckR_z (cell z coordinates)
17 #ckRILigandVar (ckLigand Reference)
18 #ckRIckComplexVar (ckComplex Reference)

G

CLV3_Peptide
2 #clv3PeptideProdP (CLV3 Peptide Translation Rate)
0.07 #clv3PeptideDegP (Degradation Rate)
0 #clv3Peptide_Freeze (CLV3 Peptide Dynamics Freeze)
0 #clv3Peptide_ActivationOnlyFlag (Flag for translation only with no accumulation)
0.0 #innerLayerEffectiveness (Parameter for modifying Translation in inner layers)
7 #clv3RnaSource (CLV3 RNA reference)
0 #clv3P_X (cell x coordinate)
1 #clv3P_Y (cell y coordinate)
2 #clv3P_Z (cell z coordinate)
diffusionSimple 1 0
0.1 #clv3Peptide_diffusionP (CLV3 Peptide diffusion rate)

H

CLV3 RNA
CLV3 RNA Dynamics
3.0 #clv3_Clv3P (CLV3 RNA Production Rate)
0.1 #clv3_DecayP param42 (Decay Rate)
1 #clv3_CrmactivityCo (CRM activity rate (speed of CRM activity))
3 #clv3_SourceWidth (CLV3 Expression Gradient Width)
1 #clv3_TimeStep (Size of overall timestep for stochastic purposes)
425 #clv3_WusSatPoint (Saturation point for effect that WUS concentration has on CLV3 binding)
0.01 #clv3_CooptMonEffect (Cooperativity among monomers, less = more binding)
0.20 #clv3_CooptDimEffect (Cooperativity among dimers, less = more binding)
0.1 #clv3_Bind1 (950 CRM binding rate)
0.1 #clv3_Bind2 (970 CRM binding rate)
0.1 #clv3_Bind3 (997 CRM binding rate)
0.1 #clv3_Bind4 (1007 CRM binding rate)
0.1 #clv3_Bind5 (1060 CRM binding rate)
0.096 #clv3_Unbind1 (950 CRM unbinding rate)
0.019 #clv3_Unbind2 (970 CRM unbinding rate)
0.037 #clv3_Unbind3 (997 CRM unbinding rate)
0.057 #clv3_Unbind4 (1007 CRM unbinding rate)
0.12 #clv3_Unbind5 (1060 CRM unbinding rate)
5 #clv3_Barrier (CLV3 gradient bottom height)
8 #clv3_ActivationMech (Activation Mechanism used to convert binding to expression)
0 #clv3_FrozenWUS (Freeze WUS dynamics when binding to CLV3 gene)
0 #clv3_M4Flag (Flag for if mutant has an M4 core)
3 #clv3_HABonusCoopt (Bonus cooperativity for high affinity 970M4 core)
2 #clv3_NeighborOnlyCoopt (Flag for neighbor only cooperativity)
1 #clv3_dimerBonusBindP (Bonus to dimerization)
0.1 #clv3_polBaseBindAffinity (Binding rate of the RNA polymerase)
4 #clv3_polTimeLimit (time till polymerase generates activation)
1000 #clv3_monFireLimit (time monomer can recruit polymerase)
1 #clv3_dimerUnbindP1 (950 Dimer Unbind Modifying Parameter)
1 #clv3_dimerUnbindP2 (970 Dimer Unbind Modifying Parameter)
1 #clv3_dimerUnbindP3 (997 Dimer Unbind Modifying Parameter)
1 #clv3_dimerUnbindP4 (1007 Dimer Unbind Modifying Parameter)
1 #clv3_dimerUnbindP5 (1060 Dimer Unbind Modifying Parameter)
0 #clv3_L1nodimer (disables dimerization in L1)
100 #unbindTimer (unbind timer)
5 #clv3_WusNuc (WUS Nuclear Reference)
0 #clv3_X (cell x coordinate)
1 #clv3_Y (cell y coordinate)
2 #clv3_Z (cell z coordinate)
9 #clv3_StochasticOverflow (overflow Reference)

Fig. 2.15. Equation parameters of the Feedback Model.
Equation parameters for the simulated species of the feedback model in the WT configuration. **(A)** WUS RNA parameters **(B)** WUS Nuclear parameters. **(C)** WUS Cytoplasmic parameters **(D)** CK Ligand parameters. **(E)** CK Complex parameters **(F)** CK Receptor parameters. **(G)** CLV3 Peptide parameters. **(H)** CLV3 RNA parameters.

Stochastic Simulation

In concert with the ODE protein and RNA system the second part of the simulation is the stochastic subcellular dynamics modeling the interaction between *CLV3* DNA and WUS protein. This is contained within the reactions.derivs portion of the main simulation loop highlighted in yellow (Fig. 2.14D).

The overall subcellular portion of the simulation is depicted in Fig. 2.16. For clarity this is described in 3 portions. In the first portion Fig. 2.16A; setup for the subcellular loop takes place. In Fig. 2.16B, the event possibilities and timestep are generated and one event selected and the CRM is updated, in Fig. 2.16C, the cleanup steps after the loop is finished take place.

The heart of the subcellular dynamics is the event selection process which is shown in Fig. 2.16B and diagrammed conceptually in Fig. 2.17. As diagrammed, the CRM sites are evaluated based on their status. Either Empty: 0, monomer occupied: 1, or dimer occupied: 2. Depending on this, a different possible set of events are generated as depicted in Fig. 2.17. A random value is generated to select an event from the set which is then used to update the CRM. In a similar fashion the timestep size is updated based on the probability information. The end result is the CRM occupancy evolving over the simulation time.

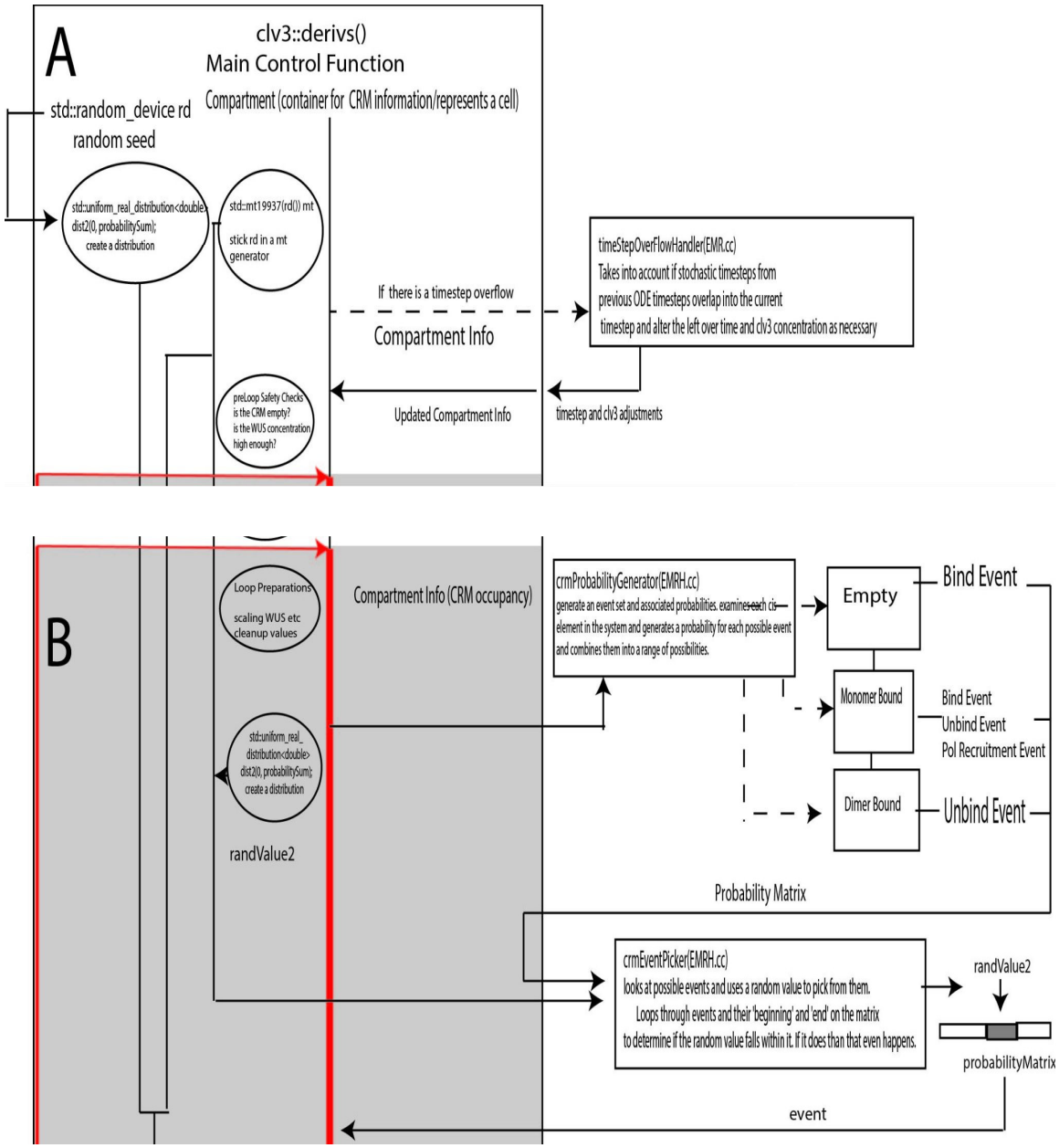
A
clv3::derivs()
Main Control Function
Compartment (container for CRM information/represents a cell)
std::random_device rd
random seed
std::uniform_real_distribution<double>
dist2(0, probabilitySum);
create a distribution
std::mt19937(rd()) mt
stick rd in a mt
generator
If there is a timestep overflow
Compartment Info
timeStepOverFlowHandler(EMR.cc)
Takes into account if stochastic timesteps from
previous ODE timesteps overlap into the current
timestep and alter the left over time and clv3 concentration as necessary
preLoop Safety Checks
is the CRM empty?
is the WUS concentration
high enough?
Updated Compartment Info
timestep and clv3 adjustments
B
Loop Preparations
scaling WUS etc
cleanup values
Compartment Info (CRM occupancy)
crmProbabilityGenerator(EMRH.cc)
generate an event set and associated probabilities. examines each cis-
element in the system and generates a probability for each possible event
and combines them into a range of possibilities.
Empty
Bind Event
Monomer Bound
Bind Event
Unbind Event
Pol Recruitment Event
Dimer Bound
Unbind Event
std::uniform_real_
distribution<double>
dist2(0, probabilitySum);
create a distribution
randValue2
Probability Matrix
crmEventPicker(EMRH.cc)
looks at possible events and uses a random value to pick from them.
Loops through events and their 'beginning' and 'end' on the matrix
to determine if the random value falls within it. If it does than that even happens.
randValue2
probabilityMatrix
event

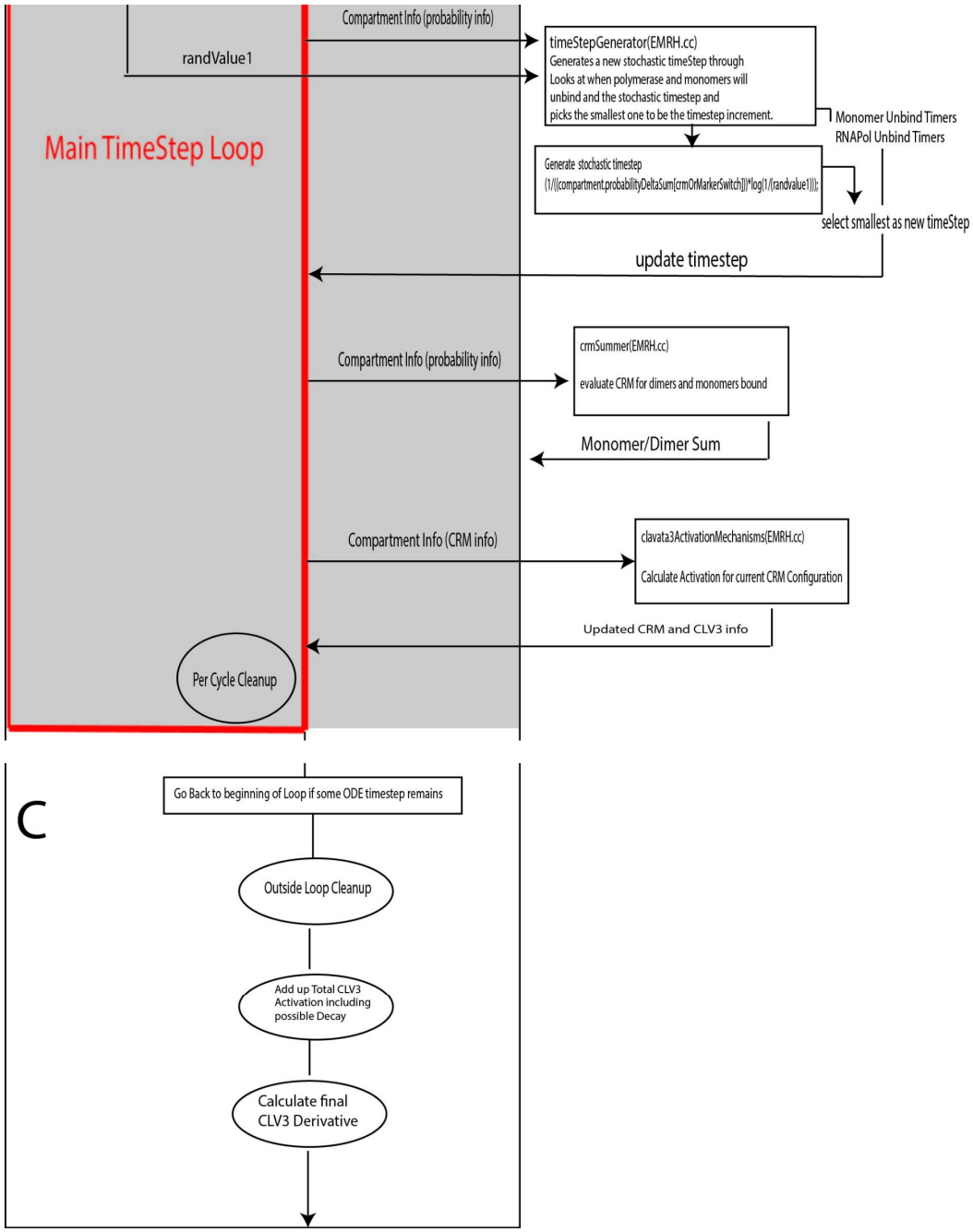
Compartment Info (probability info)
randValue1
timeStepGenerator(EMRH.cc)
Generates a new stochastic timeStep through
Looks at when polymerase and monomers will
unbind and the stochastic timestep and
picks the smallest one to be the timestep increment.
Monomer Unbind Timers
RNAPol Unbind Timers
Main TimeStep Loop
Generate stochastic timestep
(1/[compartment.probabilityDeltaSum[crm0rMarkerSwitch]])*log(1/(randvalue1));
select smallest as new timeStep
update timestep
Compartment Info (probability info)
crmSummer(EMRH.cc)
evaluate CRM for dimers and monomers bound
Monomer/Dimer Sum
Compartment Info (CRM info)
clavata3ActivationMechanisms(EMRH.cc)
Calculate Activation for current CRM Configuration
Updated CRM and CLV3 info
Per Cycle Cleanup
C
Go Back to beginning of Loop if some ODE timestep remains
Outside Loop Cleanup
Add up Total CLV3
Activation including
possible Decay
Calculate final
CLV3 Derivative

Fig. 2.16. Data flow outline of the stochastic simulation loop.
Programmatic outline of the stochastic portion of the feedback model. **(A)** Setup of the stochastic functions. **(B)** Main stochastic loop. **(C)** Data generation and cleanup

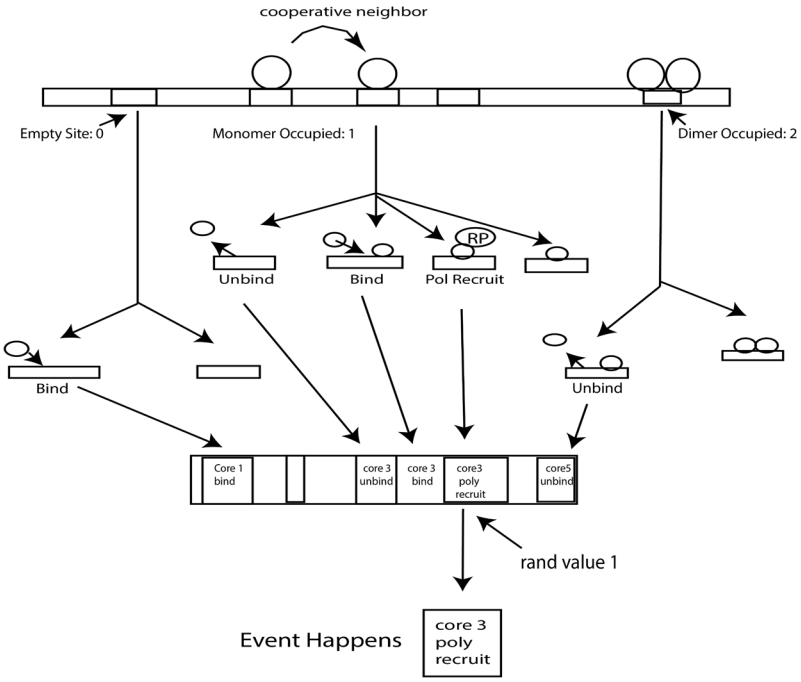

Fig. 2.17. Conceptual outline of stochastic event selection.
The sites of the CRM are evaluated and based on their states, event probabilities are generated. Empty sites can bind a monomer. Monomer occupied sites can unbind, bind and transform into dimer, or recruit a polymerase. Dimer occupied sites can unbind and transform into a monomer. The event probabilities are summed and a random value is used to select the event that occurs.

The ODE and subcellular model are connected and run atop the SAM lattice as shown in Fig 2.18. The simulation moves from cell to cell updating the different species via the ODE model and updating *CLV3 RNA* via the subcellular model.

Mutants and Results Plots

The same CRM mutants used in Chp1 are used in the feedback model simulations. As before, WT is a whole CRM with all cis-elements, 'm' mutants like *970m* and *950m* have one cis-element removed (970 and 950 respectively), *970M4* has a special high affinity 970 site, and intrinsic 'i' mutants like *970i* and *950i* are mutants with all but one cis-

element removed (970 and 950 respectively). *CLV3null* is a mutant with CLV3 peptide production disabled.

Results graphs (Fig 2.2-12) for the different species have expression or dimerization/monomerization amount on the y axis and SAM layer on the x axis. The graphs track cells in the central portion of the SAM. Specifically every cell within 2.5 units of the center of the SAM when viewing it from the top where 8.5 units would be the length to the edge.

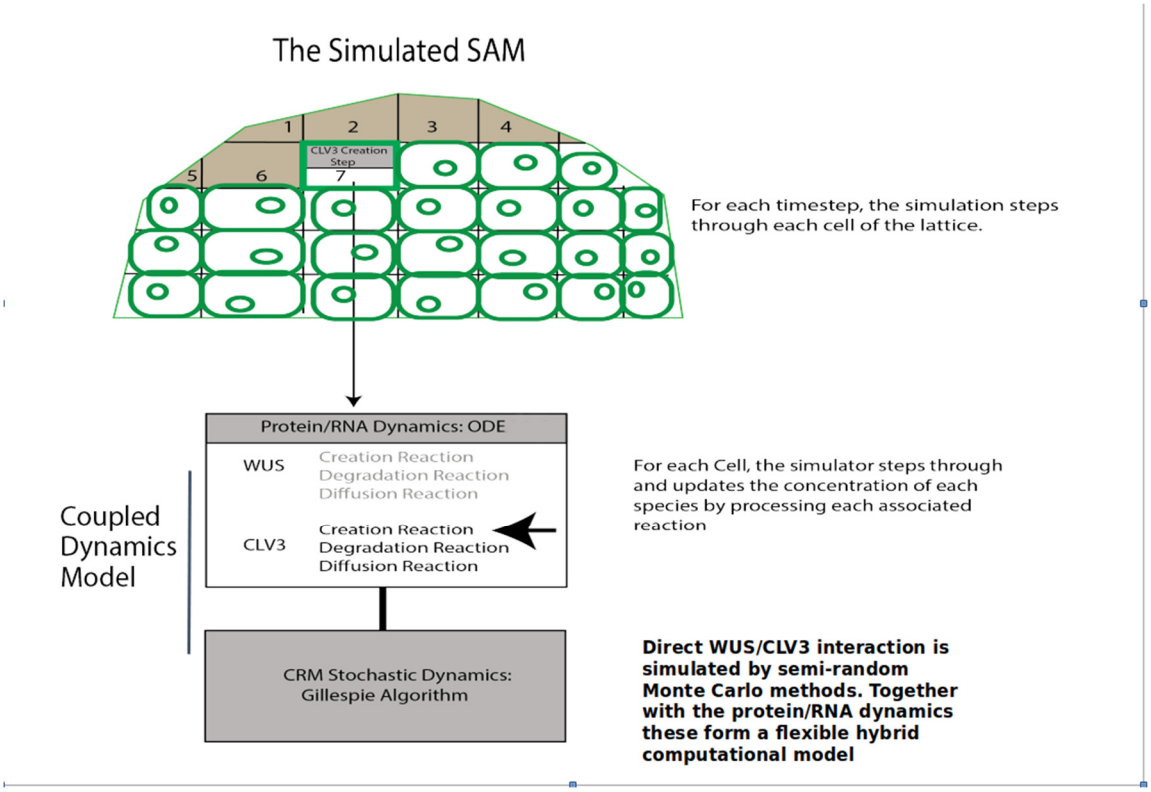

Fig. 2.18. Components of the Coupled Feedback Model.
The coupled feedback model consists of the simulated SAM tissue lattice. The ODE portion which drives the dynamics of the proteins and RNA. And the subcellular stochastic WUS/CLV3 DNA binding portion.

Perturbations

Perturbations to the model can be introduced simply by changing the values in the model, init, or solver parameter file which controls most of the parameters in the simulation.

References

1. H. Jönsson, M. Heisler, G. V. Reddy, V. Agrawal, V. Gor, B. E. Shapiro, E. Mjolsness, E. M. Meyerowitz, Modeling the organization of the WUSCHEL expression domain in the shoot apical meristem. Bioinformatics. 21, i232–i240 (2005

2. M. Perales, K. Rodriguez, S. Snipes, R. K. Yadav, M. Diaz-Mendoza, G. V. Reddy, Threshold-dependent transcriptional discrimination underlies stem cell homeostasis. Proceedings of the National Academy of Sciences. 113, E6298–E6306 (2016).

3. S. V. Nikolaev, S. I. Fadeev, A. V. Penenko, V. V. Lavrekha, V. V. Mironova, N. A. Omelyanchuk, E. D. Mjolsness, N. A. Kolchanov, A systems approach to morphogenesis in Arabidopsis thaliana: II. Modeling the regulation of shoot apical meristem structure. BIOPHYSICS. 51, 83–90 (2006).

4. K. Postawa, J. Szczygieł, M. Kułażyński, A comprehensive comparison of ODE solvers for biochemical problems. *Renewable Energy*. **156**, 624–633 (2020).

Chapter 3: The Structure of WUS Target Regions

Abstract

The landscape and structure of WUS targets was examined with a combination of experimental and computational techniques. Chromatin Immunoprecipitation (ChIP) was used to measure the binding of WUS and the openness of chromatin around the *CLV3* locus. It was found that WUS binding increased on treatment with dexamethasone bringing more WUS into the nucleus. Treatment with leptomycin B decreased the openness of chromatin which varied across the locus, perhaps through the retaining of histone deacetylases (HDACs) in the nucleus. Chromatin conformation capture (3C) suggested the 3' CRM1 region of *CLV3* contacted sequences close to it on the 3' end of the gene and had other lesser peaks of interaction across the locus. Electromobility shift assays (EMSA)s showed that the CRM2 and CRM3 WUS interaction clusters in *CLV3* had distinct binding affinities and interaction with WUS of generally lower affinity than CRM1 but distinct from each other. Computational analysis of WUS targets showed similarities in structure between downregulated and upregulated genes in the areas of motif numbers, size, and location relative to the gene. On the other hand, they also showed increased suitability for WUS binding in the gene body itself relative to areas immediately outside the gene.

Introduction

As a transcription factor WUS exerts its effect by altering the expression of gene targets. WUS has been found to bind across the genome and has many targets (1). The effect on these targets appears to differ individually, some being downregulated and others being upregulated to different degrees (1). The binding site of WUS on the *CLV3* gene is

not a simple singular binding motif but the CRM which is an array of motifs/cis-elements (2) It appears that WUS interacts with its targets in a more complex manner than simpler paradigms of TF behavior such as the French Flag model could account for (3). In order to untangle the behavior of this mechanism and more fully understand how WUS directs its control this study can focus on breaking down the fundamental parts of what is already known about what the WUS/CLV3 circuit and what goes into defining a TF and how it affects and is in turn affected by the chromatin landscape around it (4).

One of the most fundamental aspects of a TF is what motifs it binds too. Motifs are specific characteristic sequences that can be recognized by TFs. Motifs combined together can create larger binding sites that give fine tuned control to the organism to dictate expression in a variety of contexts (5). For WUS, specifically it is believed to directly interact with cis-elements which contain what are known as TAAT cores which are nucleotide sequences of TAAT/ATTA and slight variations. These cis-elements form larger CRMs which form the core regions of binding sites in *CLV3* and presumably other targets (6).

In addition to motifs in the DNA sequence, findings from other studies show the importance of other aspects of the chromatin landscape in controlling interaction (7). These include the epigenome and 3D structure which encompass characteristics of the genome beyond the nucleotide bases such as the openness of the chromatin and the interactions regions get from other looping distant sequences. Expression of genes is a highly complex and coordinated system bringing together many different mechanisms.

Bringing the contribution of the epigenome and other aspects of the chromatin landscape into the context of the WUS/CLV3 network will go far in showing how CRM based expression and WUS differs or is similar to other mechanisms and TFs (8).

Combined strategy to investigate target landscape

Several techniques were used to quantify the characteristics of WUS target genes, primarily *CLV3* but other targets were also examined. Experimental assays combined with computational techniques were used to study the genomic and epigenomic landscape of these targets. *CLV3* has long been used as a presumed canonical model for what a WUS target gene should look and behave as (2). The objective of these studies was not only to provide more insight into *CLV3* but also to generalize the information known about WUS targets to other genes.

ChIP and 3C analysis of CLV3

Chromatin Immunoprecipitation (ChIP) (9) was used extensively to map patterns of binding around *CLV3* and to improve previous data. WUS ChIP was conducted several times to measure WUS binding in target regions in mock and dexamethasone (Dex) treated tissue which allowed WUS/glucocorticoid receptor (GR) fusions to be localized to the nucleus. Antibodies against WUS itself and against GFP were employed and data for *CLV3* was quantified via PCR, sqPCR, and qPCR. Openness of the chromatin, which could play a major role in protein accessibility and by extension gene activity, was measured using an anti-histone antibody specific for the H3K9ac acetylation marker, associated with open active chromatin (10). These studies will provide a useful pilot for future genomewide surveys of WUS binding. Rather than being a linear sequence, DNA

is a complex spatial structure of coils and spaced interacting regions which forms another layer of significant control beyond the sequence. The 3D structure or looping in the chromatin was investigated through the use of chromatin conformation capture (3C) which captures the interaction between one ‘bait’ region and a set of target regions (11). Electromobility Shift Assays (EMSA)s (12), measured the binding of supplemental CRMs CRM2 and CRM3 in the *CLV3* gene to get a better idea of how they cooperate in binding along with the main CRM1.

Bioinformatic analysis of WUS targets

The characteristics of the sequence which make up WUS targets was investigated on a large group of WUS targets through computational means. A bioinformatic ‘fixed motif’ analysis scanning for TAAT cores/CRMlike clusters was performed on suspected upregulated and downregulated WUS target genes. This information was used to generate summary statistics concerning the properties of the cores and the differences between patterns in the different groups.

In addition to this, a second strategy of data driven machine learning based analysis was used to examine the WUS target list to further tease out possible patterns. Rather than relying on fixed patterns, HMMs derive the binding targets to scan for based on training data, potentially removing the biases of preselecting sites and allowing for more complex binding sites to be tested for (13).

Results

WUS binding to *CLV3* increased when treating *ap1cal WUS-GR* tissue with dexamethasone.

Binding of WUS was measured through a series of ChIP assays and then quantified either by PCR, sqPCR, or qPCR. The first WUS ChIP was with antibodies against WUS peptide sequence RERQKKRFNGTNMTC derived directly from animal blood aliquots and was quantified via PCR targeted toward the *CLV3* locus. The assay was conducted at two temperatures 45C and 55C. Treatments were divided into Leaf tissue, Mock treated, and Dex treated SAM tissue. The tissue used was from *ap1cal WUS-GR* for Mock and Dex and *ap1cal* for Leaf treatment. As shown in Fig. 3.1A, bands were seen at 45C and 55C. There was a strong band for the positive control of *CLV3* construct plasmid, faint bands were seen for Leaf and Mock tissue (in 45C), and a stronger band was seen at Dex treated tissue.

A second ChIP using purified antibodies toward the same locus as the previous run was quantified via PCR targeted toward the promoter and 3' UTR region of *CLV3* (Fig. 3.1B). In this instance both pulldowns and inputs for Mock and Dex were tested. For both regions strong positive control bands appeared. A strong band appeared for the Mock input for the promoter with a weak larger than expected band in the Dex pulldown. For the UTR, the Mock input showed a faint band of the expected size and a strong smaller band. Mock and Dex pulldowns also had faint bands but these are larger than expected and in the case of Dex a possible very weak band of expected size.

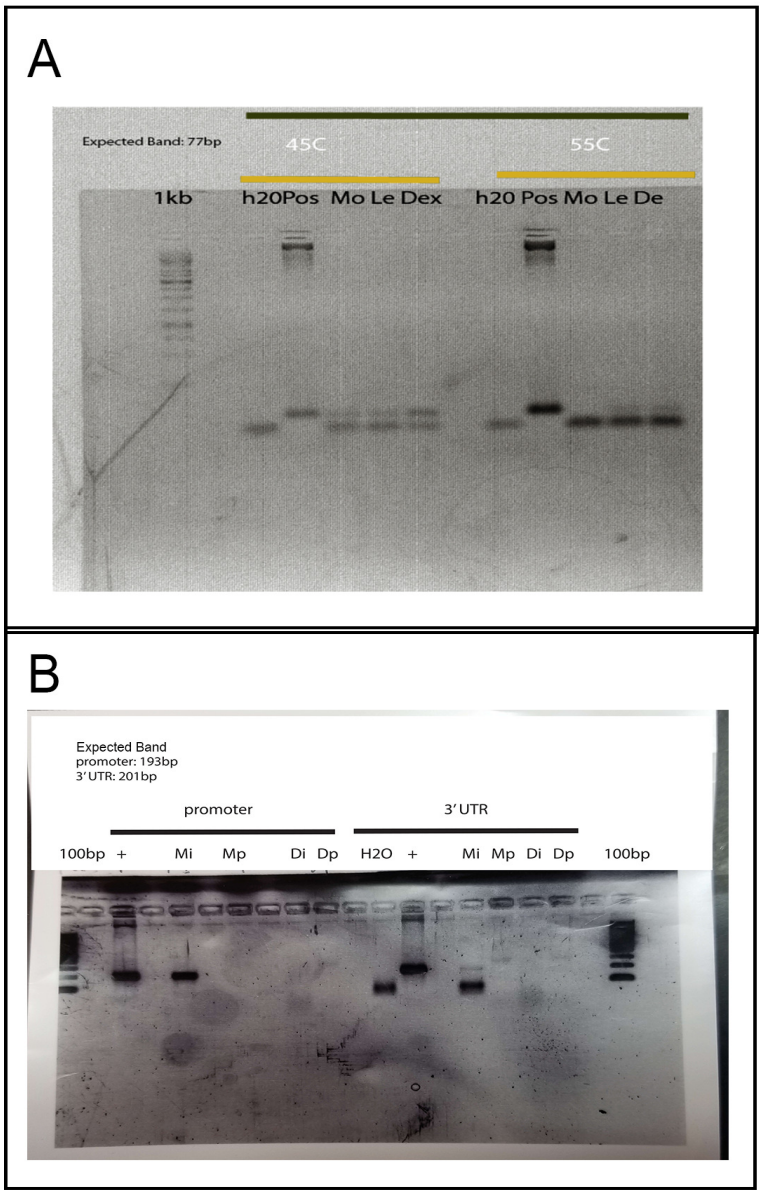

Fig. 3.1. PCR of WUS ChIP.
(A) PCR of 1st ChIP utilizing bleed derived antibodies at 45C and 55C. H20 is PCR with water template, Pos is positive control of CLV3 plasmid. Mo is Mock, Le is Leaf, and De is Dex. **(B)** is PCR of 2nd ChIP utilizing purified antibodies for the *CLV3* promoter and 3' UTR region. Mi is Mock Input, Mp is Mock Pulldown, Di is Dex Input, Dp is Dex Pulldown, H2O is templateless negative control, and + is positive control of *CLV3* plasmid.

QPCR captures increased WUS binding to *CLV3* under Dex induction in *ap1cal eGFP WUS-GR* tissue.

ChIP was also performed against GFP. The tissue treatment categories were; *ap1cal* Leaf and Mock treated and Dex treated *ap1cal eGFP-WUS-GR* SAMs. The ChIPs were then quantified through qPCR measuring pulldown percentage compared to input (Fig. 3.2). In run 1; Leaf had the highest pulldown percentage at roughly 30% while Mock was 9.3% and Dex was around 26%. Run 2 used an identical tissue set but different primers and had Leaf as the lowest pulldown at 4.7%, Mock intermediate at 43%, and Dex had the highest pulldown at 81%

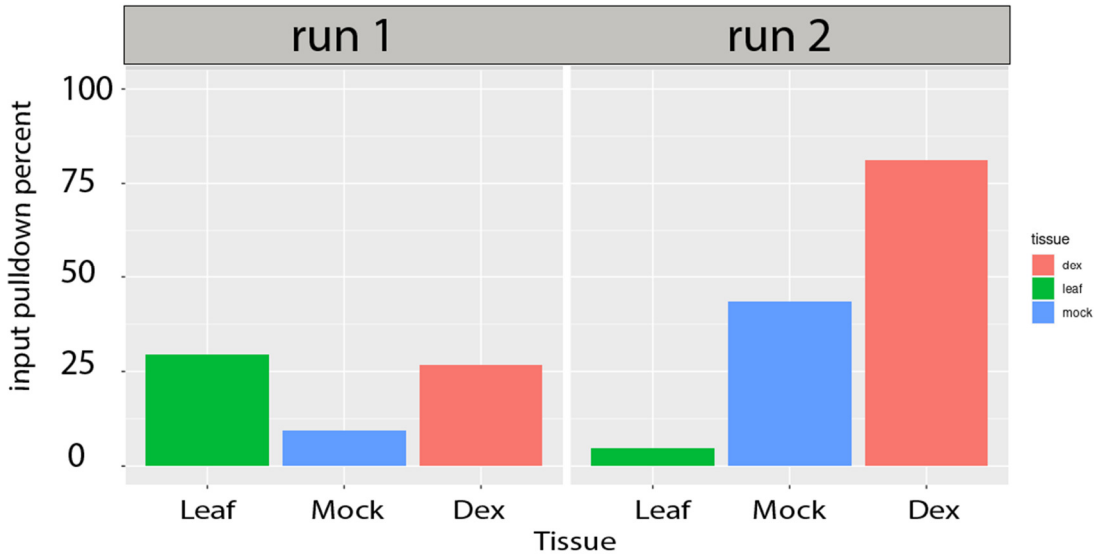

Fig. 3.2. Dex treatment leads to higher WUS accumulation on *CLV3*
QPCR of the *CLV3* region for anti-GFP ChIPped chromatin of *ap1cal eGFP-WUS-GR* tissue. Run 1 and Run 2. Pulldown percent compared to input is on the y axis. Treatment group is on the x axis.

Leptomycin treatment reduces acetylation in the *CLV3* region

ChIP was conducted on *clv3-2 pWUS::eGFP* tissue using antibodies against the H3K9ac histone mark correlating with open active DNA. The treatments were mock H20 treated and 20nM leptomycin treated SAMs harvested after 24hr from treatment. The tissue was subjected to qPCR with primers against the -1080, CRM1, CRM2, and CRM3 loci where the first is in the 5' end of the gene and the rest are in the 3' end respectively, and the *ACTIN7* locus as a control. Two qPCR runs were performed as shown in Fig. 3.3. In Run 1, fold enrichment, measured against an IgG negative control pulldown was consistently higher in all loci for Mock treated tissues with the difference vs Lep being more than 2x greater in the -1080, CRM1, and CRM3 loci. Mock was slightly higher in the CRM2 loci while both treatments are nearly identical for *ACTIN7* (Fig. 3.3A). Run 2 also shows generally higher levels of fold change in Mock pulldowns vs Lep but the difference is much smaller. The difference in CRM1 is slightly larger than in *ACTIN7*. -1080 has a large difference while CRM2 and CRM3 are visually nearly identical (Fig 3.3B).

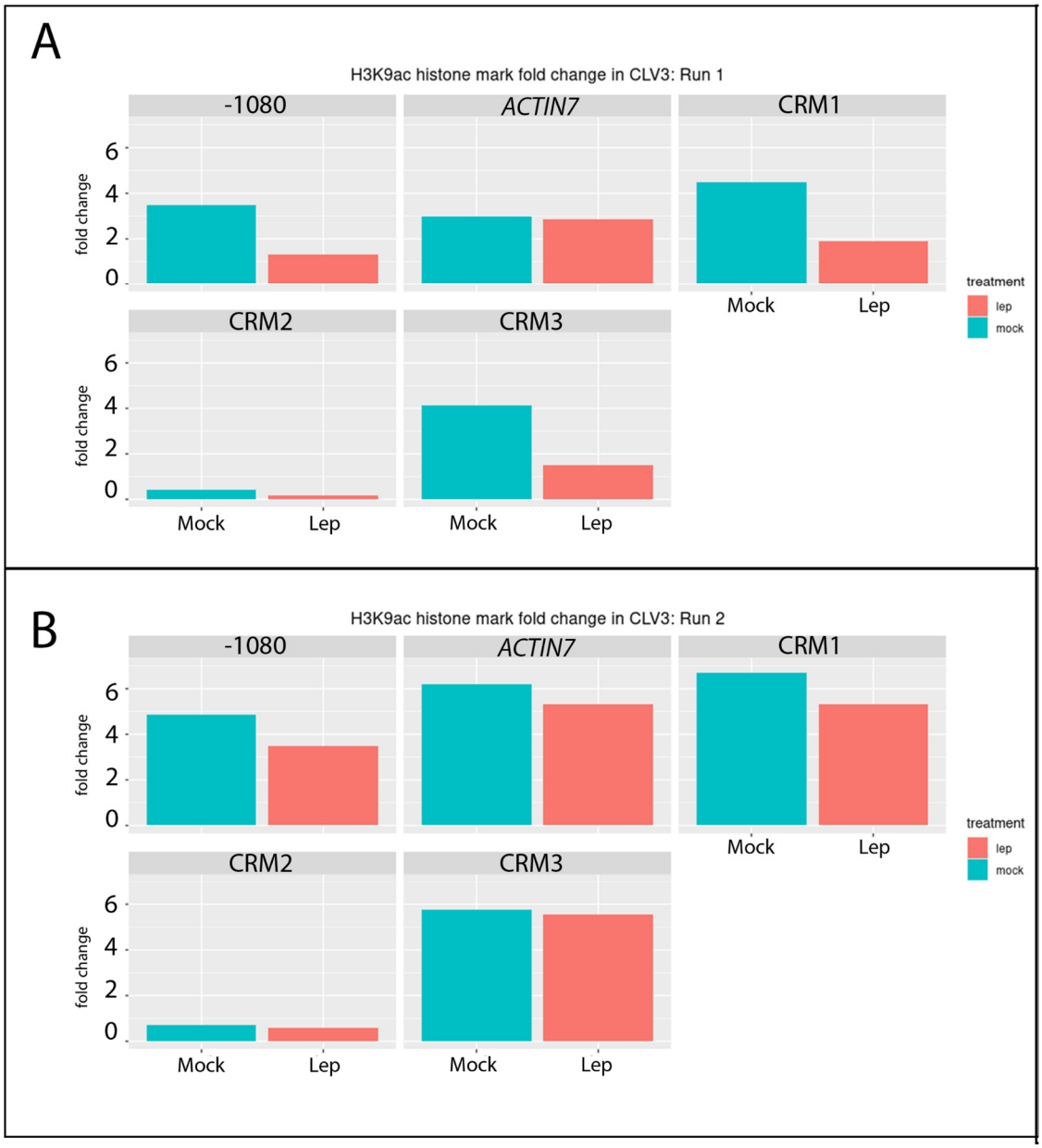

Fig. 3.3. Leptomycin treatment reduces H3K9ac marks on *CLV3* regions.
QPCR of the *CLV3* region of anti-H3K9ac ChIPped chromatin. **(A)** Run 1; -1080, CRM1, CRM2, and CRM3 are regions on *CLV3*. *ACTIN7* is a region on the *ACTIN7* gene. Fold enrichment is on the y axis. Treatment group is on the x axis. **(B)** Run 2

The 3' promoter region of *CLV3* contacts sequence in close proximity.

Chromatin looping and possible contact points in *CLV3* were investigated through chromatin conformation capture (3C). The experimental groups were defined into 3 broad categories. Mock treated and Dex treated *ap1cal eGFP-WUS-GR* tissue and *pCLV3::LHG4/6XOP::WUS-NLS* tissue. Dex tissue was used to examine looping formed under conditions of gene activation, the *WUS-NLS* tissue (which should accumulate more WUS in the nucleus) was used to study looping under repressive conditions and the Mock was for comparison to the Dex. The 3C procedure was performed with two different restriction enzymes yielding two different sets of fragments tested for interaction against the bait region. The DpnII set tests the 3' bait region against 4 fragments shown in Fig 3.4A. The NlaIII set tests a smaller bait region also at the 3' end against 13 fragments (Fig. 3.4A).

3C pulldowns were quantified in different ways. Through sqPCR which was then visualized on a gel and through qPCR that was quantified through raw Cq value (indicating the first qPCR cycle product is detected).

3C interaction is displayed in Fig. 3.4B-C and is aligned with the maps in Fig. 3.4A. Overall the qPCRs of the Mock and Dex NlaIII data both show higher interaction at the 3' UTR and 3' end of the gene relative to the rest of *CLV3* along with small peaks of higher local interaction across the rest of the gene. *WUS-NLS* qPCR has peaks of interaction around the same areas as those found in Dex but at lower levels. Dex interaction seems to be at the same level or higher than Mock (Fig. 3.4B). What patterns that can be seen

in the sqPCR also show higher interaction at the 3’ end of the gene with interaction elsewhere only sporadically attested (Fig. 3.4C).

Local peaks of interaction are defined as having an interaction value higher than both the surrounding regions with the exception of regions on the margin. Dex NlaIII qPCR had peaks of interaction (relative to surrounding regions) around N13, N9, N7, and N2. Dex DpnII had peaks in the D3 and the D1 fragments.

For Mock, NlaIII peaks occurred around N11, N7, and N1. DpnII Mock peaks followed DpnII Dex peaks with slightly higher interaction. NlaIII *WUS-NLS* had peaks around N12, N11, N9, N7, and N2 (Fig. 3.4B).

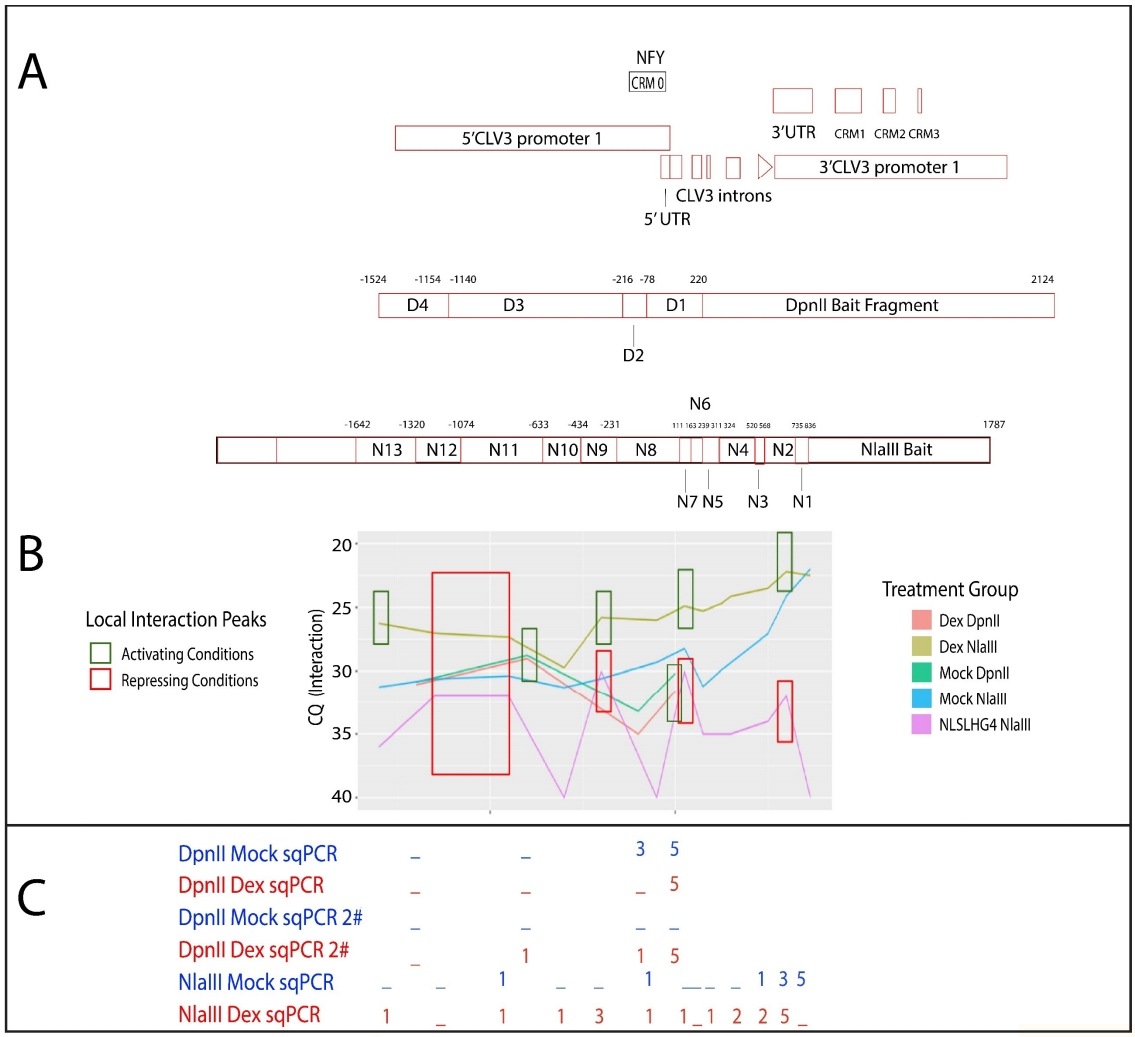

Fig. 3.4. The 3' region of *CLV3* interacts across other regions of the gene.
3C results for the *CLV3* locus. **(A)** Schematic of the *CLV3* locus and DpnII and NlaIII digest fragments. **(B)** qPCR of tissue. Cq value is on the y axis. Region on the x axis corresponds to the aligned region map in A. Green boxes corresponds to local activating condition peaks. Red boxes corresponds to local repressed conditions peaks **(C)** SqPCR results for Mock and Dex treatment. Numbers indicate qualitative assessment of band brightness. (higher is more)

Cis-elements of CRM2 and CRM3 have characteristic affinities and interaction patterns with WUS.

A series of EMSA binding studies were used to measure the strength and pattern of binding in the CRM2 and CRM3 regions. The EMSAs tested *CLV3* sequence containing the different CRM sites against full length (FL) WUS in increasing volumes from 0uL to 16uL. The results shown in Fig. 3.5 showed distinctive characteristics for each cis-element similar to but of generally lower affinity then the cis-elements of CRM1 in Chp1 with increased shifting of bands with increasing WUS concentrations and different CRM sites showing different affinities and shift patterns. For example, 1245 and 1186 of CRM2 start shifting before the others with 1245 appearing to skip over monomeric binding which others enter.

The control 970 cis-element shifts almost completely to dimers by 16ul. For CRM3, S32 and S31 show the greatest change between 12ul and 16ul with a proportion shifting to monomer and dimer bound. For CRM2, cis-element 1245 largely shifts by 12uL. 1233 and 1213 shift to monomer/dimer and dimer significantly by 16ul respectively. 1186 shifts to a mix of monomer and dimer at full 16ul concentration. CRM3 overall is weak compared to 970 and CRM2. A significant amount of protein for S32 and S31 remains unbound even at 16ul. 1245 appears to be strong, maybe the strongest in CRM2, although results are obscured by the probe sometimes getting stuck in the well. 1233 appears to be a weak cis-element while 1213 and 1186 are stronger cis-elements.

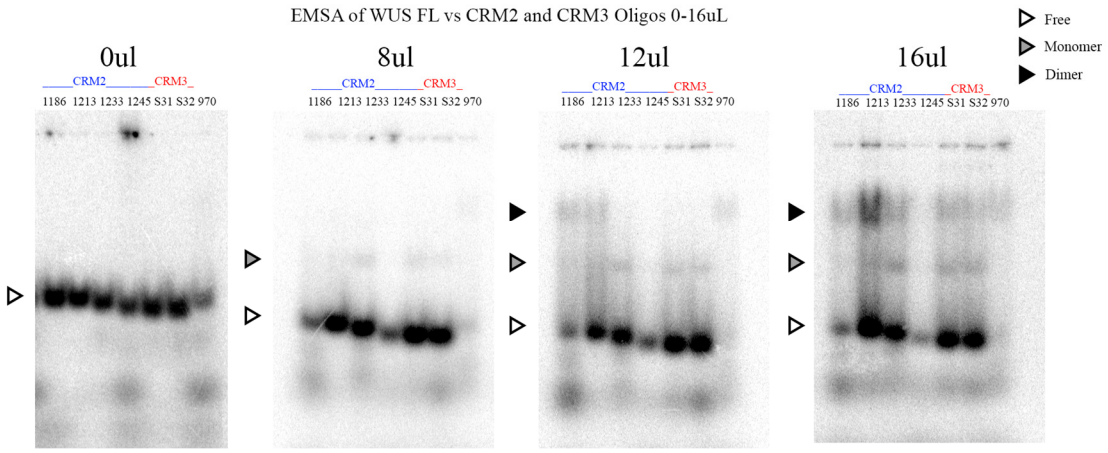

Fig. 3.5. CRM2 and CRM3 cis elements have distinct interaction patterns with WUS
EMSAs of CRM2 and CRM3 cis-elements vs WUS full length protein. EMSAs listed by volume of WUS FL protein used to treat them from 0ul to 16uL. The order of cis-elements in each EMSA is 1186, 1213, 1233, and 1245 for CRM2, S31 and S32 for CRM3, and 970 for CRM1.

Motif Analysis shows similarities between upregulated and downregulated WUS targets.

Binding between WUS and its targets was further explored through computational means. Here two general strategies were employed. The first scanned for clusters of the TAAT core motif/CRMlike clusters in a set of WUS targets and gathered different statistics (Fig. 3.6). This is called the 'fixed motif' approach. The number of clusters, the cluster size, and the cluster locations were quantified for upregulated and downregulated genes. For the number of TAAT clusters both up and downregulated genes varied along similar distributions peaking at 3 clusters per gene with very few above 10. TAAT cluster size for both down regulated and upregulated genes started around 13 nucleotides and went up to 40 nucleotides with similar distributions for both except for minor differences such as a peak around 26 for downregulated. Cluster location was measured by dividing the area within and around the gene into 9 parts. The first three being 1kb segments of a three kb interval before the gene at the 5' end. The next four segments are the transcribed gene/gene body divided into quarters. And the last two segments are a 2 kb

stretch (1kb each) at the 3’ end of the gene. Here again the distribution between downregulated and upregulated genes are similar except for a slightly higher bias toward the 5’ end for downregulated.

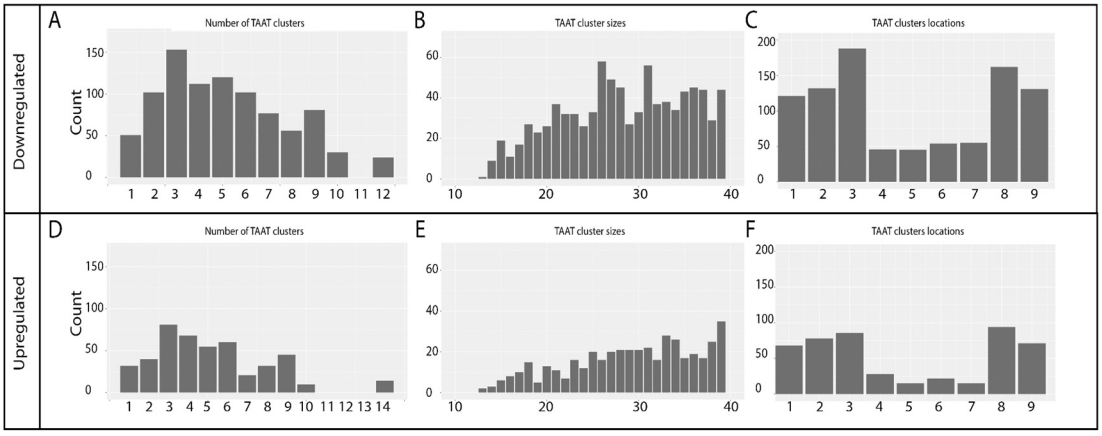

Fig. 3.6. Motif scanning shows similarities between downregulated and upregulated WUS targets. Fixed motif analysis of WUS targets. **First Row:** Downregulated statistics: Count on y axis. **(A)** Number of clusters per target, **(B)** cluster size, and **(C)** cluster location on x axis. **Second row:** Upregulated statistics. **(D)** Number of clusters per target. **(E)** cluster size **(F)** cluster location.

The WUS target list used for fixed motif analysis, was also analyzed via an HMM machine learning based approach which was trained on ChIPseq data to differentiate between highly bound and lightly bound WUS regions. This strategy relies on developing two HMM models for highly bound and lightly bound regions based on cis-element structure. Novel sequences can then be run though these models using the forward algorithm which yields probabilities they were generated by the model. The sequence is then classified as the model with the highest probability. More details about this approach are available in Methods. Using this strategy, a small test on novel ChipSeq

data outside the training set revealed it was capable of 90% accuracy in classification between the two groups (unpublished data). The strategy was then used for the target list.

Like the fixed motif analysis, several statistics were also quantified between upregulated and downregulated genes. The down regulated and upregulated gene lists were used to generate 3 different lists each. One for the transcript region/gene body of the target and its 5’ and 3’ ends which were 1kb regions outside the gene boundary.

These 6 lists were fed into the HMM to classify them as lightly bound and highly bound regions. The results were plotted by bar graph (Fig. 3.7A). The downregulated and upregulated genes both had gene bodies which were more likely to be classified as highly WUS bound. And both had margins on the 5’ and 3’ end that were more likely to be classified as lightly bound.

The now 12 classified lists (divided by highly bound and low bound classified) were then analyzed for strength/conformity which corresponds to how well they fit with the HMM model of the sequence type they were classified as. Again, the theme was upregulated and downregulated genes were similar to each other in conformity patterns for all regions. For both down and upregulated genes and high and low binding sets, the conformity of the sequences for both the 3’ and 5’ ends cluster around the same value. For the gene bodies, conformity distribution is the same across the categories with a slight bias toward weaker conformity (Fig 3.7B).

Finally, for each of the 6 lists of sequences classified as highly WUS bound. (Upregulated: 5', Gene body, 3' and Downregulated: 5', Gene body, 3'). The gene identifiers of the 48-50 strongest/most conformist sequences were put through PANTHER GO-Slim analysis at go.pantherdb.org to see which types of molecular pathways were represented. For upregulated genes which were classed as highly WUS bound, the function of catalytic activity dominated for both the gene body and the margins. For downregulated highly WUS bound targets, binding, catalytic activity, and ATP dependent activity were strongly represented (Fig. 3.7C).

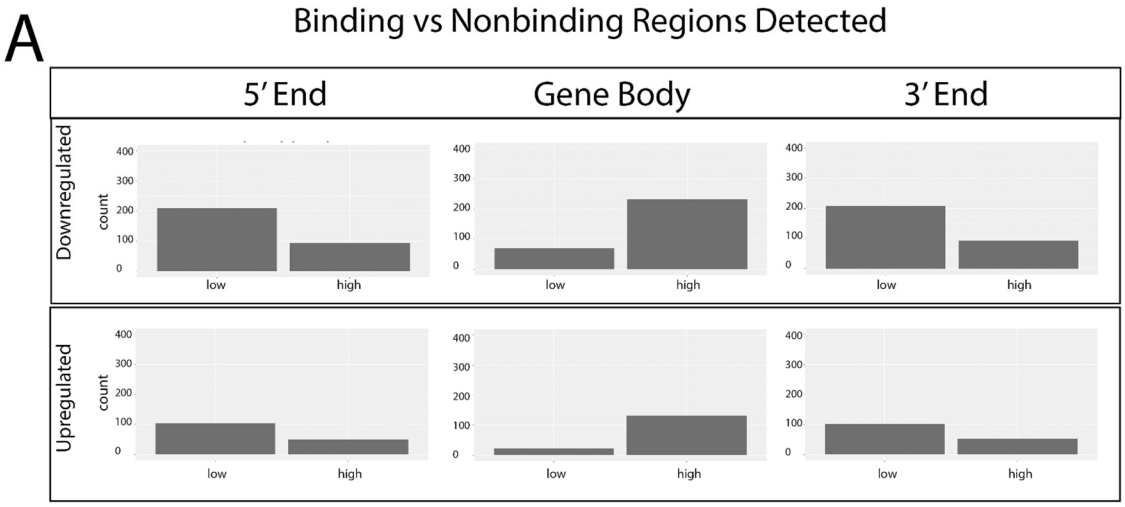
A
Binding vs Nonbinding Regions Detected
5′ End
Gene Body
3′ End
Downregulated
Upregulated
count
low
high

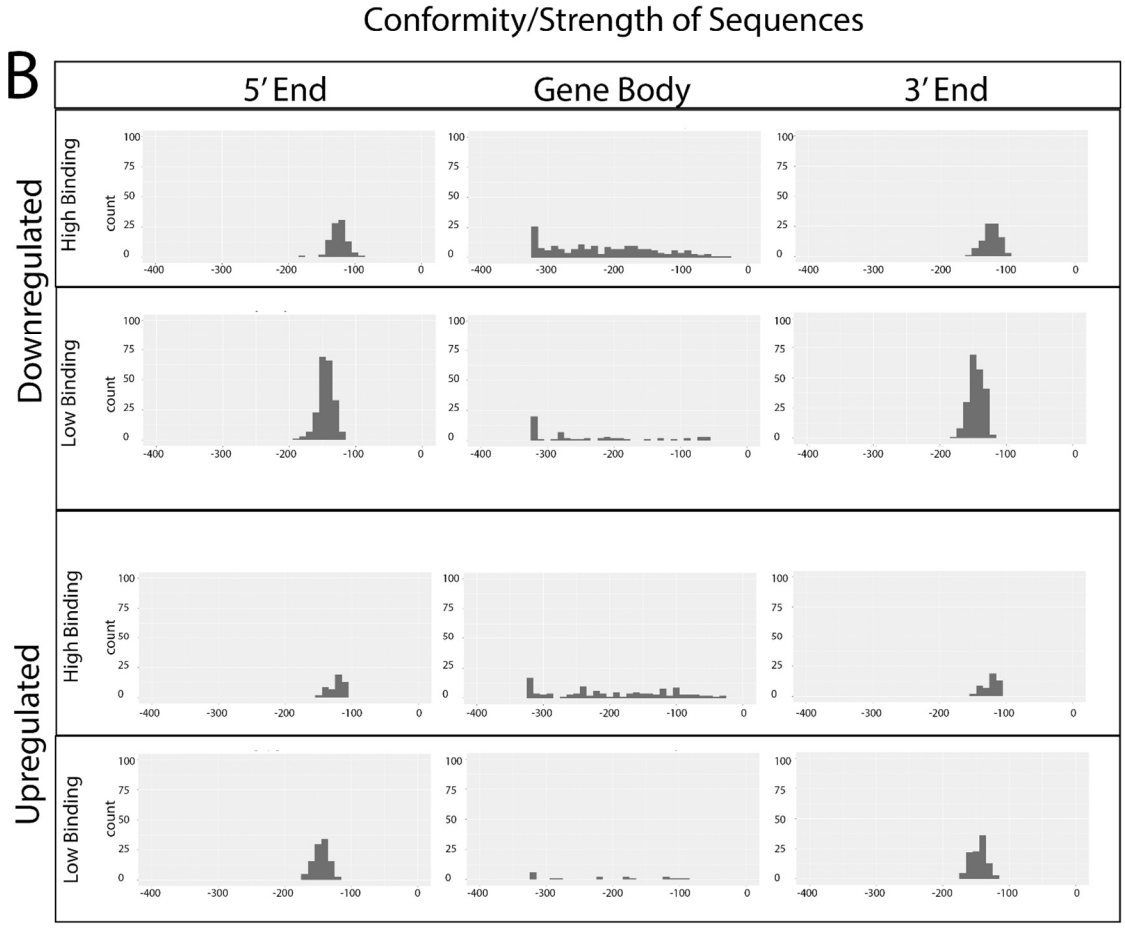
B
Conformity/Strength of Sequences
5′ End
Gene Body
3′ End
Downregulated
Upregulated
High Binding
Low Binding
count

C

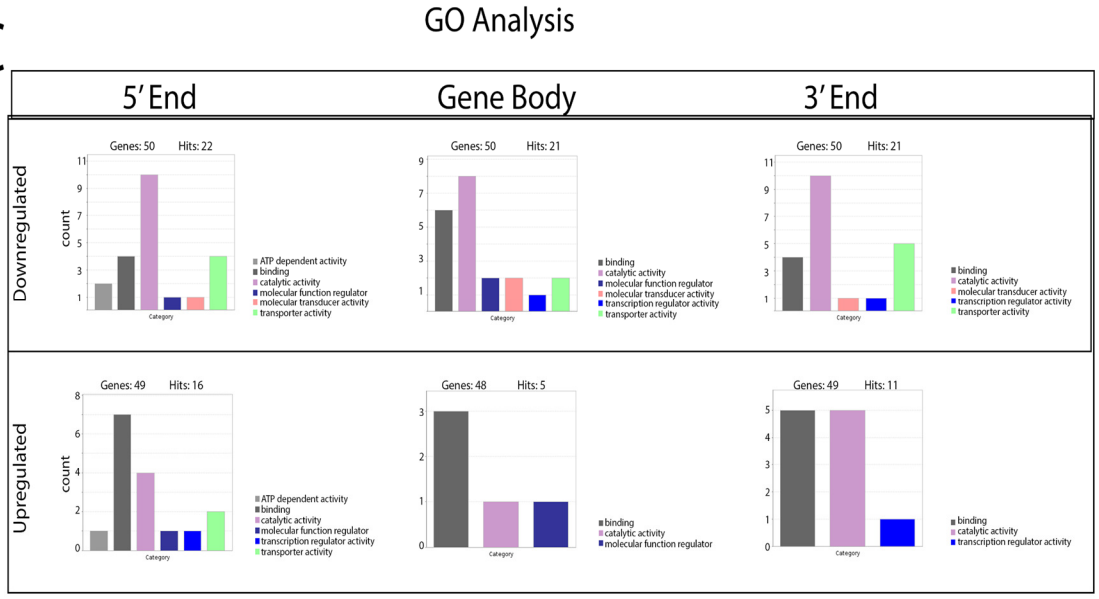
GO Analysis
5′ End
Gene Body
3′ End
Downregulated
Upregulated
count
Category
Genes: 50 Hits: 22
ATP dependent activity
binding
catalytic activity
molecular function regulator
molecular transducer activity
Genes: 50 Hits: 21
binding
catalytic activity
molecular function regulator
molecular transducer activity
transcription regulator activity
transporter activity
Genes: 50 Hits: 21
binding
catalytic activity
molecular transducer activity
transcription regulator activity
transporter activity
Genes: 49 Hits: 16
ATP dependent activity
binding
catalytic activity
molecular function regulator
transcription regulator activity
transporter activity
Genes: 48 Hits: 5
binding
catalytic activity
molecular function regulator
Genes: 49 Hits: 11
binding
catalytic activity
transcription regulator activity

Fig. 3.7. HMM analysis of WUS targets
(A) Binding vs Nonbinding regions found. First Row: Downregulated targets. Second Row: Upregulated targets. Column 1: 5' End. Column 2: Gene body. Column 3: 3' End. **(B)** Conformity of sequences to model. Row 1-2 Downregulated targets. Row 3-4: Upregulated targets. **(C)**GO analysis of Molecular function. Row 1: Downregulated targets. Row 2: Upregulated targets.

Discussion

By interrogation of the epigenomic neighborhood around *CLV3,* more detailed data can be gathered to fill in the context in which WUS interacts with *CLV3*. Progress has even started on extending these findings to other WUS targets.

Several antibody trials were run to test different strategies for ChIPing WUS targets. Both direct WUS and anti-GFP antibodies seem to function adequately with binding increasing from Leaf to Mock to Dex, some variability perhaps coming from primer choice. In future experiments scaling up the procedure to ChIPseq anti-GFP antibody may be a more suitable choice as it is easier to obtain and standardized and as a bonus the marker in *eGFP-WUS-GR* plants is a good way to quality control for suitable tissue.

In addition, the first steps have been taken to begin to collect info about the 3D structure of target regions and how it is controlled and varies under different conditions. Openness of the chromatin varied from region to region of *CLV3*. Leptomycin treatment which shuts off nuclear export appears to lead to a marked reduction in acetylation and by extension a reduction in the openness of the chromatin. This is perhaps an effect of leptomycin preventing the export of important HDACs (14). Comparing the binding sites leads to other possibly interesting observations. CRM2 has less acetylation than other sites, indicating it is less open and less involved with the machinery for WUS mediated CLV3 expression. CRM1 and CRM3 have high levels of acetylation while -1080 has slightly lower. CRM1 makes sense as having the highest acetylation since it is the primary CRM and expected to be heavily involved with WUS. CRM3 is harder to explain but perhaps it also is contacted more than expected by WUS.

Preliminary results show a complex looping arrangement across *CLV3* which varies under different conditions. But with some distinct patterns. 3C shows the greatest amount of looping interaction at 3' near CRM1. Local interaction peaks are dotted across the gene. These peaks tend to occur in the same place across conditions. Dex appears to have greater interaction than Mock (at least for NlaIII 3C) which seems to indicate more looping occurs under activating conditions. Both are greater than looping under repressive conditions measured under *WUS-NLS.* It makes sense that activating conditions would have more looping as more transcriptional machinery could come into the site from other sequences during times of high activity. On the other hand, during repression less activity and thus looping would be expected. While some tentative data points may be drawn from these results, the DpnII data set was of lower resolution than the NlaIII set so for additional confirmation in the future the locus can be tested with different restriction enzymes generating more testable fragments, different primer sets can be vetted for similar efficiencies and used. Additional experimental replicates should also be conducted to confirm the results.

The results of the CRM2/CRM3 EMSAs follows along with the findings in Chp1 for CRM1. Each of the cis-elements has their own particular binding affinity and pattern and these differences potentially play a role in how they collectively interact with and control WUS and other transcriptional machinery. It may be that for these regions the relatively stronger cis-elements work together with the weaker ones in a similar way to how 970 works with weak cis-elements in CRM1 where it is the major interaction site with WUS and the other cis-elements play supplementary roles. As CRM2 and CRM3 themselves are subordinate in role and of overall weaker affinity than CRM1 (unpublished data) the

balance between the strong and weak cis-elements in this module probably does not affect the expression distribution in the same way but the relationship between the cis-elements within the CRMs still can be similar. CRM3 appears to be weakly binding overall compared to CRM2. This may be a bit surprising seeing how the histone analysis indicated that the chromatin around CRM3 was more open than CRM2. One might expect regions set up to be more active might have greater affinity but perhaps regulation is a bit more complex. Or it may be due to size differences between the CRMs.

Bioinformatic analysis helped to expand data on WUS targets outside of the *CLV3* locus and generalize it. Fixed motif analysis found that TAAT clusters follow very similar patterns in upregulated and downregulated WUS target genes. The number of clusters per gene in each group was similar and peaks at 3 and the size of clusters have the same distribution in both. While potentially coincidental, 3 cis-elements is around the ballpark for the number of CRMs in targets where they are known. And this is possibly a sign of how CRMs among targets are similar. In terms of differences that could be found, more clusters seemed to appear in the margins per bin than the gene body. While this may be reflective of regulatory regions in the margin, care must be taken when comparing the margins and the gene body directly as they are divided up in different fashions as explained in Methods. While this analysis may be able to narrow down interesting sites similar to the *CLV3* CRMs, this should be combined with other techniques to confirm their biological relevance.

Unlike the fixed motif analysis, HMM analysis can at least theoretically more directly extrapolate whether there is WUS binding from sequences rather than rely on the substitute measure of cluster properties. Like the fixed motif scan, HMM analysis showed great overall similarity in the patterns between downregulated and upregulated targets. The binding enrichment patterns and strength/conformity of the sequences was largely the same in the 5' region, the gene body, and 3' region between the two groups.

There was greater variability of strength of the sequences in the gene body compared to the margins although this is likely due to the variability of length of the gene bodies of the different targets.

However, the analysis also showed gene bodies were much more likely to be highly WUS bound, whereas the margins had lower numbers of WUS binding sequences. By being able to independently, if indirectly, distinguish between transcribed genes identified through other means and margin sequences, this algorithm shows promise as a way to computationally identify other binding regions and perhaps even zero in on biologically relevant WUS target sequences. It also provides more possible evidence of the importance of the TAAT motifs/CRMs and associated spacing structure in defining the binding regions. This data would appear to clash with finding more clusters at the margins although perhaps number of clusters and WUS binding aren't always linearly related. Or it could be a limitation of one or both of the algorithms. In the end, comparisons should be considered carefully as relating the fixed motif cluster detection directly with the HMM classification is problematic as the algorithm for each, particularly how they divide the sequence varies significantly.

GO terms for both downregulated and upregulated genes which were highly bound overlapped, suggesting less bias between biological functions WUS preferentially upregulates or downregulates.

All in all the structural similarity between the WUS downregulated and upregulated targets suggest WUS binds in a similar fashion to both upregulated and downregulated genes. Perhaps the fact that the model found such similarities would indicate that many of these WUS targets may also be switchable just like *CLV3* in certain circumstances.

Methods

ChIP

CHIP was conducted according to the method presented in (16) and also with the Epiquik™ plant ChIP kit for the histone ChIP procedure. *Arabidopsis* tissue preparation consisted of harvesting tissue of 6-week-old plants and deep freezing with liquid nitrogen. The tissue was then stored at -80C and ground when needed before formaldehyde fixation at 1% formaldehyde for 10 mins. The ChIP procedure then continued on as outlined in the relevant protocol. ChIP DNA was then quantified by regular PCR where the products were visualized in agarose gel after a set number of cycles, sqPCR where bands were visualized in agarose at a series of increasing cycles, and finally qPCR, where the products were measured every cycle using the BioRad CFX96 machine. Afterward the qPCR was quantified via input percentage for the anti-GFP Wus-ChIP and fold enrichment vs a negative IgG control for the histone ChIP. WUS/GFP ChIP was divided into treatments Mock and Dex where the SAMs were

treated with either (1ul/5mL) silwet/water or (1ul/5mL) silwet/water with 10uM dexamethasone for 5hr and leaf tissue from untreated plants. The histone ChIP was divided into 2 treatments, Mock and Lep, where mock was treated with silwet/water (1ul/6.02ml) or leptomycin with 20nM leptomycin B with the same amount of silwet for 24hr. *Clv3-2 pWUS::eGFP-WUS* tissue was used for the histone ChIP. While *ap1cal* was used for Leaf treatment and *ap1cal1 WUS-GR* and *ap1cal eGFP-WUS-GR* was used for the Dex and Mock WUS and GFP ChIPs respectively.

3C

The 3C procedure was carried out based on (17) and (16) with frozen *ap1cal eGFP-WUS-GR Arabidopsis* SAM tissue crushed and incubated in nuclear extraction buffer with 1% formaldehyde for 10 mins and quenched with 2M glycine. Two restriction enzymes, DpnII and NlaIII were used, giving rise to two different sets of bait and target fragments to measure interaction between. The bait and target fragments for each set are shown in Fig. 3.4A. The DpnII set tests the 3' bait region against 4 fragments. They are from 3' to 5', D1-D4. D1 is in the gene region, the 5' UTR, and the 5' promoter. Regions D2-D4 are in the 5' promoter and further in the 5' direction respectively. The NlaIII set tests a bait region at the 3' end against 13 fragments. They are from 3' to 5' N1- N13. N1 falls in the 3' UTR region, N2 in the 3' UTR and gene region. N3-N7 fall into the gene region. N8 spans the gene region, 5' UTR, and the 5' promoter. N9-N13 are located in the 5' promoter region.

The experiment was further categorized by treatment and tissue type. The *ap1cal1 eGFP-WUS-GR* tissue was divided between Mock and Dex fixed similarly to the ChIP

treatments. *pCLV3::LHG4/6XOP::WUS-NLS* tissue was also used for NlaIII. The DNA was taken through the 3C protocol referenced above and digested, ligated, and purified. It was then quantified through both sqPCR and qPCR. Interaction for sqPCR was based on band brightness at the last cycle. QPCR interaction was measured through the Cq value, which indicates the first qPCR cycle with detectable product, lower roughly corresponding to more interaction. This y scale was inverted in the graph so higher interaction would be higher visually (Fig. 3.4B).

Antibodies used as well as primers for ChIP analysis and the 3C bait and target primers are shown below (Fig. 3.8).

<u>WUS ChIP: Anti-WUS</u>	
WUS Chip 1+2	
Antibody	
AB WUS 95aa (Antibody 1) Target aa RERQKKRFNGTNMTC	
Wus Binding Location 94-127 RERQKKRFNGTNMT	
Other Binding:	
wox transport RERQKKRF	
Primers	
WUS chIP 1:SqPCR	
1642	AAGGGTGGGCGCGCCGACCCAGCTTTCTTG
2810	TTGCCGGCGCCGTATCGAG
WUS ChiP 2 SQPCR:	
Promoter:	
1787	TCACTATTGTTGAGAACGTTGGCCTATAGTGAGTCGTATTACGC

2813	AGAGTATCAAATCAATGGCAA
3’ UTR:	
1788	CGACGTGAATTCTAAGATCGTCTCGCATACACTG
2829	CCCTCCAATGGATCCTCG
WUS ChiP 3 anti-GFP	
Antibody	
ABCAM ab290	
Primers	
Run1 4/19	
1788	CGACGTGAATTCTAAGATCGTCTCGCATACACTG
3662	GTTTAATTGTGACTATCACATCC
Run2 5/19	
2729	TTTGACACTGACACTGCCTG
3673	ACGCGTAAAATTTATTAGTACGTTTTCAATTGTC
Histone ChIP	

Antibody	
ABCAM ab10812	
Primers	
CRM1	
Forward primer	CAAAGCAATGTACCGTTGGGA
Reverse primer	CCTGTCACTGCCCCAAAGTC
Product length	167
CRM2	
Forward primer	TGCAAATTGAATGGTGGAGGAG
Reverse primer	TCGCCAGTGTCACATCTCAA
Product length	193
CRM3 primer	
Forward primer	ACGTCACCACTTTTCCCACC

Reverse primer	TGACATTGGAGGAACGAAAGAAAT
Product length	180
-1080 Primer	
Forward primer	CGTATGATCGGACGGCTGTG
Reverse primer	GGCTGATGTCATGAGGCAGAG
Product length	94
Actin7 Control	
Forward primer	CGTTTCGCTTTCCTTAGTGTTAGCT
Reverse primer	AGCGAACGGATCTAGAGACTCACCTTG
Product Length:	134
CLV3 3C	

Primers	
DpnII	
CLV3_2_3pBait	AAACAATCAAACAAAAAGGAACAGAGGG
CLV3_n144_5pP2F4 D2	TTTGTCCTAAACGTGTATCATAGTT
CLV3_CDS_5pP4F1 D1	AGAGAGAGTGAGACCAGAAGCATCA
CLV3_n1573_n1204P1 D4	TGAATTCAACACCACCATACTGCT
1783 D3	GTATCGAGGGTACCATCGGCTGATGTC
NlaIII	
Nbait	ACTTGCTTTGGAATCGTATGACA
NTF0 N1	CACTTCAGCAACAAACGTAATGC
NTF1 N2	AGGTCAAGGGAGCTGAAAGT
NTF1p5 N3	ATGATGGTGCAACGGGTCAG
NTF2S N4	CTCGTGACAACTAAAGCAATGA
NTF3S N5	GCGGTTGGAAAGTCCTTGAAC
NTF4Hand N6	GAGCTTGAGTGAGATCTGGTGAAAT

NTF5S N7	AGACATATAGAGGAGTGAAAGAGAGAG
NTF6Hand N8	GCCTACAAGGGCGAGAAATG
NTF7S N9	AGTTGTATAAAACGGCAGGGGT
NTF8Hand N10	GGCACCGGCACATACTCTAATATAT
NTF9S N11	TGGATTATATGAGCCTTGCCG
NTF10S N12	TTTGGGCCAATAAGGTGCCA
NTF11S N13	GGCCAACAATTTATTAGATCAGAAGAC
NTF12S	ACTGCCATATCGATCAGGTTTCT
NTF13S	ACTTGCACACTTTCATTTCTCCC

Fig. 3.8. List of ChIP and 3C antibodies and primers

EMSA

EMSA was used to measure the binding behavior between WUS and various cis-elements. The general procedure is to create a polyacrylamide gel and place it in the gel apparatus and prerun for 30 min at 175V. Mixtures of previously radioactively labeled ^{32}P DNA probes corresponding to the tested cis-elements are mixed with varying concentrations of WUS protein then run on the gel for 90 mins at 175V. Afterwards the gel is placed in a developing cassette overnight and the film sheet is then imaged in the Typhoon 9410.

Data for Computational Analysis

Both the fixed motif analysis and the HMM analysis was used on microarray data from (1). This list consisted of genes believed to be significant WUS targets due to large changes in their expression level. Treatment with cycloheximide was used to ensure the genes were direct targets of WUS. These genes were arranged into downregulated and upregulated lists. The HMM model was also trained on previous unpublished WUS-ChipSeq data.

Fixed Motif Analysis

Motifs in WUS target genes were investigated by examining the sequences for various fixed patterns of TAAT cores which can be seen as potential cis-elements. Data was collected using the following ruleset (version 101115) running on WUS target genes. ruleset: Select inverted or tandem repeat ATTA/TAAT with 2 TAAT/ATTA cores within 41 bp.

Algorithm:

For each gene on list

1. Extract sequence to search (3000 upstream and 2000 downstream of CDS)

2. Search for all TAATTAAT, ATTAATTA, TAATAT, and ATTATA motifs which are the "central motif"

3. Take each found motif one at a time

4. Take 41 bases before and 41 bases after the motif

5. Search each side for ATTA/TAAT

6. Take the two closet right side hits, the two closest left side, and the closet right and left side hits

7. Measure the chain they form with the "central motif".

8. Pick the shortest one and record its coordinates and sequence if it is less than 41 bp in length.

9. Move to the next motif until all inverted/tandem repeats for the gene have been processed.

10. move to the next gene.

Three different summary statistics were collected from this data. The number of clusters per target gene, the size of these clusters, and the location of the clusters defined as a sequence of segments from 1-9 where the first three segments correspond to a 3kb region (1kb each) at the 5’ end of the gene, the next 4 are the 4 quarters of the gene body and the last two are in the 2kb region (1kb each) at the 3’ end of the gene.

HMM motif analysis

In contrast to the previous fixed motif analysis, the HMM motif analysis, rather than looking for a predefined motif, is trained on existing data (specifically ChIPseq) and uses this to build an HMM model. This model can then be used to classify an unknown sequence input through the use of the aforementioned HMMs and the forward algorithm which uses the probabilities from these models to calculate the probability of generating a specific sequence and is outlined in (15). In this instance models were trained corresponding to a highly bound WUS sequence (enriched) and a lightly bound sequence (clear). The HMM analysis operates as outlined below and visually in Fig. 3.9-3.10.

The model runs as follows

1. Training data in the form of ChIPseq files are extracted and split into highly bound (enriched) and poorly bound (clear) coordinates.
2. The coordinates are associated, using chromosome sequence files, into enriched and clear sequences. Enriched is defined as greater than 30 reads within a 1000bp sequence and clear is defined as less than 7 reads.
3. The enriched and clear sequences are translated into emission sequences suitable to be analyzed by the model. The emissions are cores defined as TAAT/ATTA motifs, miscores which are cores with single nucleotide differences, complex cores which are multiple cores 4 bases apart or less. Spacers; gaps between cores which are of sizes that are multiples of 10, and are 40 or less bp. And noise which are the rest of the emissions.

4. The states of High, Medium, and Low Core (corresponding core emission percentages out of all emissions, where High Core has greater than 5%, Medium Core has 5% to greater than 1% and Low Core is 1% or less.) sequences and their associated emission and transition probabilities are gathered from the training data.
5. The HMM models for enriched and clear sequences are created and filled with the gathered information.
6. The forward algorithm is used to calculate the probability of a given input sequence of unknown identity for both models.
7. The sequence is classified as of the type of the model with the highest probability.

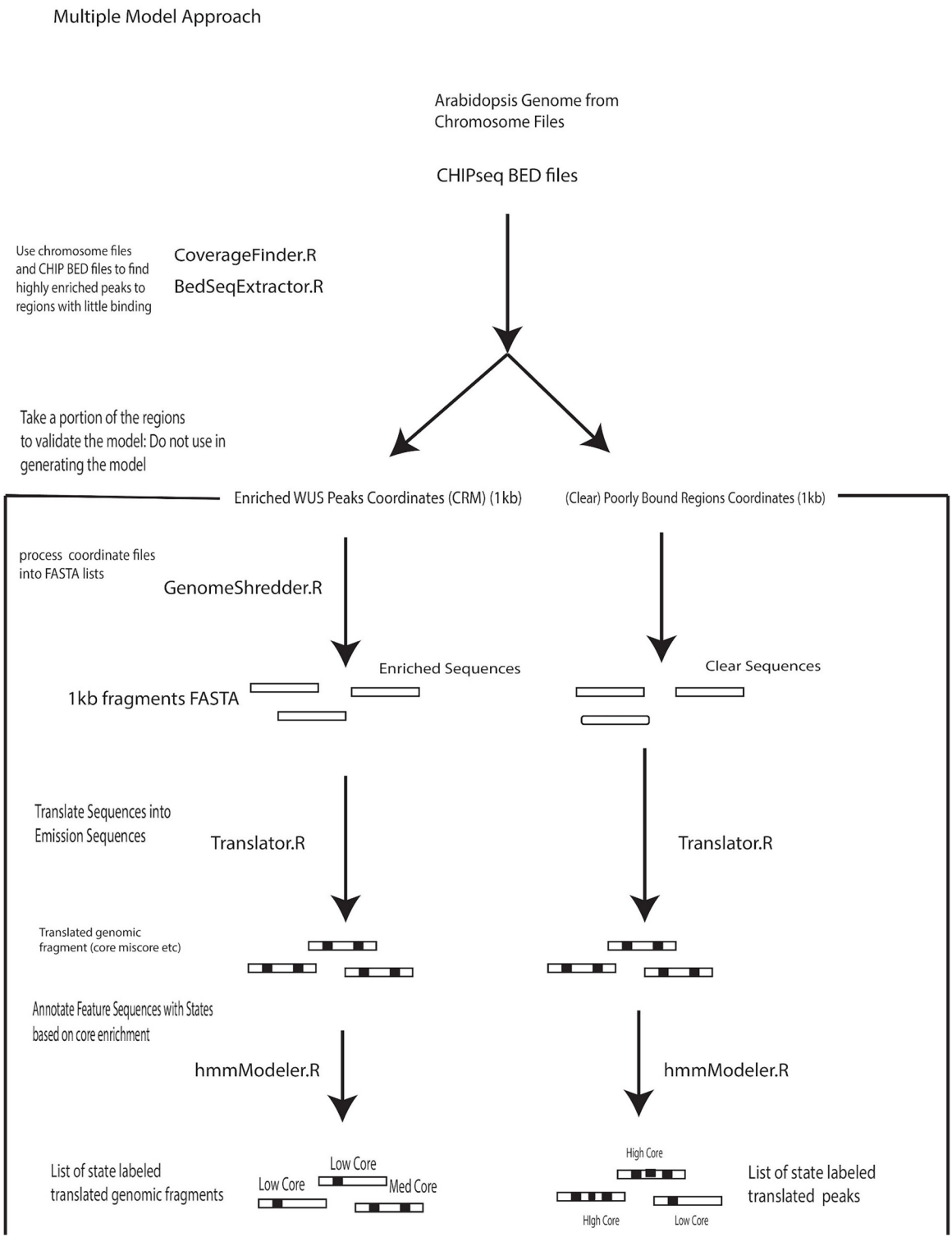

Fig. 3.9. Conceptual diagram of the HMM analysis process. Part I.

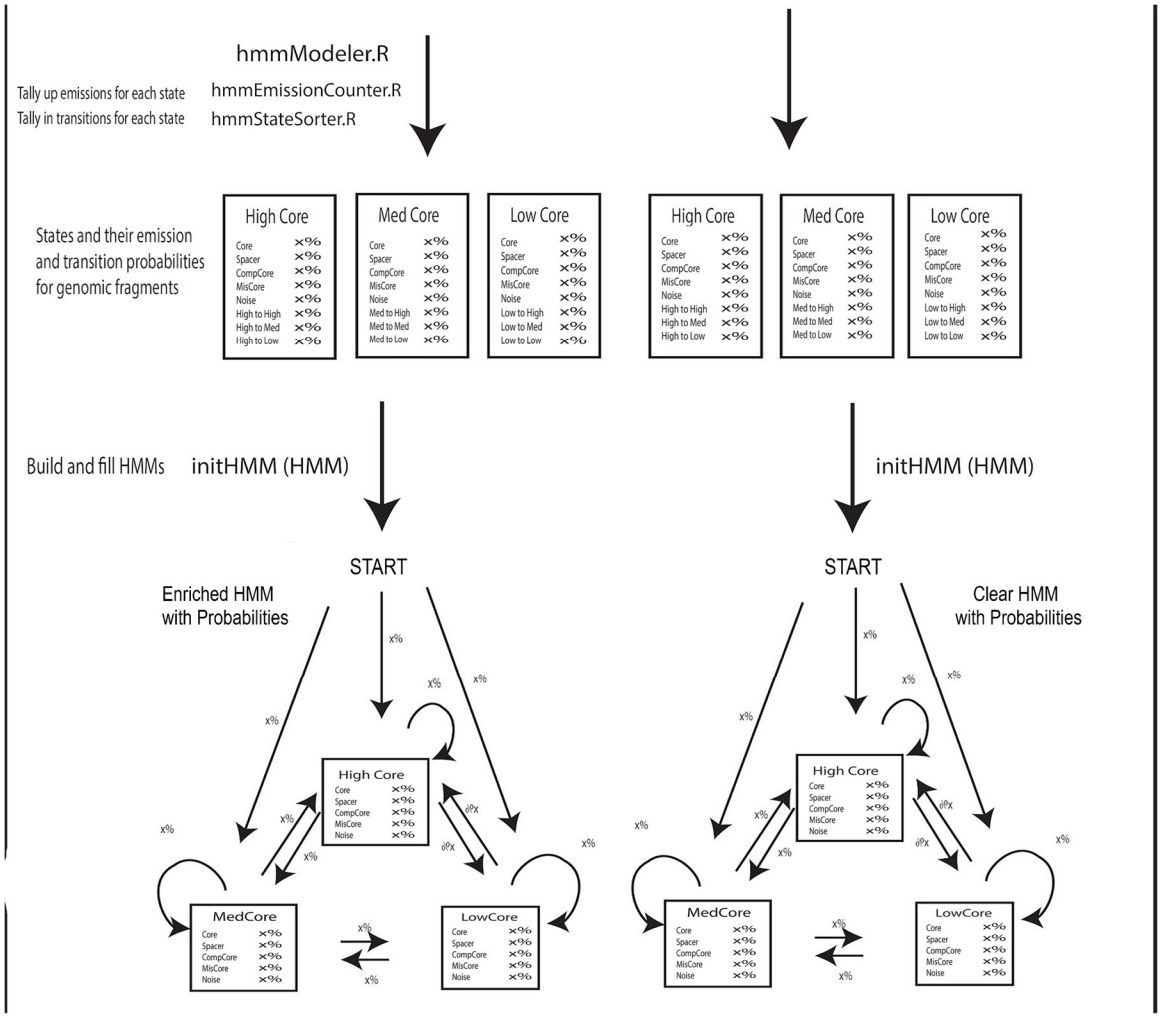
hmmModeler.R
Tally up emissions for each state
hmmEmissionCounter.R
Tally in transitions for each state
hmmStateSorter.R
States and their emission and transition probabilities for genomic fragments
High Core
Med Core
Low Core
Core x%
Spacer x%
CompCore x%
MisCore x%
Noise x%
High to High x%
High to Med x%
High to Low x%
Med to High x%
Med to Med x%
Med to Low x%
Low to High x%
Low to Med x%
Low to Low x%
Build and fill HMMs
initHMM (HMM)
initHMM (HMM)
START
START
Enriched HMM with Probabilities
Clear HMM with Probabilities
x%
∂θx
MedCore
LowCore

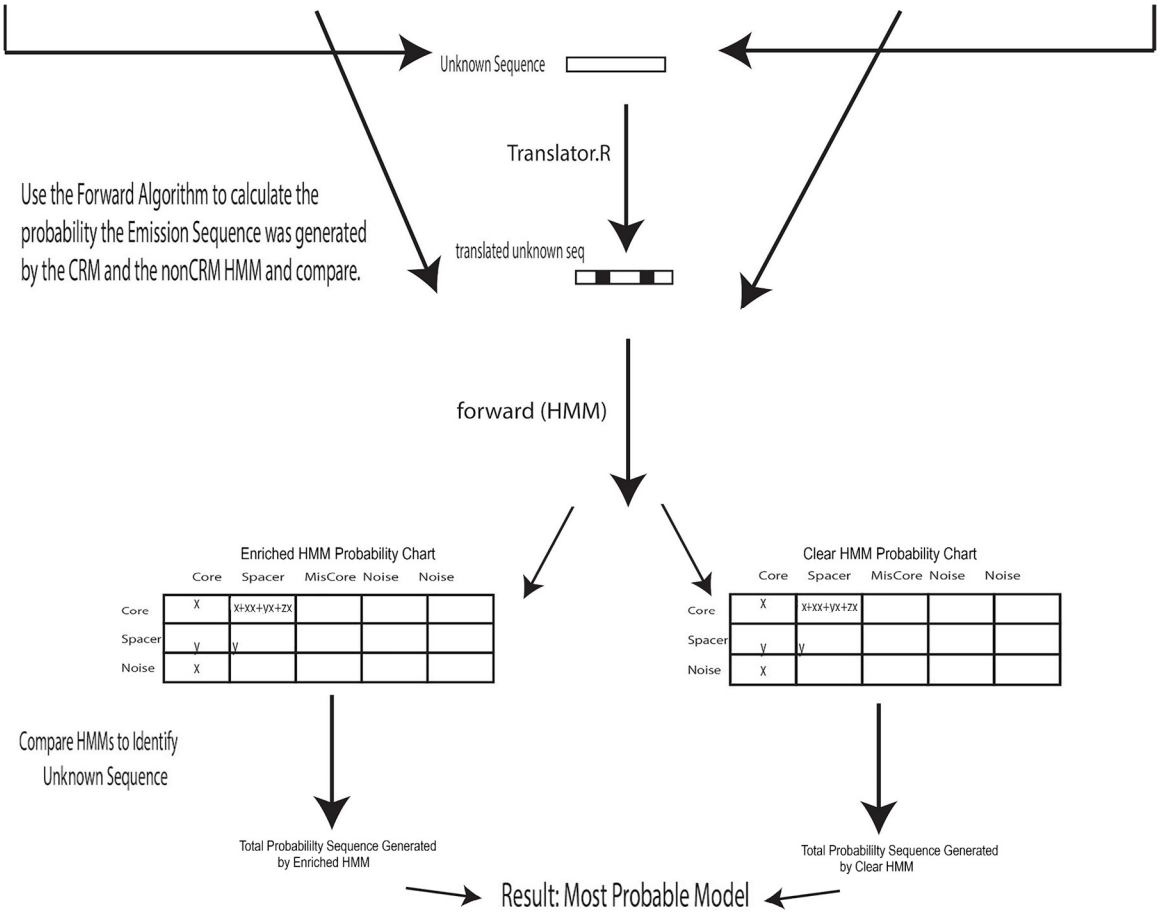
Unknown Sequence
Translator.R
Use the Forward Algorithm to calculate the probability the Emission Sequence was generated by the CRM and the nonCRM HMM and compare.
translated unknown seq
forward (HMM)
Enriched HMM Probability Chart
Core Spacer MisCore Noise Noise
Core
Spacer
Noise
X
X+XX+YX+ZX
Y
Y
X
Clear HMM Probability Chart
Core Spacer MisCore Noise Noise
Core
Spacer
Noise
X
X+XX+YX+ZX
Y
Y
X
Compare HMMs to Identify Unknown Sequence
Total Probability Sequence Generated by Enriched HMM
Total Probability Sequence Generated by Clear HMM
Result: Most Probable Model

Fig. 3.10. Conceptual diagram of the HMM analysis process. Part II

The model results were then used to classify and create summary statistics for the same WUS target genes examined in the fixed motif scan. The lists of downregulated and upregulated genes were divided into 6 different lists. The upregulated and downregulated; 5' end, gene body, and the 3' end of the targets, where the 5' and 3' end were 1kb intervals outside the gene. Three different main summary statistics were generated from these categories. The first counted the number of sequences predicted to be low bound or high bound. This yielded bar graph results of counts for each category, and 12 categories where the previous six lists were now split into low and high bound sequences.

The second statistic is the 'strength/conformity' of the sequence which tested how closely it conforms to its classified HMM model. This is calculated by taking the probability the sequence is generated from the model using the forward algorithm. Because the probability number is very small the base 10 log is taken where higher corresponds to greater strength/conformity. This method was used to test the 12 categories generated previously and generate a new set of histograms of counts showing the distribution of sequences based on conformity.

The third statistic tested the 48-50 strongest entries in each 'highly bound' category (Down and upregulated 5', gene body, 3') with the Panther GO-Slim molecular function test and counting the GO annotation hits.

References

1. R. K. Yadav, M. Perales, J. Gruel, C. Ohno, M. Heisler, T. Girke, H. Jönsson, G. V. Reddy, Plant stem cell maintenance involves direct transcriptional repression of differentiation program. Molecular Systems Biology. 9, 654 (2013).

2. M. Perales, K. Rodriguez, S. Snipes, R. K. Yadav, M. Diaz-Mendoza, G. V. Reddy, Threshold-dependent transcriptional discrimination underlies stem cell homeostasis. Proceedings of the National Academy of Sciences. 113, E6298–E6306 (2016).

3. B. V. L. Vadde, A. H. K. Roeder, Can the French flag and reaction–diffusion models explain flower patterning? Celebrating the 50th anniversary of the French flag model. Journal of Experimental Botany. 71, 2886–2897 (2020).

4. M. Geertz, S. J. Maerkl, Experimental strategies for studying transcription factor–DNA binding specificities. Briefings in Functional Genomics. 9, 362–373 (2010).

5. C. Sayou, M. H. Nanao, M. Jamin, D. Posé, E. Thévenon, L. Grégoire, G. Tichtinsky, G. Denay, F. Ott, M. Peirats Llobet, M. Schmid, R. Dumas, F. Parcy, A SAM oligomerization domain shapes the genomic binding landscape of the LEAFY transcription factor. Nat Commun. 7, 11222 (2016).

6. R. K. Yadav, M. Perales, J. Gruel, T. Girke, H. Jönsson, G. V. Reddy, WUSCHEL protein movement mediates stem cell homeostasis in the Arabidopsis shoot apex. Genes Dev. 25, 2025–2030 (2011).
7 10 21

7. U. C. Lange, R. Schneider, What an epigenome remembers. BioEssays. 32, 659–668 (2010).

8. W. Ouyang, Z. Cao, D. Xiong, G. Li, X. Li, Decoding the plant genome: From epigenome to 3D organization. Journal of Genetics and Genomics. 47, 425–435 (2020).

9. M. F. Carey, C. L. Peterson, S. T. Smale, Cold Spring Harb Protoc, in press, doi:10.1101/pdb.prot5279.

10. Z. Du, H. Li, Q. Wei, X. Zhao, C. Wang, Q. Zhu, X. Yi, W. Xu, X. S. Liu, W. Jin, Z. Su, Genome-Wide Analysis of Histone Modifications: H3K4me2, H3K4me3, H3K9ac, and H3K27ac in Oryza sativa L. Japonica. Molecular Plant. 6, 1463–1472 (2013).

11. M. Simonis, J. Kooren, W. de Laat, An evaluation of 3C-based methods to capture DNA interactions. Nat Methods. 4, 895–901 (2007).

12. L. M. Hellman, M. G. Fried, Electrophoretic mobility shift assay (EMSA) for detecting protein–nucleic acid interactions. Nat Protoc. 2, 1849–1861 (2007).

13. A. Krogh, Two methods for improving performance of an HMM application for gene finding. Cent. Biol. Seq. Anal. Phone. 45, 4525 (1997).
24-25

14. T. A. McKinsey, C.-L. Zhang, J. Lu, E. N. Olson, Signal-dependent nuclear export of a histone deacetylase regulates muscle differentiation. *Nature*. **408**, 106–111 (2000).

15. D. Jurafsky, J. H. Martin, Speech and Language Processing: An Introduction to Natural Language Processing, Computational Linguistics, and Speech Recognition (Prentice Hall, 2009).

16. C. Bowler, G. Benvenuto, P. Laflamme, D. Molino, A. V. Probst, M. Tariq, J. Paszkowski, Chromatin techniques for plant cells. *The Plant Journal*. **39**, 776–789 (2004).

17. M. Louwers, E. Splinter, R. van Driel, W. de Laat, M. Stam, Studying physical chromatin interactions in plants using Chromosome Conformation Capture (3C). *Nature Protocols*. **4**, 1216–1229 (2009).

Chapter 4: WUS and CLV3 Tissue Level Dynamics

Abstract

A series of genetic constructs and chemical treatments were used to study WUS and CLV3 dynamics on the tissue level. The box-B stemloop construct with *CLV3* sequence was transformed into plants expressing the LambdaN protein to see if they would be suitable to quantify expression as an alternative to protein fusion techniques. But this did not generate any noticeable localized signal. Treating *pCLV3::H2B-mYFP* chromatin with trichostatin also did not lead to noticeably altered CLV3 signal. Attempts to measure diffusion of WUS yielded varying values perhaps as a result of microvibrations. Measuring the effect of dimeric WUS appeared to yield an association with lowered expression and altered organ phenotype. More evidence was gathered that HAIRY MERISTEM (HAM) proteins have an influence on the concentration dependent mechanism and by extension the distribution of WUS and expression of *CLV3*.

Introduction

Signaling networks are highly complex and coordinated systems bringing together many different mechanisms and species to drive highly controlled pathways (1). These converge to lead to phenotypic patterns which become obvious on the tissue level which provides a convenient vantage point to study both WT and perturbed systems (2). One of the most effective straightforward strategies to study these systems is to employ tailored chemical treatments and genetic constructs with relevant markers and visualize the dynamics of these markers through confocal microscopy (3). This strategy was

applied to the study of the SAM signaling network investigating different aspects of the function and distribution of CLV3 and WUS.

RNA stem loop based expression quantification

Currently expression in the SAM system is being measured through methods such as GFP and YFP protein fusions (4). While offering some flexibility there are limitations to this strategy. Relying on a protein signal adds an additional layer of regulation between the expression and the marker. There may be a substantial time delay between expression and signal, regulation can affect the amount of protein generated vs the expression and the resolution, i.e., the precise amount of expression and its trends up and down at given time intervals can be poor (5). A possible solution to these issues is a signaling method which measures RNA expression more directly than using a protein with a fluorescent signal. The λN_{22} or LambdaN system was set up for use in measuring WUS interaction with the *CLV3* target gene. LambdaN is an alternative to the more common MS2 tagging system (5) (6) which was used in this system unsuccessfully previously, that can potentially directly measure RNA expression. In the LambdaN system the gene in question is cloned with a box-B 15nt repeat sequence. The repeat sequence is transcribed as a stemloop that assembles with a 22AA LambdaN peptide fused with GFP produced constitutively in the system (6). By measuring the expression more directly and bypassing the additional step of generating a labeled protein after transcription, this strategy can solve the problems inherent in more traditional labeled protein approaches (5). Plants expressing LambdaN protein were transfected with constructs of *pCLV3::box-B* and examined under microscopy to determine if the new marker system would function *in vivo* in this system.

Effects of opening chromatin structure on expression

As important as the raw sequence of the gene is the structure and conformation of the strand can also be of great importance (7). The 3D structure of chromatin of WUS targets is studied from a genetic and computational perspective in Chp2 but imaging studies can provide further data on the effect of chromatin structure on tissue level expression patterns (8).

Trichostatin is a chemical which exerts a powerful effect on the structure of the chromatin by inhibiting histone deacetylases (HDACs). HDACs deacetylate histones which wrap the DNA leading to tighter binding (8). Treatment with trichostatin effectively may loosen DNA binding leading to increased access for WUS and changes in activity for certain target genes (8). In order to measure this possible change; SAMs with the CLV3 marker *pCLV3::H2B-mYFP*, were treated with 10uM trichostatin and observed to see what would happen if the neighborhood around *CLV3* was opened up.

Effects of dimeric WUS

In addition to *CLV3*, other investigations focused on WUS. As touched on in Chp1, WUS can bind target genes as a monomer or in multimeric form (9). In *in vivo* systems it is difficult to untangle the different forms and study them in isolation (9). A forced dimer (FD) is a set of two WUS proteins modified to be attached together through a hydrophilic linker which seeks to recreate the effect of dimeric WUS in an *in vivo* system without the inconvenience of the transient nature and concentration based factors affecting dimer formation that need to be overcome when dealing with a natural dimeric WUS. The artificial dimeric construct in addition to separating the effects of the dimer from

monomeric WUS and other forms allowed for a degree of control and could be cloned into different constructs to extract different data. The form investigated in detail was from the construct *pWUS::FD*, a forced dimer driven by a regular WUS promoter (Fig. 4.1). This would allow for observation of what effect the FD has in the absence of any other factors.

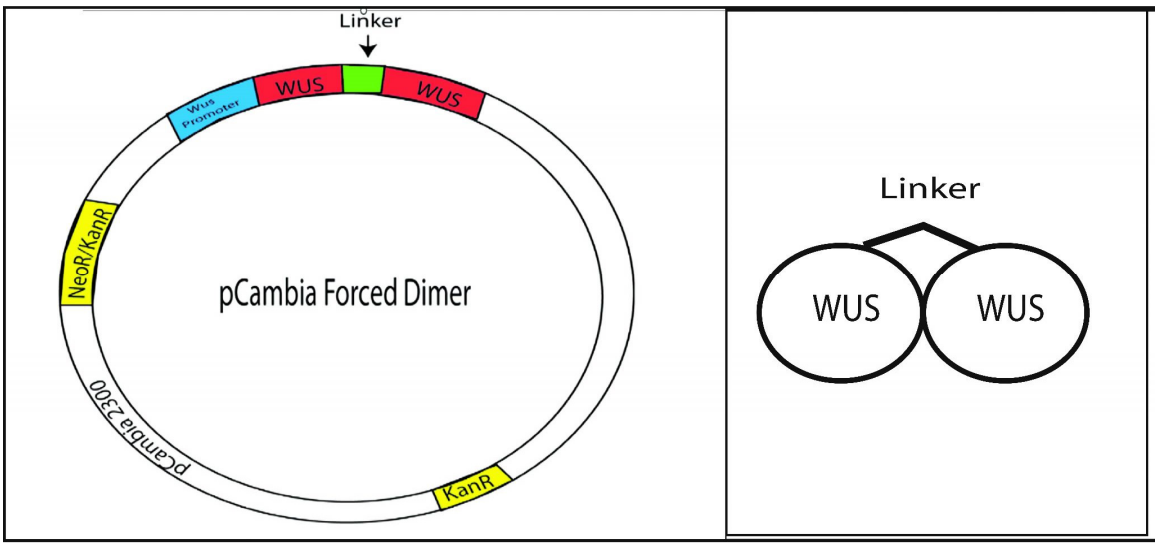

Fig. 4.1. Diagram of the Forced Dimer construct.
WUS FD plasmid and protein product.

Diffusion of WUS across the SAM

The extent and speed of diffusion within cells, specifically of WUS in the SAM remain to be characterized. Diffusion can be an important factor in signaling throughout the SAM governing the travel and distribution of species. It helps set up the subsequent expression patterns seen for WUS and CLV3 as well as its effects on its downstream targets (10). Observed diffusion can be used to derive quantitative values for conditions indicative of different behaviors such as dimerization (11) and aid in constructing future simulations. The method used to measure diffusion was fluorescence correlation

spectroscopy (FCS) specifically a version called raster image correlation spectroscopy (RICS) (12). In this method, plant tissue with genes encoding three different types of GFP were visualized over a period of time. These systems were *Arabidopsis* SAMs with free eGFP where the GFP protein alone was produced, *WUS-eGFP*, and *eGFP-wus-7ΔHOD2 or (ΔHOD7)*, a form of WUS which lacks the ability to dimerize due to the knockout of its homodimerization domain. Plants containing these constructs were grown and their SAMs were scanned under confocal microscopy in time courses.

The resultant time datasets were then analyzed computationally. The RICS procedure first takes a point spread function value (PSF) and then compares images in the time series in order to measure the diffusion coefficient (D1) and collect data on how diffusion in the cell varies, and the behavior and formation of WUS complexes (12).

Inducing *pin* phenotype in plants.

In order to obtain an isolated SAM which is more easily mounted for side views for the diffusion assay data collection, a *pin* phenotype (which simulates the knockout of one or more of the *PIN-FORMED* (*PIN)* auxin transporters) (13) was induced into each of the different plant types through spraying twice daily with 100uM naphthylphthalamic acid (NPA) in 1ul/5mL silwet/H2O. The three GFP background types used in the diffusion studies are also currently being crossed with *pin1* plants to hopefully gain an intermediate *pin* phenotype between WT and the *pin* phenotype introduced by spraying.

Effect of HAM proteins on WUS Distribution

HAIRY MERISTEM, (HAM) proteins are GRAS-domain transcription factors which interact with WUS protein as cofactors and are believed to play a role in governing its distribution across the SAM (14). In order to determine how the HAMs work together with WUS to gauge its distribution, several mutants were generated with different *HAM* genes knocked out and were visualized under confocal microscopy.

Results

Different chemical and genetic assays were performed to quantify different aspects of CLV3.

LambdaN does not seem to interact with the box-B construct when attempting to make a working expression quantification system for CLV3

The box-B repeat construct was transformed into several plants already expressing the LambdaN protein. The offspring were selected via antibiotic and visualized under confocal microscopy to see if there were any relevant changes. Several meristems were visualized, some of which are shown in Fig. 4.2. While spots containing LambdaN protein could be identified, (Fig. 4.2B) the patterns looked very similar to plants carrying the protein without the box-B construct (Fig. 4.2A) and there was no clearly visible shift in distribution to the central region of the meristem that would indicate that the box-B was interacting with the LambdaN protein as expected.

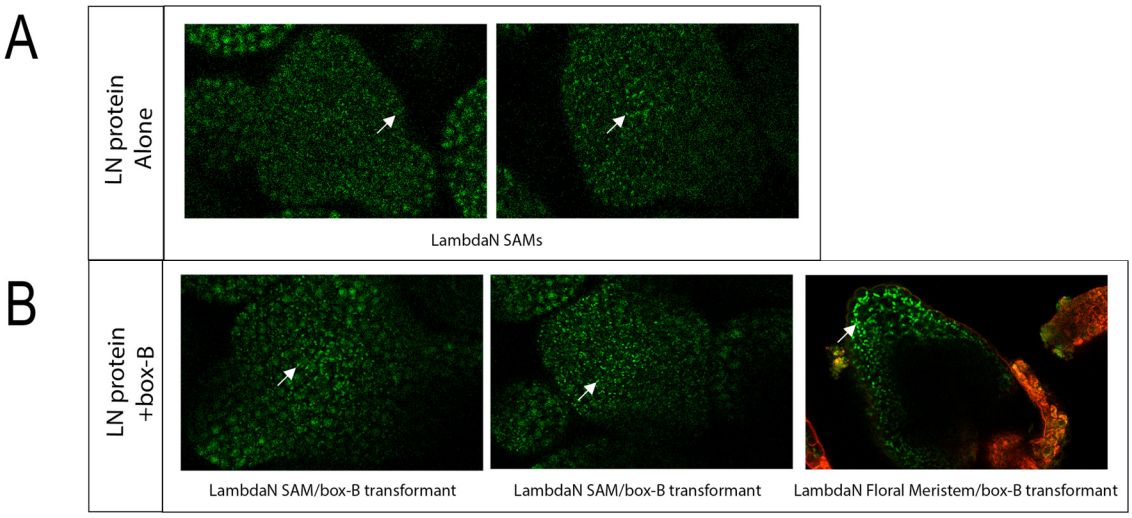

Fig. 4.2. The box-B sequence does not have a noticeable effect on LambdaN protein distribution. **(A)** Confocal images of SAMs with LambdaN protein only. **(B)** meristems with LlambdaN transformed with box-B construct.The first two being SAMs and the last being a side view of a floral meristem. **(A-B)** white arrows indicate LambdaN-GFP-NLS protein

Opening chromatin through trichostatin treatment does not lead to a significant shift in *CLV3* expression.

pCLV3::H2B-mYFP plants were treated with trichostatin at a concentration of 10uM and left for 24hr (Fig. 4.3B). These treated plants were compared to a similarly DMSO treated set of plants (Fig 4.3A) and examined for any changes in distribution and expression across the tissue. Both groups appeared to express the marker *H2B-mYFP* at roughly the same level and pattern.

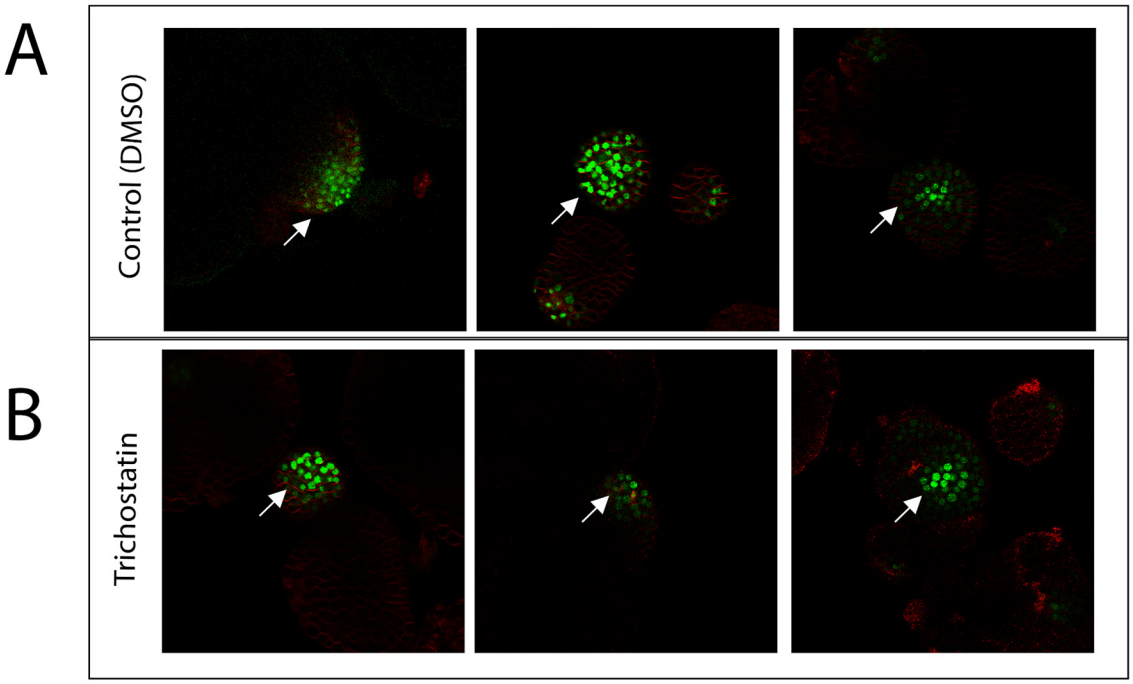

Fig. 4.3. CLV3 expression is not significantly altered by trichostatin.
(A) DMSO treated SAMs. **(B)** trichostatin treated SAMs. **(A-B)** White arrows indicate CLV3 expression pattern

In tandem with CLV3, different properties of WUS and how it behaves in the wider context of the signaling network and the SAM were also investigated.

Dimeric WUS leads to repressive phenotypes.

The forced dimer was transformed into *pCLV3::H2B-mYFP* plants and examined visually and under confocal microscopy to quantify any changes in phenotype.

The most extensively examined FD was the *pWUS::FD* construct under an LER or *wus1-1* null background with a *pCLV3::H2B-mYFP* marker. The general physical phenotypes are shown in Fig. 4.4A. Compared to the regular LER plant shown in (6) plants transformed with FD showed a mix of phenotypes from stunted (1) to stringy (2) to

WTlike (4) in general appearance. The floral organs of the FD transformed plants were examined in detail. (Fig. 4.4B) Compared to LER flowers (1) flowers of FD transformants often had a lower number of anthers and were more likely to have terminated SAMs (3, 6) SAMs of FD transformants were also compared with WT plants for differences in *CLV3* expression. (Fig. 4.4C) Compared to the WT first row in Fig 4.4C, the heterozygous FD transformant SAM in row 2 shows lower expression of CLV3 in all layers. For the *wus1-1* background with FD transformant in the third row, a tiny bit of expression seems to be returning in the central zone in contrast to regular *wus1-1*.

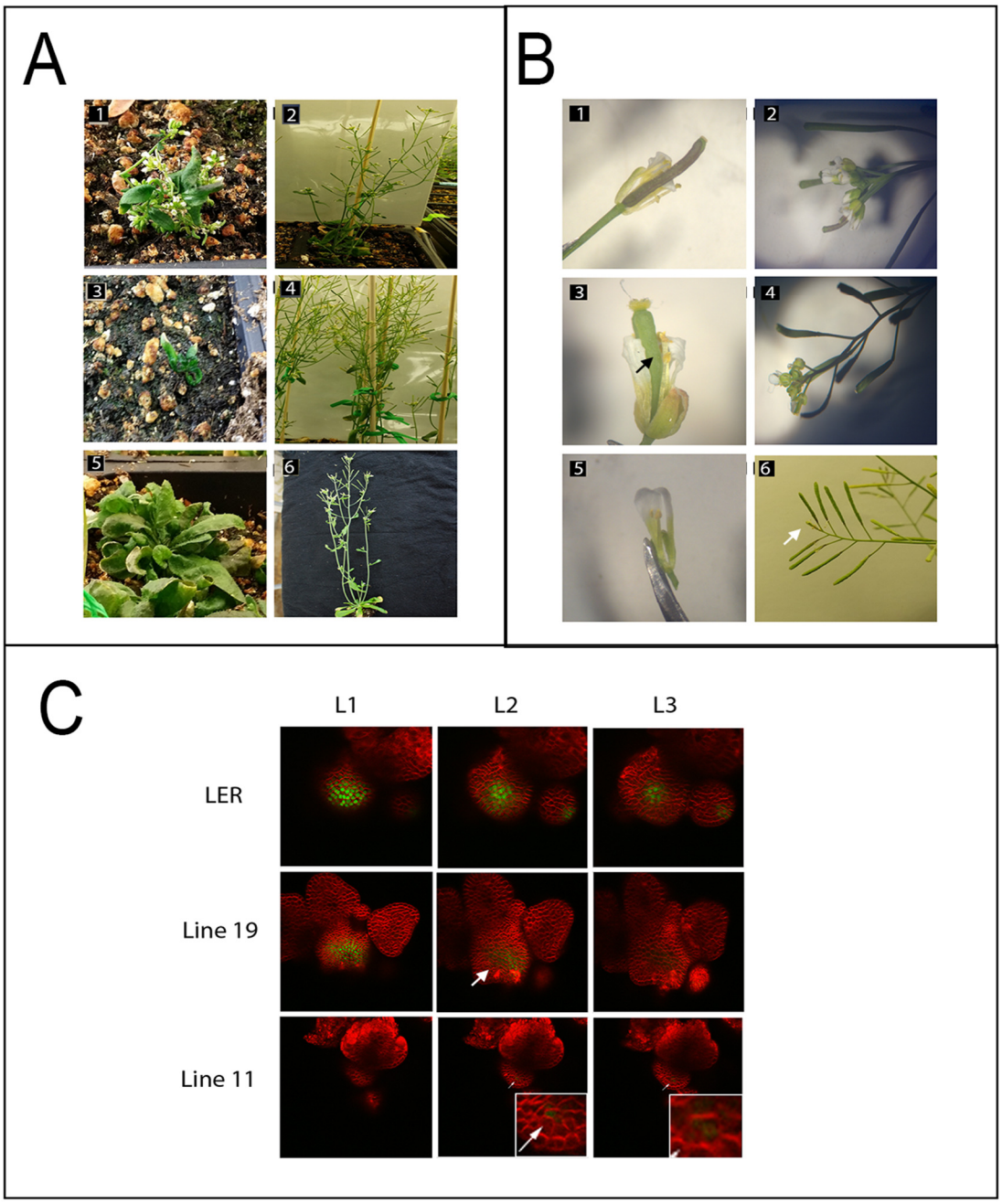
A
1
2
3
4
5
6
B
1
2
3
4
5
6
C
L1
L2
L3
LER
Line 19
Line 11

Fig. 4.4. Dimeric WUS appears to introduce repressive and subnormal structural phenotypes. **(A)** Plant structure phenotypes from plants transformed with *pWUS::FD* plasmid: 1. Stunted 2. Stringy. 3. Stunted 4. Near Normal 5. *wus1-1* null transformant. 6. WT LER. **(B)** Floral phenotypes of plants transformed with FD plasmid. 1. LER flower (control) 2. LER inflorescence (control) 3. FD flower. White arrow points to thickened style and reduced number of anthers. 4. FD inflorescence. 5. *wus 1-1* background FD flower. 6. FD terminated meristem. Arrow points to terminated meristem. (**C)** Confocal imaging of expression of *CLV3:H2B-mYFP* LER plants meristems transformed with FD through the different meristem layers. Rows: plant lines. Columns: meristem layers. First row: LER, Second row: FD line 19. Arrow points to reduced CLV3 expression. Third row: FD *wus1-1* homozygous line 11.1

Measuring diffusion through RICS

Diffusion of WUS in the SAM was investigated through a series of time trials where the tissue was visualized over time periods and the changes in fluorescence were quantified. The table of results is listed in Fig. 4.6 along with the PSF values from eGFP solutions. Several trials to calculate the dilution coefficient (D1) in um2/s were performed and are listed after the 'Raster Image Correlation' heading with their conditions as the three lefthand columns in Fig. 4.6. Trial 1 tested *eGFP-WUS* plants and show low D1 ranging from 0.000002 to 0. Trial 2 tested *eGFP-WUS* plants that were treated with 100uM NPA in order to develop *pin* mutant structures where the SAM juts out more prominently (Fig. 4.5) and can be more easily fixed for side views for more data collection. These show much greater D1 values ranging from 117 to 606. Trial 3 tested *eGFP-WUS* plants under different pixel dwell times and had D1 values mostly similar to Trial 2 ranging from 0.000035 to 805.

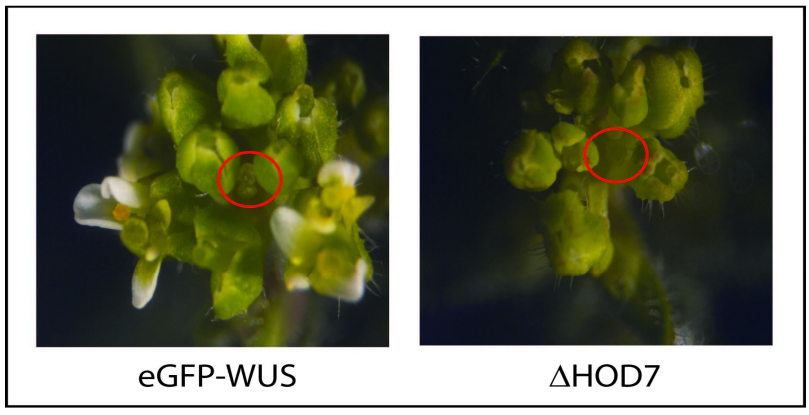

Fig. 4.5. *pin* phenotypes after NPA treatment.
pin phenotypes observed after treating *eGFP-WUS* and *ΔHOD7* plants with NPA.

FCS DATA

A

Point Spread Function	Wo (1/e2)
fresh gfp	0.27996
	0.28665
	0.53767
	0.28894
old gfp	0.28278
	0.27994
	0.28574
average	0.284001667 excluding fresh 3 Wo (1/e2)

Raster Image Correlation

B

	Diffusion Coefficient	um2/s
EGFP-WUS trials		
Test 1	0	E1
Test 2	2E-06	E1
Test 3	1E-06	E1
Test 4	0	E1
test 4half	0	E2
test hlaf	2E-06	E3

C

eGFP-WUS trials (NPA treated)		
Plant 1	190	N1
Plant 1	104	N1
Plant 1	121.111256	N1
Plant 1	358.05787	N1
Plant 3	606.164767	N1
Plant 3	117.566219	N1

D

EGFP-WUS Dwell times Trials		
dwell0.98:	3.7E-05	T1
dwell1.7:	805.123958	T2
dwell4.1:	545.928619	T3
dwell8:	445.187847	T4

E

Conditions	
EGFP-WUS Conditions	
E1	(pt 8.19 lt 0.00024 ft 1.26 ps 0.1)
E2	(changed parameters pt 4.10)
E3	(changed parameters pt 4.10 ft 0.62915)
NPA Conditions	
N1	pt 8.19 us lt 0.000240ms ft 1.26s ps 0.07um)
Dwell Time Conditions	
T1	(pt 0.98us lt 0.000240ms ft 0.26051s ps 0.07um)
T2	(pt 1.70us)
T3	(changed parameters: pt 4.1us ft 0.149s)
T4	(changed parameters: ft 0.62915s)
pt	pixel time
ps	pixel size
lt	line time
ft	frame time not used in rics

Fig. 4.6. Raster Image Correlation Spectroscopy values.
(A) Point spread function values from GFP solutions. **(B-D)** Diffusion coefficient values from different RICS trials. Trial conditions are indicated by right column alphanumeric value. **(E)** Trial condition legend. Changed parameters indicates change from default values listed in topmost group condition.

HAMs exert a powerful effect on WUS distribution and *CLV3* expression

The effect of HAM mutants on the distribution of WUS are quantified in Fig. 4.7. In Fig 4.7A, A WT *pWUS::eGFP-WUS* in the first column is compared with various mutants where *HAM1* and *HAM2* are either fully or partially knocked out. Compared to the WT, WUS expression is barely or not seen at all for the mutants. In Fig. 4.7B, a *pCLV3(970M4)::H2B-mYFP* plant with intact HAM genes is compared with *ham1 -/-*

/ham2 +/- mutants of the same plant. These consistently show strengthened CLV3 expression over the SAM with fully intact HAM.

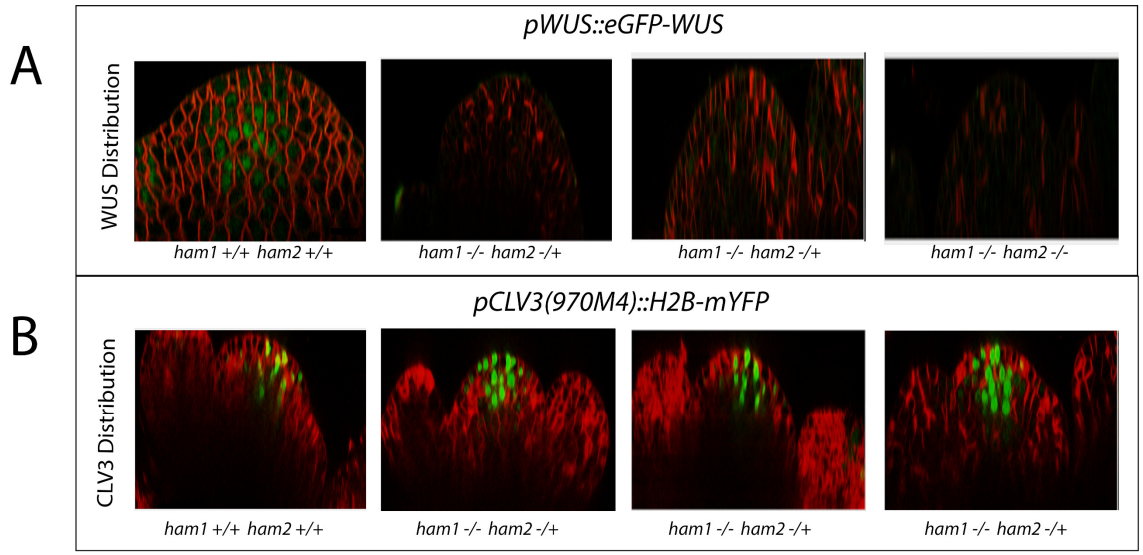

Fig. 4.7: HAM protein exerts a strong influence on WUS distribution and CLV3 expression.
(A) WUS distribution quantified through *pWUS::eGFP-WUS* marker. HAM genotypes are below images.
(B) CLV3 distribution quantified through *pCLV3(970M4)::H2B-mYFP*.

Discussion

Imaging studies are a powerful way to investigate the WUS/CLV3 SAM dynamics at the tissue level. Through these studies more information and supporting evidence has been gathered for systems such as the concentration dependent mechanism investigated in Chp1.

Even though some of the imaging studies did not work as expected, data was still gathered about the possible properties and behavior of CLV3 and WUS in each case.

The attempt to use the LambdaN system to measure expression appeared to not be successful. Although free LambdaN protein was seen throughout the meristems tested,

there did not seem to be any significant hallmark that would indicate interaction with *CLV3* transcripts. Perhaps the system does not work as the protein does not interact as expected with the box-B RNA stemloop. Perhaps something in the system prevents the box-B sequence from integrating into the genome after transformation due to the repeats which could have caused the plant to reject the gene while keeping the selective marker. In this case, a redesign of the vector, reducing repeats would possibly help. Attempts to use the similar MS2 system to measure *CLV3* expression also failed, pointing to a possible underlying incompatibility with these systems when measuring CLV3.

Treatment with trichostatin to open up the chromatin through HDAC inhibition and test increased WUS access, did not seem to have a specific pronounced effect on expression of the *CLV3* gene. The open chromatin itself is just one component of increasing expression and chemical treatment may not have been enough to alter it specifically. There might be some feedback mechanism at play restricting expression from going out of control. The amount of trichostatin used can possibly be adjusted as the treatment may not have enough getting into the meristem to make a difference or the time between treatment and visualization may be too long and can be reduced.

Attempts are ongoing to quantify diffusion of different forms of WUS through RICS analysis. This will among other things help quantify the effect of dimerization and visualize the concentration dependent mechanism in action as well as provide data for more accurate simulation studies. Current attempts have been thwarted by microvibrations that make collecting stable images at levels needed to track molecules difficult. Current measures of D1 in plants tend to have diffusion coefficients around the

100s of um/s which seems large compared to the diffusion coefficients of other proteins in plants (15) but additional work to create plants with less extreme *pin1* phenotypes which can be more easily mounted and stabilized continues to confirm if the collected values are accurate or if better data can be collected.

Analysis of WUS's dimerization through the FD revealed some interesting properties which further bore out the repressive aspects of WUS dimerization and the importance of the concentration dependent mechanism. CLV3 appeared to have lower expression in plants transformed with the FD. Some of the plant phenotypes were abnormal and appeared to be intermediate between WT and WUS mutants like *wus1-1* including signs like terminated SAMs, lower anther number etc.

Visualizing systems with mutant HAM showed the importance of HAMs in maintaining WUS distribution. The WUS gradient dissipated under HAM mutants, CLV3 concentration actually increased with the dispersal of WUS again reinforcing the nature of WUS as having a repressive effect on CLV3 at very high concentrations while activating CLV3 at lower concentrations.

Methods

LambdaN System

The LambdaN system is composed of the 22AA λN_{22} or LambdaN protein and the 15nt box-B sequence and is more fully described in (6). The LambdaN protein with a connected marker binds to an RNA transcript of box-B as it forms a stemloop sequence opening up a possible way to measure expression of a gene. A box-B repeat sequence

was cloned alongside the *CLV3* promoter and plants already expressing the *UBQ10: LambdaN-GFP-NLS* locus were transformed with the construct.

Trichostatin

Trichostain inhibits HDACs, which theoretically should lead to loosening of the chromatin. *pCLV3::H2B-mYFP* plants were treated with trichostatin at 10uM and then left for 24hrs and treated again at 3hr before visualization.

Diffusion Studies and RICS Analysis

Diffusion of WUS was studied through Raster Image Correlation Spectroscopy (RICS). RICS expands on traditional FCS measuring the temporal fluctuations in fluorescence of several spatial points by scanning tissue rapidly over time. This study followed the protocol laid out in (12) where tissue was scanned under the confocal microscope for a period of time and the fluorescence patterns were analyzed. Several parameters in the visualization were adjusted to achieve optimal results. These were pixel time: which controls the time in which a single pixel is scanned, line time: which is the time between line scans, and pixel size. For analysis the program SimFCS 4 was used to conduct analysis on a background of free GFP in solution for the point spread function (PSF) value (Wo) in two sets named Old and fresh GFP. The point spread function is a measure of blurring of a point in the optical system and is necessary as a value for the next step of RICS

The average PSF minus an outlier was used for RICS analysis comparing the image stack to correlate and track particle movement. This yielded the diffusion coefficient (D1)

in units of um2/s which measured the speed at which a particle flows from high to low concentrations. By using this coefficient and comparing different regions and systems the diffusion behavior in these systems could be quantified. The tissues analyzed were LER plants containing *eGFP-WUS*, free eGFP, and *WUS(⊿HOD7)*, a mutant lacking dimerization ability.

PIN **mutant plants**

In order to obtain tissue that could more easily be mounted to conduct the imaging needed for FCS. *eGFP-WUS*, free eGFP and *WUS(⊿HOD7)* plants were treated with 100uM NPA. NPA interferes with the activity of PIN proteins leading to phenotype shown in Fig. 4.5.

HAM Mutants

Mutants of HAM were genotyped and visualized under the microscope.

Forced Dimer

The forced dimer construct sequence was composed of two WUSCHEL sequences with the linker GGCGGCGGCTCTGGCGGCGGCTCTGGCGGCGGCTCTGGCGGCGGCTCTGGCGGCGGCTCTGGCGGCGGCTCT in between, controlled by the pWUS promoter.

References

1. J. Sheen, Master regulators in plant glucose signaling networks. J. Plant Biol. 57, 67–79 (2014).

2. Á. Soria-García, M. C. Rubio, B. Lagunas, S. López-Gomollón, M. de los Á. Luján, R. Díaz-Guerra, R. Picorel, M. Alfonso, Tissue Distribution and Specific Contribution of Arabidopsis FAD7 and FAD8 Plastid Desaturases to the JA- and ABA-Mediated Cold Stress or Defense Responses. Plant and Cell Physiology. 60, 1025–1040 (2019).

3. J. Sheen, S. Hwang, Y. Niwa, H. Kobayashi, D. W. Galbraith, Green-fluorescent protein as a new vital marker in plant cells. The Plant Journal. 8, 777–784 (1995).

4. C. Akgul, D. A. Moulding, M. R. H. White, S. W. Edwards, In vivo localisation and stability of human Mcl-1 using green fluorescent protein (GFP) fusion proteins. FEBS Letters. 478, 72–76 (2000).

5. S. Alamos, A. Reimer, K. K. Niyogi, H. G. Garcia, Quantitative imaging of RNA polymerase II activity in plants reveals the single-cell basis of tissue-wide transcriptional dynamics. Nat. Plants. 7, 1037–1049 (2021).

6. J. Schönberger, U. Z. Hammes, T. Dresselhaus, In vivo visualization of RNA in plants cells using the λN22 system and a GATEWAY-compatible vector series for candidate RNAs. The Plant Journal. 71, 173–181 (2012).

7. W. Ouyang, Z. Cao, D. Xiong, G. Li, X. Li, Decoding the plant genome: From epigenome to 3D organization. Journal of Genetics and Genomics. 47, 425–435 (2020).

8. L. C. Huber, J. H. W. Distler, F. Moritz, H. Hemmatazad, T. Hauser, B. A. Michel, R. E. Gay, M. Matucci-Cerinic, S. Gay, O. Distler, A. Jüngel, Trichostatin A prevents the accumulation of extracellular matrix in a mouse model of bleomycin-induced skin fibrosis. Arthritis & Rheumatism. 56, 2755–2764 (2007).

9. M. Perales, K. Rodriguez, S. Snipes, R. K. Yadav, M. Diaz-Mendoza, G. V. Reddy, Threshold-dependent transcriptional discrimination underlies stem cell homeostasis. Proceedings of the National Academy of Sciences. 113, E6298–E6306 (2016).

10. H. Fujita, K. Toyokura, K. Okada, M. Kawaguchi, Reaction-Diffusion Pattern in Shoot Apical Meristem of Plants. PLOS ONE. 6, e18243 (2011).

11. K. A. de Villiers, C. H. Kaschula, T. J. Egan, H. M. Marques, Speciation and structure of ferriprotoporphyrin IX in aqueous solution: spectroscopic and diffusion measurements

demonstrate dimerization, but not μ-oxo dimer formation. J Biol Inorg Chem. 12, 101–117 (2007).

12. N. Clark, R. Sozzani, "Measuring Protein Movement, Oligomerization State, and Protein–Protein Interaction in Arabidopsis Roots Using Scanning Fluorescence Correlation Spectroscopy (Scanning FCS)" in Methods in Molecular Biology (2017), vol. 1610, pp. 251–266.

13. M. Sassi, O. Ali, F. Boudon, G. Cloarec, U. Abad, C. Cellier, X. Chen, B. Gilles, P. Milani, J. Friml, T. Vernoux, C. Godin, O. Hamant, J. Traas, An Auxin-Mediated Shift toward Growth Isotropy Promotes Organ Formation at the Shoot Meristem in Arabidopsis. Current Biology. 24, 2335–2342 (2014).

14. Y. Zhou, A. Yan, H. Han, T. Li, Y. Geng, X. Liu, E. M. Meyerowitz, HAIRY MERISTEM with WUSCHEL confines CLAVATA3 expression to the outer apical meristem layers. Science. 361, 502–506 (2018).

15. H. Hao, L. Fan, T. Chen, R. Li, X. Li, Q. He, M. A. Botella, J. Lin, Clathrin and Membrane Microdomains Cooperatively Regulate RbohD Dynamics and Activity in Arabidopsis. *The Plant Cell*. 26, 1729–1745 (2014).

Concluding Discussion

Through this study, progress has been made toward a fuller understanding of several aspects of WUS biology and how it interacts and influences the network around it from protein to DNA. This work is part of a larger goal to move beyond observing the behavior of the meristem network to developing a quantitative mechanistic explanation for the dynamics that are observed. It is important as a clearer picture of the biology continues to be developed that important new targets are identified to focus on and put into context as well. The next step is to expand beyond the WUS/CLV3 pathways and to go genomewide and in the direction of generalization where possible, integrating computational techniques to process and analyze the large complex datasets that are generated. Some of the projects presented here are steps along that path providing valuable biological information or being direct precursors to large scale experiments.

One of the key components of the network that has been fleshed out, is the CRM and the concentration dependent switch it coordinates through temporal, spatial, and biochemical factors. A quantitative explanation of the molecular dynamics behind this switch has been a big step forward in understanding the biology of the meristem and providing a possible model for similar systems for other WUS targets as well as other TFs in *Arabidopsis* and beyond. The cooperative action among the different cis-elements is an important subcomponent of the CRM system and another divergent mechanism from traditional models of gene expression. Collectively the unique features of the *CLV3* CRM shows that there is a greater diversity of regulatory schemes for genes that possibly are better suited for different contexts than previously suspected. Uncovering this and other more recent expression paradigms (1) may signal a shift that will allow

researchers to more effectively untangle the regulation of other gene systems or even reexamine what is known about systems thought to be understood. Work is now progressing on to other CRMs in *CLV3* and other genes to see how they interact with WUS, and what role they play in the SAM.

The simulation model used to examine the CRM in Chp1 was expanded into a coupled feedback model with fluctuating WUS species added. Data is currently being gathered on its properties and how the system balances with multiple competing species. But preliminary results indicate that the concentration dependent mechanism and cooperativity still play the same role in this system. But work still remains to thoroughly characterize its properties and behavior under a comprehensive set of conditions. Also, further refinement of the core dynamics is needed as the feedback model does not fully match up with new experimental results for *clv3-2* complemented plants coming in that are showing resetting of the CLV3 gradient to the outer layers across most mutants. Understanding this phenomenon is important as it may explain the robustness of the meristem phenotype to CLV3 levels.

Looking into the landscape of *CLV3*, is an important complement to the study of the CRM to give a fuller picture of how WUS coordinates its interaction with targets. This study has also gathered some limited information about genes other than *CLV3*, the logical next step is to expand the scope of the assays that have been conducted to a larger level.

The ChIP of WUS and histone marks to *CLV3* can be scaled up to ChIPseq that will quantify WUS binding and histone acetylation under the conditions previously tested, on a genomewide scale (2). WUS ChIPseq has been performed previously but was deemed to have excessive background, but higher quality data could still be useful. Similarly, the 3C testing for interactions between *CLV3* fragments with a bait at the 3' end can be scaled to HiC which tests for interactions between all combinations of fragments generated by restriction digest using essentially a very similar protocol, greatly increasing the data generated and removing bias from selecting arbitrary fragment sets (3). The major challenge will be to obtain the large amounts of properly processed chromatin for these scaled up assays. As the small scale assays are very similar to the large scale assays in their initial steps, it would be helpful to perform additional replicates of the smaller scale ChIP and 3C experiments with other targets such as *YABBY* and *KAN1* in order to experiment with further quality control for the technique and optimize for larger yields as well as confirm previous findings.

The upscaled datasets from genomewide assays will provide more data to work with that will require even greater computational resources for interpretation but should also provide more robust broad results and more ways to segment the data to draw useful conclusions. The fixed motif and machine learning based HMM analysis, which has shown promise in identifying WUS target regions, can be integrated into an even more powerful strategy with the larger data availability and can be reoriented to different purposes such as determining whether significant subgroups of highly WUS bound sequences exist and how they differ from each other. Additionally, the data will provide a superior training pool for the HMM model.

Imaging studies have been mixed. In some cases, like the LambdaN expression system the solution may be to slightly alter the repeats of the box-B or diagnose some technical problem. But such stemloop expression systems might not function for *CLV3*.

Work is ongoing to overcome the technical challenges in some studies. Some difficulties are well understood and attempts are in progress to mitigate them such as reducing vibrations when attempting to quantify diffusion. In other cases, such as opening the chromatin with trichostatin to observe how it alters gene expression, the strategy simply didn't lead to any changes and the cause is more ambiguous.

However, some data has been gathered regarding the effect of the dimeric form of WUS and the effect of interactors like HAM on WUS distributions. And these results back up mechanisms established in earlier chapters regarding the dynamics governing WUS and CLV3 expression. *In vivo* imaging remains one of the gold standards for studying most experimental chemical and genetic perturbations to the meristem at the tissue level but must be carefully crafted to the purpose at hand.

The new data from this and other studies have helped the research of meristem and WUS biology to move past the observational stage to begin to develop quantitative mechanistic explanations for the behavior that has been characterized. Combining experimental and computational approaches and designing the investigation to tackle the issues from multiple angles has been invaluable in solving this complex problem.

The integration of computational methods will become more critical as work proceeds to the next stage of upscaling from *CLV3* to other targets and eventually the genome/proteome level to generalize findings. The larger datasets will not only help to refine computational and bioinformatic analysis but also require tools to provide meaningful analysis leading to a stronger symbiotic relationship between experimental and computational techniques.

References

1. C. Sayou, M. H. Nanao, M. Jamin, D. Posé, E. Thévenon, L. Grégoire, G. Tichtinsky, G. Denay, F. Ott, M. Peirats Llobet, M. Schmid, R. Dumas, F. Parcy, A SAM oligomerization domain shapes the genomic binding landscape of the LEAFY transcription factor. Nat Commun. 7, 11222 (2016).

2. P. J. Park, ChIP–seq: advantages and challenges of a maturing technology. *Nat Rev Genet*. **10**, 669–680 (2009).

3. E. de Wit, W. de Laat, A decade of 3C technologies: insights into nuclear organization. *Genes Dev.* **26**, 11–24 (2012).